(4)

GL-TR-89-0133

Regional Phases: Oceanic and Continental Propagation

John A. Orcutt

University of California, San Diego
Scripps Institution of Oceanography
La Jolla, CA 92093

4 March 1989

Final Report
4 March 1987-4 March 1989

GEOPHYSICS LABORATORY
AIR FORCE SYSTEMS COMMAND
UNITED STATES AIR FORCE
HANSCOM AIR FORCE BASE, MASSACHUSETTS 01731-5000

SPONSORED BY
Defense Advanced Research Projects Agency
Nuclear Monitoring Research Office
ARPA ORDER NO. 5299

MONITORED BY
Geophysics Laboratory
Contract No. F19628-87-K-0013

This technical report has been reviewed and is approved for publication.

JAMES F. LEWKOWICZ
Contract Manager
Solid Earth Geophysics Branch
Earth Sciences Division

JAMES F. LEWKOWICZ
Branch Chief
Solid Earth Geophysics Branch
Earth Sciences Division

FOR THE COMMANDER

DONALD H. ECKHARDT, Director
Earth Sciences Division

This report has been reviewed by the ESD Public Affairs Office (PA) and is releasable to the National Technical Information Service (NTIS).

Qualified requestors may obtain additional copies from the Defense Technical Information Center. All others should apply to the National Technical Information Service.

If your address has changed, or if you wish to be removed from the mailing list, or if the addressee is no longer employed by your organization, please notify AFGL/DAA, Hanscom AFB, MA 01731-5000. This will assist us in maintaining a current mailing list.

Do not return copies of this report unless contractual obligations or notices on a specific document requires that it be returned.

REPORT DOCUMENTATION PAGE

Form Approved OMB No. 0704-0188

1a. REPORT SECURITY CLASSIFICATION: Unclassified	1b. RESTRICTIVE MARKINGS
2a. SECURITY CLASSIFICATION AUTHORITY	3. DISTRIBUTION/AVAILABILITY OF REPORT: Approved for public release; distribution unlimited.
2b. DECLASSIFICATION/DOWNGRADING SCHEDULE	
4. PERFORMING ORGANIZATION REPORT NUMBER(S)	5. MONITORING ORGANIZATION REPORT NUMBER(S): GL-TR-89-0133
6a. NAME OF PERFORMING ORGANIZATION: Univ. of California, San Diego; 6b. OFFICE SYMBOL (If applicable)	7a. NAME OF MONITORING ORGANIZATION: Geophysics Laboratory
6c. ADDRESS (City, State, and ZIP Code): Scripps Institution of Oceanography, La Jolla, CA 92093	7b. ADDRESS (City, State, and ZIP Code): Hanscom Air Force Base, Massachusetts 01731-5000
8a. NAME OF FUNDING/SPONSORING ORGANIZATION: Defense Advanced Research Projects Agency; 8b. OFFICE SYMBOL (If applicable): NMRO	9. PROCUREMENT INSTRUMENT IDENTIFICATION NUMBER: F19628-87-K-0013
8c. ADDRESS (City, State, and ZIP Code): 1400 Wilson Blvd., Arlington, VA 22209-2308	10. SOURCE OF FUNDING NUMBERS

PROGRAM ELEMENT NO.	PROJECT NO.	TASK NO.	WORK UNIT ACCESSION NO.
61101E	7A10	DA	CJ

11. TITLE (Include Security Classification): Regional Phases: Oceanic and Continental Propagation

12. PERSONAL AUTHOR(S): John A. Orcutt

13a. TYPE OF REPORT	13b. TIME COVERED	14. DATE OF REPORT (Year, Month, Day)	15. PAGE COUNT
Final	FROM 3/4/87 TO 3/4/89	3/4/89	146

16. SUPPLEMENTARY NOTATION

17. COSATI CODES			18. SUBJECT TERMS (Continue on reverse if necessary and identify by block number)
FIELD	GROUP	SUB-GROUP	Seismic discrimination, quarry blasts, sonograms, impulse response, resonance microseisms

19. ABSTRACT (Continue on reverse if necessary and identify by block number)

In this report we present the results of several investigations dealing with two diverse topics:

We compare ambient noise levels on islands with those present at and beneath the seafloor to determine the value of permanent seafloor seismic stations. We compare signal power spectral levels expected from earthquakes with ambient noise levels at these locations to determine a lower magnitude limit of detectable events.

We study the nature of propagation of seismic waves through the continental and oceanic crusts. We investigate the influence the regular repetition of features in seismograms, introduced at the source and/or during propagation by layer resonance, has on the spectrum of the recorded coda.

20. DISTRIBUTION/AVAILABILITY OF ABSTRACT	21. ABSTRACT SECURITY CLASSIFICATION
☐ UNCLASSIFIED/UNLIMITED ☐ SAME AS RPT. ☐ DTIC USERS	Unclassified
22a. NAME OF RESPONSIBLE INDIVIDUAL: James Lewkowicz	22b. TELEPHONE (Include Area Code): (617) 377-3222 — 22c. OFFICE SYMBOL: GL/LWH

DD Form 1473, JUN 86 — Previous editions are obsolete. — SECURITY CLASSIFICATION OF THIS PAGE: Unclassified

FINAL TECHNICAL REPORT

4 March 1987 - 4 March 1989

ARPA Order: 5299

Name of Contractor: The Regents of the University of California
University of California, San Diego
Scripps Institution of Oceanography
La Jolla, California, 92093

Effective Date of Contract: 4 March 1987

Contract Expiration Date: 4 March 1989

Contract Number: F19628-87-K-0013

Principal Investigator: Dr. John A. Orcutt
(619) 534-2887

Program Manager: James Lewkowicz
(617) 377-3028

Short Title of Work: Regional Phases: Oceanic and Continental Propagation

SPONSORED BY:

Defense Advanced Research Projects Agency (DOD)
Strategic Technology Office, Geophysical Sciences Division
DARPA/STO Signal Propagation Theory Program

Issued by The Air Force Geophysics Laboratory

TABLE OF CONTENTS

TASK OBJECTIVES

There are two broad objectives in this research effort. The first of these involves the analysis of oceanic data sets for the purpose of evaluating seafloor noise levels *vis-a-vis* stations which are located on islands and confirming a propagation model for high frequency regional phases which was developed using data collected during the DARPA-sponsored NGENDEI Expedition. The second objective is to use the experience with regional phases which was gained in studying oceanic P_n and S_n in analyzing NORESS array recordings of events which have propagated over regional distances on the continents.

Specifically, the Work Statement includes the following:

- Obtaining stable estimates of the short period (>0.1 Hz) noise at island stations (*SNZO and GUMO) for comparison with typical* noise levels on the seafloor.

- Examining high frequency regional phase (P_n/S_n) data from the Wake Island Array for comparison with the P_n propagation model and the data collected in the southwest Pacific during the NGENDEI Expedition.

- Analyzing data from the NORESS array including the computation of frequency-wavenumber spectra from high frequency regional phases such as P_g and L_g. Comparing the results with computations of synthetic seismograms and frequency-wavenumber spectra in order to understand more fully the responsible wave propagation phenomena.

TECHNICAL RESULTS

ABSTRACT

In this report we present the results of several investigations dealing with two diverse topics:

- We compare ambient noise levels on islands with those present at and beneath the seafloor to determine the value of permanent seafloor seismic stations. We compare signal power spectral levels expected from earthquakes with ambient noise levels at these locations to determine a lower magnitude limit of detectable events.

- We study the nature of propagation of seismic waves through the continental and oceanic crusts. We investigate the influence the regular repetition of features in seismograms, introduced at the source and/or during propagation by layer resonance, has on the spectrum of the recorded coda.

SUMMARY

The initial goal of this project was to compare ambient noise levels on islands with those present at and beneath the seafloor. The motivation for this work stems from concern about the sparse coverage of oceanic areas provided by island based seismic stations. In chapter 1 we compare noise levels recorded by Seismic Resarch Observatory (SRO) stations on Guam, the north island of New Zealand, Taiwan and Easter Island and conclude that in the frequency band from 0.1 to 10 Hz the island noise levels are comparable to those at the seafloor, recorded by Ocean Bottom Seismometers, and somewhat higher than those recorded beneath the seafloor by the Marine Seismic System (MSS). We conclude that in this band seafloor stations are realistic alternatives when island sites are not available.

In chapter 2 we extend this study by comparing ambient noise levels recorded on and beneath the seafloor with signal levels expected at an epicentral range of 30° from events ranging in M_W from 5.0 to 9.5. We find that at this range in the Pacific events with Mw as low as 5.5 should be detectable by seafloor

sensors. Due to lower noise levels in the Atlantic, and beneath the seafloor in the Pacific, it appears that the threshold for sensors deployed in these regions is as low as 5.0. We found that in the range from 1 to 100 km from the shoreline that microseism noise levels (in the band near 250 mHz) are inversely correlated with distance from the shoreline. We extend this effort, in chapter 4, with a comparative analysis of ambient borehole noise levels present at the NORESS array in Norway and in Kazakhstan U.S.S.R. We find that the noise levels at the NORESS are 5 to 10 db lower than those in Kazakhstan except in the microseism band where they are significantly higher. We conclude this is probably due to the proximity of NORESS to the Ocean.

In chapters 3 through 6 we consider two fundamentally different processes that are capable of impressing a regular modulation onto the frequency spectrum of recorded coda. The first process we consider requires the interaction of time offset wavefields produced by sub-events within multiple-event mine explosions (ripple-fired quarry blasts). The second process involves the resonance of energy in low velocity strata.

In chapter 3 we examine recordings of regional single and multiple event explosions in central Asia. We consider the effect that the practice of ripple firing, or the detonation of several explosions closely grouped in space and time, has on the spectrum of the resultant seismic coda. We predict theoretically, and observe in seismic recordings, that this practice is capable of impressing a time-independent modulation on the spectrum of the coda. Simple events do not seem to give rise to this time-independent organization of energy. We develop an algorithm that attempts to discriminate between mine explosions and single event explosions by seeking time-independent spectral features.

In chapter 4 we extend the work discussed in the previous chapter by considering data collected in a different geographic setting. The data set considered in this study consists of recordings of earthquakes and mine explosions made by the NORESS array in Norway. Despite low digitization rates at NORESS (40 samples/s) the two types of events are easily distinguished using the algorithm developed by the previous study. These studies show that earthquakes and single event explosions can be distinguished from mining

explosions using the method we describe. In addition the algorithm appears to be independent of geologic setting and local mining practice.

One result of Scripps' 1983 S.W. Pacific Ngendei expedition was the Pn propagation model proposed by Sereno and Orcutt (1985 a,b). An important aspect of this model is a coda generation mechanism that relies solely on the resonance of energy in low velocity strata and does not invoke scattering by small scale inhomogeneities. In chapter 5 we seek to reproduce the results of Sereno and Orcutt by examining high frequency recordings of earthquakes made by Hydrophones in the Wake Island Hydrophone array and by Hydrophones and Ocean Bottom Seismometers deployed during the Ngendei expedition. Our observations are essentially consistent with those made by Sereno and Orcutt.

In chapter 6 we report on research carried out to investigate the likely dominant coda generation mechanism present in the continental crust. We use two datasets for this purpose - recordings of mine and single-event explosions made in central Asia as well as recordings of mine explosions and earthquakes made by the NORESS array in Norway. This work, which primarily involves the analysis of the evolution of frequency and wavenumber spectra as a function of time in seismic coda, is currently in progress and in this chapter we report interim results and plans for the continuation of this research.

CHAPTER 1

A COMPARATIVE STUDY OF ISLAND, SEAFLOOR AND SUB-SEAFLOOR AMBIENT NOISE LEVELS

Michael A.H. Hedlin and John A. Orcutt

Institute of Geophysics and Planetary Physics (A-025)

Scripps Institution of Oceanography, La Jolla CA, 92093

Bulletin of the Seism. Society of America (1989) vol. 79, 172-179

ABSTRACT

A study of seafloor and island stations shows that for the frequency band 0.1 - 10 Hz, the seismic noise levels on islands are comparable to the levels on the seafloor. The microseism peak at the seafloor appears to be comparable to the highest levels observed on small islands. For this band, seafloor stations are realistic alternatives when island sites are not available.

Seven year averages of the ambient noise levels recorded by Seismic Research Observatory (SRO) stations on three islands (Guam [GUMO], Taiwan [TATO] and New Zealand's north island [SNZO]) are compared to those recorded by the International Deployment of Accelerometers (IDA) station on Easter Island and on and beneath the ocean floor by Ocean Bottom Seismometers (OBS's) and the Marine Seismic System (MSS) deployed in a south Pacific DSDP drill hole at 23.8 ^{o} S., 165.5 ^{o} W (Adair et al,1986). From 0.3 to 2 Hz the SRO displacement power levels fall in the range historically observed by the Scripps' OBS's (decreasing at 70 dB/decade from 1 x 10^{6} nm^2/Hz at 0.3 Hz to 1 nm^2/Hz at 2 Hz) and are 10 to 15 dB above MSS levels. Above 2 Hz it appears that the same ratios hold (the SRO power levels decrease at 70 dB/decade to 1 x 10^{-3} nm^2/Hz at a frequency of 10 Hz), although this correlation is based on very limited, high gain, short period data. At frequencies below 0.3 Hz the SRO noise levels peak and decrease to approximately 2 x 10^{3} nm^2/Hz at 40 mHz. The noise levels recorded at Easter Island are somewhat higher (decreasing at 70 dB/decade from 1 x 10^{7} nm^2/Hz at 0.2 Hz to 1 nm^2/Hz at 10 Hz and to 1 x 10^{5} nm^2/Hz at 50 mHz). At the microseism peak near 0.2 Hz the MSS levels are from 15 to 20 dB higher than observed by the SRO stations and equivalent to those recorded at Easter Island. There appears to be little dependence of the variance in noise level estimates on frequency. The upper 95% confidence limit generally lies 10 dB above the average noise levels for all island stations.

All island noise level curves are dominated by the broad double frequency microseism peak centered between 0.15 to 0.2 Hz. The single frequency peak ranges from absent (Easter Island) to discernable (Guam and New Zealand) to obvious (at Taiwan). The center frequency of this peak ranges from 0.07 Hz at Guam and New Zealand to 0.1 Hz at Taiwan. We speculate that the increased amplitude and frequency of the single frequency microseism peak is due to

the interaction between the shallow continental shelf and surface gravity waves and/or the presence of Taiwan in a region of limited fetch.

INTRODUCTION

For the past 30 years, seismologists have deployed seismometers on and beneath the sea floor. The primary motivation for this work has been the desire to understand ocean crustal/lithospheric structure and seismicity. In addition, however, a long range goal of this research has been to use these instruments to improve the global coverage of seismometers. To demonstrate the feasibility of long term ocean bottom deployments it must be shown that noise levels at the seafloor are not significantly higher than those commonly observed on land.

This study is intended to assess the noise level change, if any, that can be expected by moving seismic sensors away from land. Toward this end this paper compares ambient noise levels on four islands with those at and below the sea-floor. In addition, the island noise level estimates are based on several noise observations spanning a number of years so that an estimate of the long term variance of these levels due to changing meterological and cultural conditions as a function of frequency will be obtained. The locations and relative magnitudes of the microseism peaks in the island spectra will also be discussed.

THE DATA

The SRO data used in this study were taken from day tapes of stations deployed on Guam, Taiwan and the north island of New Zealand, (GUMO, TATO and SNZO respectively, see table 1). Short and long period SRO data (with sampling rates of 20 and 1 sample per second respectively) have been merged to provide power estimates over the range from 40 mHz to 10 Hz. Only the vertical component data were studied since no horizontal short period SRO data are collected by the stations. Each power estimate is based on averaging 10 separate samples taken at random from 4 to 7 year time spans between 1976 and 1983 so that a wide range of meteorological conditions were incorporated. Prior to averaging, each trace was smoothed so that the final variance estimate would be largely due to changing meteorological conditions only.

Short period data are available only on event triggered records which are relatively infrequent. Each time series was examined on a visual display before transforming to ensure that data corresponding to seismic arrivals were eliminated. Each long and short period sample consisted of 853 points padded to 1024 points with zeros. The time series were demeaned and then tapered with a Hanning window prior to Fourier transformation. The SRO seismometers are equipped with a notch filter centered at roughly 0.17 Hz which is designed to reduce the effect of the microseismic noise on the long period channels. This notch causes a sharp peak in the power spectrum following a correction for the instrument response. Since this peak is unlikely to be a real feature of the data, the portion of the power spectra between .15 and .19 Hz was removed and the plotted levels were obtained by interpolation. The power levels in this frequency band are clearly not valid and should be ignored. For a discussion of SRO instrumentation the reader is referred to Peterson et al (1976).

The IRIS/IDA data were collected by the vertical component of the Streckeisen seismometers deployed on Easter Island (station RPN, see table 1). These data were treated in the same manner as the SRO data although only 9 intermediate period (5 samples/s) and 4 short period (20 samples/s) samples, taken from June, 1987 to March, 1988, were included in the final noise level estimate. For a discussion of the instrument refer to Wielandt and Streckeisen (1982).

The MSS data were collected in February of 1983 during Scripps' Ngendei Expedition and the noise analysis was originally published by Adair et al (1986). The MSS was deployed at 23.8^{o} S, 165.5^{o} W in DSDP drill hole 595b (leg 91), 124 meters below the sediment-water interface and 54 meters into the basement. The MSS data were obtained from short (40 samples/s) and mid-period (4 samples/s) channels with time series which were roughly 13 and 128 seconds long respectively. To reduce the variance, the short and mid-period curves are based on the average of 10 spectra. The OBS noise level bounds were computed from 25 noise level estimates obtained from data collected at locations and dates detailed in table 2. Each individual estimate was made after stacking from 3 to 125 noise level curves although the individual time series collected were too short to obtain high resolution at frequencies approaching 0.2 Hz. Both MSS and OBS power estimates have been corrected for instrument

response. The MSS and OBS instruments are discussed in detail in Adair et al (1986) and Orcutt et al (1987).

COMPARISON OF NOISE LEVELS

The four island stations exhibit similar time-averaged noise structure (figures 1,2,3 and 4). All records are dominated by the double frequency microseism peak centered between 0.15 and 0.2 Hz. The single frequency peak ranges from absent (Easter Island) to discernable (Guam and New Zealand) to obvious (at Taiwan). The center frequency of this peak ranges from 0.07 Hz at Guam and New Zealand to 0.1 Hz at Taiwan. At frequencies above the main microseism peak, all four spectra fall off at roughly 70 dB/decade. In all spectra the rate of decay decreases at frequencies above 2 Hz and the SRO station power levels actually increase above 5 Hz. It is felt that this apparent "levelling off" of the power spectra is not a real feature of the data but is due to digitization and instrumentation noise. The three SRO stations used in this report were selected because they are located on islands and thus are close to the shoreline. To combat the resultant high noise levels, the SRO short period station gains were reduced to a level 60 dB lower than those of all other SRO stations, (Peterson et al,1980). As a result, these records are more susceptible to digitization and instrumentation noise at high frequencies. In the early days of 1976 at GUMO, however, the short period data were collected with high gain. The spectrum from 12 January 1976 is shown in figure 5. At frequencies above 2 Hz the power spectral levels continue to decay at roughly 70 dB/decade. This spectrum is clearly more representative of the true power level in this frequency band. Because the average long term power levels at all stations were desired it was obviously not possible to base the average power level estimates solely on these high gain data.

At frequencies above 0.2 to 0.3 Hz the island power levels fall within the OBS noise level bounds and are 10 to 15 dB above MSS levels. At frequencies below 0.2 Hz the MSS levels are comparable to those recorded at Easter Island and 10 to 15 dB above noise levels recorded on the 3 SRO islands. This enhanced island noise level is probably a reflection of the oceanic origin of the microseisms. The upper 95% confidence limit, lying two standard deviations above the average, is plotted on figures 1 to 4 with the average power level curve. The

lower confidence limit was excluded since it was negative in places. These curves track each other fairly well and indicate that each frequency band has approximately the same variance.

THE ISLAND MICROSEISM PEAKS

The traditional explanation of the origin of the double frequency microseism peak involves the non-linear interference of gravity waves traveling in opposite directions, Longuet-Higgins (1950). In deep water this non-linear interaction is effective in producing acoustic energy at twice the frequency of the interacting gravity waves. This acoustic energy subsequently excites microseismic activity in the basement rock at the same frequency. The explanation of the single frequency microseism peak is fundamentally different. Early observations of this peak were made by Wiechert (1904), Oliver and Ewing (1957) and Haubrich et al (1963). The generally accepted explanation holds that when surface gravity waves propagate through shallow water the decaying pressure oscillations they cause are "felt" directly by the substrate. These pressure oscillations thus excite seismic energy at the same frequency as the source surface gravity waves. A generally accepted rule of thumb holds that this interaction is significant when the water depth is less than 60% of the wavelength of the surface gravity waves. The pressure fluctuations caused by such a wave on the bottom is greater than 4.6% of the static water pressure. At 0.07 Hz a typical wavelength is on the order of 350 m. This crude calculation suggests that in water shallower than about 200 m, single frequency microseisms can be excited.

Adair (1985) discussed previous continental microseismic studies which have generally detected the small, single frequency microseism peak at 0.07 Hz and the larger amplitude, double frequency, peak at 0.14 Hz. The single frequency microseism peaks in the GUMO and SNZO spectra agree with each other and conform to these continental studies. However, at TATO the fundamental microseism peak is more apparent and both peaks are shifted to higher frequencies (0.1 and 0.2 Hz). The single frequency peak is absent from the Easter Island data.

Plausible explanations for these differences may be found by considering the bathymetric and geographic settings of the four islands. Taiwan is located on the continental shelf of China and is 150 km from the mainland. There is a broad expanse of water less than 200 m deep in the vicinity of this island (the shallowest water, generally less than 100 m deep, lies to the north and west). The north island of New Zealand, Guam and Easter Island, however, are located far from major land masses. The local water depths increase rapidly away from the shore to greater than 200 m so that the generative area for primary microseisms is small (relative to Taiwan). This is especially true at Guam and Easter Island. It seems likely that the increased amplitude of the primary microseismic peak at TATO relative to GUMO, SNZO and especially RPN is due to the broad expanse of shallow water surrounding Taiwan which facilitates the direct conversion of gravity wave pressure fluctuations to seismic energy in the basement.

Hasselmann and Collins (1967) discussed the influence of shallow water on the frequency content of surface gravity waves. As these waves travel in shallow water, the long period components that interact directly with the sea floor are preferentially dissipated. In the vicinity of Taiwan where the surface gravity waves most likely have traveled a great distance over the shallow basement before approaching the island it seems that this mechanism would strip away the low frequencies preferentially and cause the apparent shift of the single frequency microseism peak to a slightly higher frequency.

It is widely known that the frequency (f_m) of the main energy peak in the spectrum of surface gravity waves depends on the fetch and the local wind speed (commonly represented by U_{10}, the velocity of wind 10 meters above the sea surface). Hasselmann et al (1973) found that f_m was proportional to $(U_{10})^{-.34}$ in the North Sea, a region of limited fetch. In theory f_m is proportional to $(U_{10})^{-1.0}$ in unlimited fetch. The waves grow until the phase velocity, which is inversely proportional to the frequency, equals that of the wind. The proximity of Taiwan to mainland China restricts the local wind fetch and thus could plausibly explain the increased frequency of the single frequency microseism peak. The dependence of f_m on the wind speed itself could provide an alternative explanation for the shift in Taiwan's single frequency microseism peak provided that the long term average wind speed was

significantly lower in the vicinity of Taiwan than near the other islands. However, wind speed data published by the U.S. Naval Weather Service indicate little difference between the average scalar wind speeds at these locations. At Taiwan, Guam, New Zealand and Easter Island the average wind speeds are 14.0, 12.7, 14.5 and 13.0 knots.

CONCLUSION

We have computed and compared estimates of noise levels on four islands, on the seafloor and beneath the seafloor. Over a limited frequency band the ocean bottom and island power levels are comparable and thus no degradation of the signal to noise ratio should be expected by moving sensors from land to the seafloor. We have shown that over this frequency band a sensor located beneath the ocean bottom will display significantly lower noise levels than seismometers deployed on the ocean bottom or on islands. This is true except at the lowest frequencies (below 0.2 Hz). These observations are particularly encouraging with regard to sea floor stations over the bulk of the Pacific and Indian oceans where few islands are available for station siting.

It seems plausible that the increased amplitude and frequency of the single frequency microseismic peak in the TATO record relative to GUMO, SNZO and RPN is due to the interaction between the shallow continental shelf surrounding Taiwan and surface gravity waves and/or the presence of Taiwan in a region of limited fetch.

ACKNOWLEDGMENTS

We would like to express our appreciation to Jean Francois Fels for providing us with the IRIS/IDA Easter Island data and to Spahr Webb and Chip Cox for their useful comments.

REFERENCES

Adair, R.G., 1985, Microseisms in the Deep Ocean: Observations and Theory, Ph.D. thesis, 166 pp., Univ. of Calif., San Diego, La Jolla, CA.

Adair, R.G., Orcutt, J.A., Jordan, T.H., 1986, Preliminary Analysis of Ocean-Bottom and Sub-Bottom Microseismic Noise during the Ngendei Experiment, Init. Repts. of DSDP, 88/91, 357-375.

Hasselmann, K., Barnett, T. P., Bouws, E., Carlson, H., Cartwright, D. E., Enke, K., Weing, J. A., Gienapp, H., Hasselmann, D. E., Kruseman, P., Meerburg, A., Muller, P., Olbers, D. J., Richter, K., Sell, W., Walden, H., 1973, Measurement of wind-wave growth and swell decay during the Joint North Sea Wave Project (JONSWAP). Erganzungsheft zur Deutschen Hydrographischen Zeitschrift Reine A (8^{o}) (12), 122 pp.

Hasselmann, K., Collins, J.I., 1967, Spectral Dissipation of Finite-depth Gravity Waves Due to Turbulent Bottom Friction, Journal of Marine Research, 26, 1-12.

Haubrich, R.A., Munk, W.H., Snodgrass, F.E., 1963, Comparative Spectra of Microseisms and Swell, Bull. Seism. Soc. Am., 53, 27-37.

Longuet-Higgins, M.S., 1950, A theory of the origin of microseisms., Phil. Trans. Roy. Soc., A., 243, 1-35.

Oliver, J., Ewing, M., 1957, Microseisms in the 11 to 18 second period range, Bull. Seism. Soc. Am., 47, 111-127.

Orcutt, J.A., Moore, R.D., Jordan, T.H., 1987, Description and Performance of the Scripps Ocean Bottom Seismographs during the Ngendei Experiment, Initial Reports of the Deep Sea Drilling Project, 88/91, 347-356.

Peterson, J., Butler, H.M., Holcomb, L.G., Hutt, C.R., 1976, The Seismic Research Observatory, Bull. Seism. Soc. Am., 66, 2049-2068.

Peterson, J., Gutt, C.R., Holcomb, LG., 1980, Calibration of the Seismic Research Observatory, United States Dept. of the Interior Geological Survey Open-File report 80-187.

U.S. Navy Marine Climatic Atlas of the World, Vols 2 and 5, Naval Weather Service Detachment, Asheville N.C.

Wiechert, E., 1904, Verhandlungen der Zweiten Internationalen Seismologischen Kouferenz. Gerl. Geitr. Geophyus., Ergänzungsbd., 2, 41-43.

Wielandt, E. and Streckeisen, G., 1982, The Leaf-Spring Seismometer: Design and Performance, Bull. Seism. Soc. of Am., 72, 2349-2367.

TABLE AND FIGURE CAPTIONS

Table 1. The geographic coordinates of the four island-based seismometers incorporated in this study. The areas of the islands on which these seismometers are deployed are included.

Table 2. The geographic coordinates and dates at which the OBS noise samples used in this study were collected.

Figure 1. Noise power spectral density in displacement units for the SRO station on Guam. The lower solid curve is the average noise level obtained from seven years of data while the upper curve is a 95% confidence limit on the power. The frequently dashed curve is the power spectral density from the Marine Seismic System deployed during the southwest Pacific Ngendei Expedition. The broadly dashed bounds represent upper and lower limits of noise levels observed by the Scripps' OBSs over a twelve year period in the Pacific Basin.

Figure 2. Noise power spectral density in displacement units for the SRO station on the north island of New Zealand. The other curves are explained in the caption for Figure 1.

Figure 3. Noise power spectral density in displacement units for the SRO station on Taiwan. The other curves are explained in the caption for Figure 1.

Figure 4. Noise power spectral density in displacement units for the IRIS/IDA station on Easter Island. The other curves are explained in the caption for Figure 1.

Figure 5. Power spectral levels in displacement units for GUMO for records in 1976 when the SRO station was operating at higher gain. The other curves are explained in the caption for Figure 1. Note that the noise levels continue to decay at higher frequencies indicating that the higher noise levels observed at this and the other island stations are probably associated with digitization noise.

Table 1 Island Data

SITE	LATITUDE	LONGITUDE	ISLAND AREA (Square Km)
GUMO	13° 35' 17" N	144° 51' 58" W	541
SNZO	41° 18' 36" S	174° 42' 16" W	115,000
TATO	24° 58' 32" N	121° 29' 18" W	36,000
RPN	27° 08' 37" S	109° 26' 10" W	118

Table 2 OBS data

NUMBER OF SAMPLES	LATITUDE	LONGITUDE	DATE
6	41° 30' N	127° 20' W	JUN 1976
2	16° 0' N	145° 0' W	OCT 1977
1	29° 30' N	122° 0' W	OCT 1977
3	18° 0' N	145° 20' W	JAN 1976
8	16° 30' N	100° 30' W	JUN 1977
4	20° 50' N	109° 6' W	APR 1979
1	23° 48' S	165° 30' W	FEB 1983

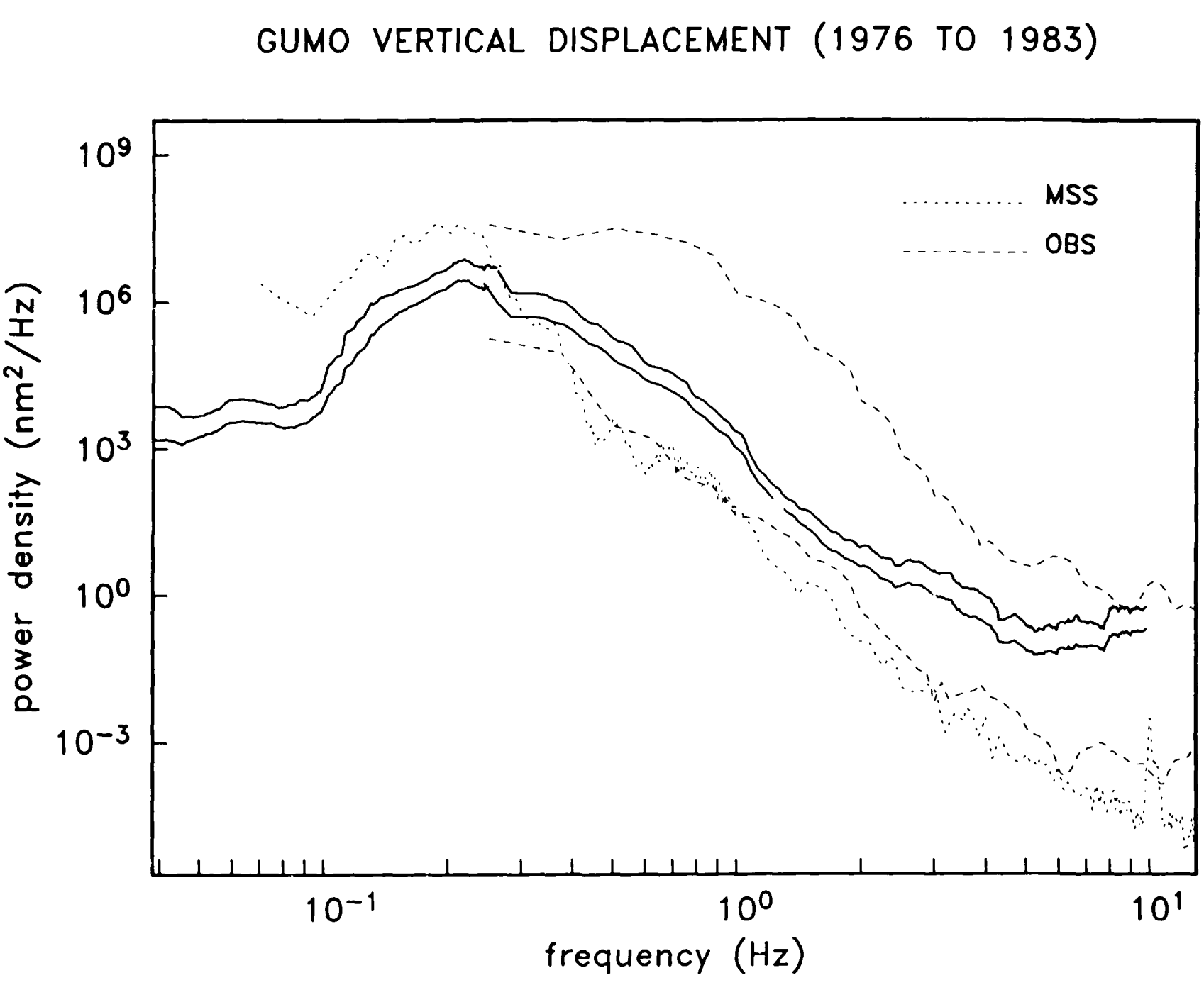
GUMO VERTICAL DISPLACEMENT (1976 TO 1983)
MSS
OBS
power density (nm²/Hz)
10⁹
10⁶
10³
10⁰
10⁻³
10⁻¹
10⁰
10¹
frequency (Hz)

Figure 1

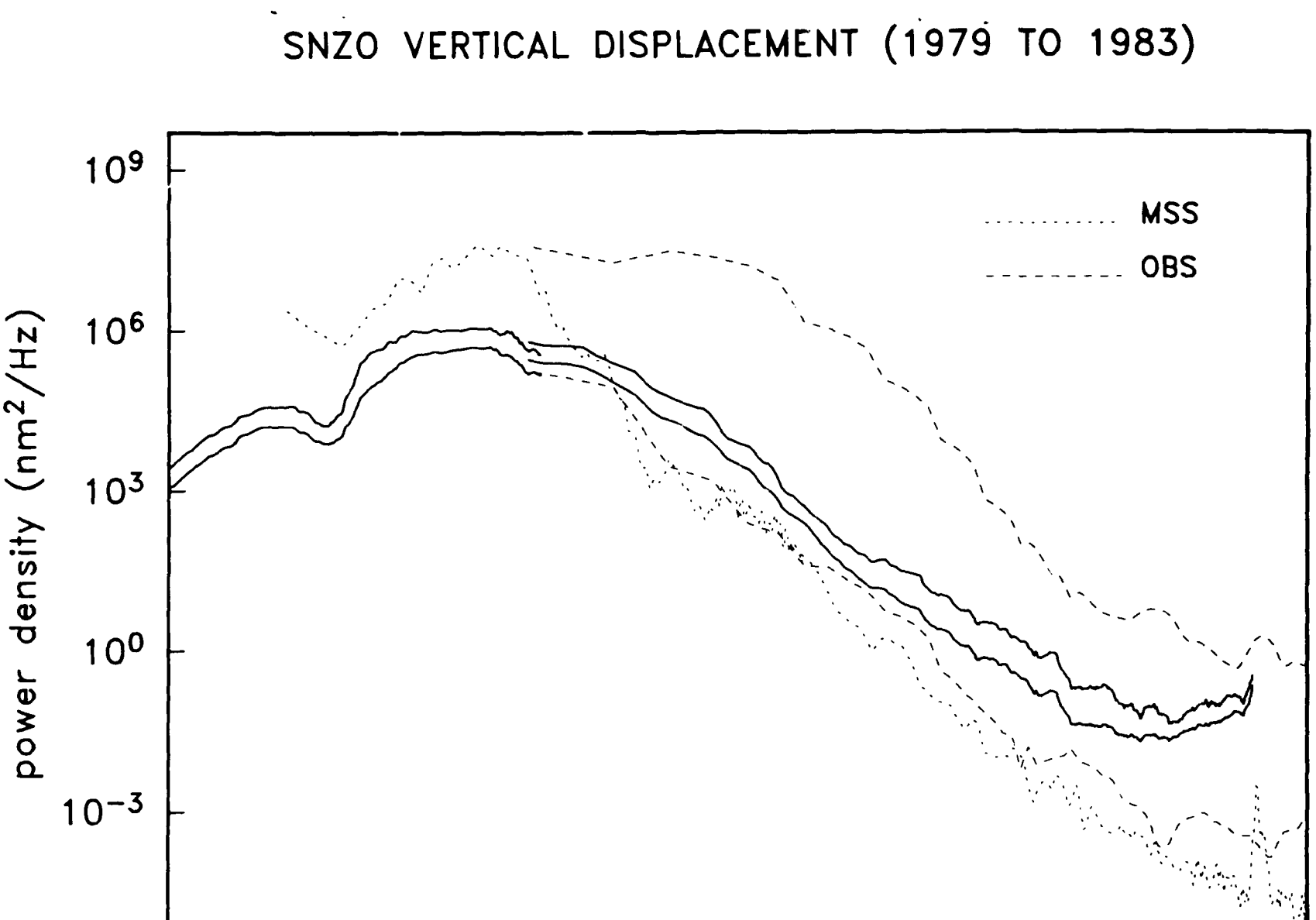
SNZO VERTICAL DISPLACEMENT (1979 TO 1983)
MSS
OBS
power density (nm²/Hz)
10⁹
10⁶
10³
10⁰
10⁻³
10⁻¹
10⁰
10¹
frequency (Hz)

Figure 2

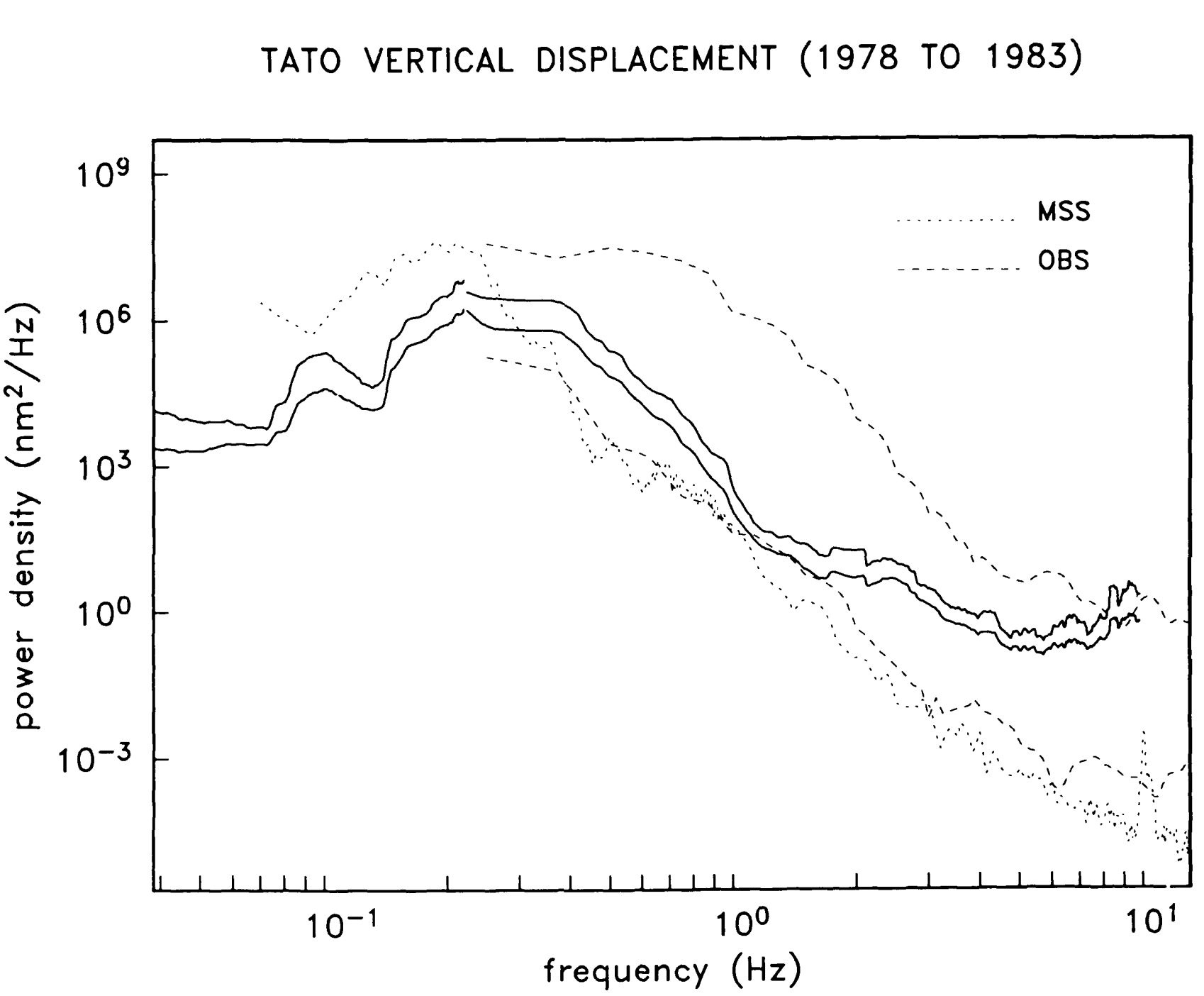
TATO VERTICAL DISPLACEMENT (1978 TO 1983)
MSS
OBS
power density (nm²/Hz)
10⁹
10⁶
10³
10⁰
10⁻³
10⁻¹
10⁰
10¹
frequency (Hz)

Figure 3

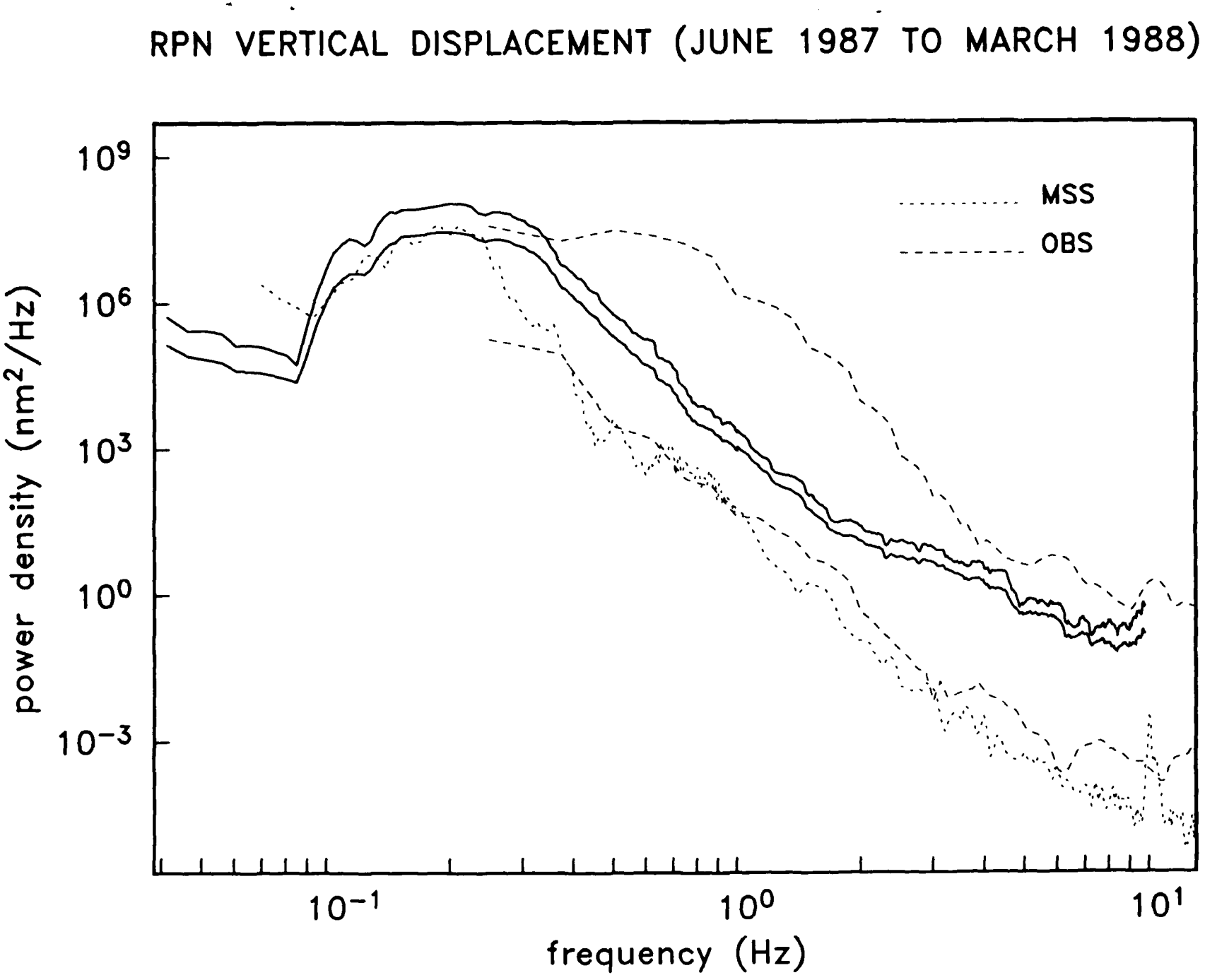
RPN VERTICAL DISPLACEMENT (JUNE 1987 TO MARCH 1988)
MSS
OBS
power density (nm²/Hz)
10⁹
10⁶
10³
10⁰
10⁻³
10⁻¹
10⁰
10¹
frequency (Hz)

Figure 4

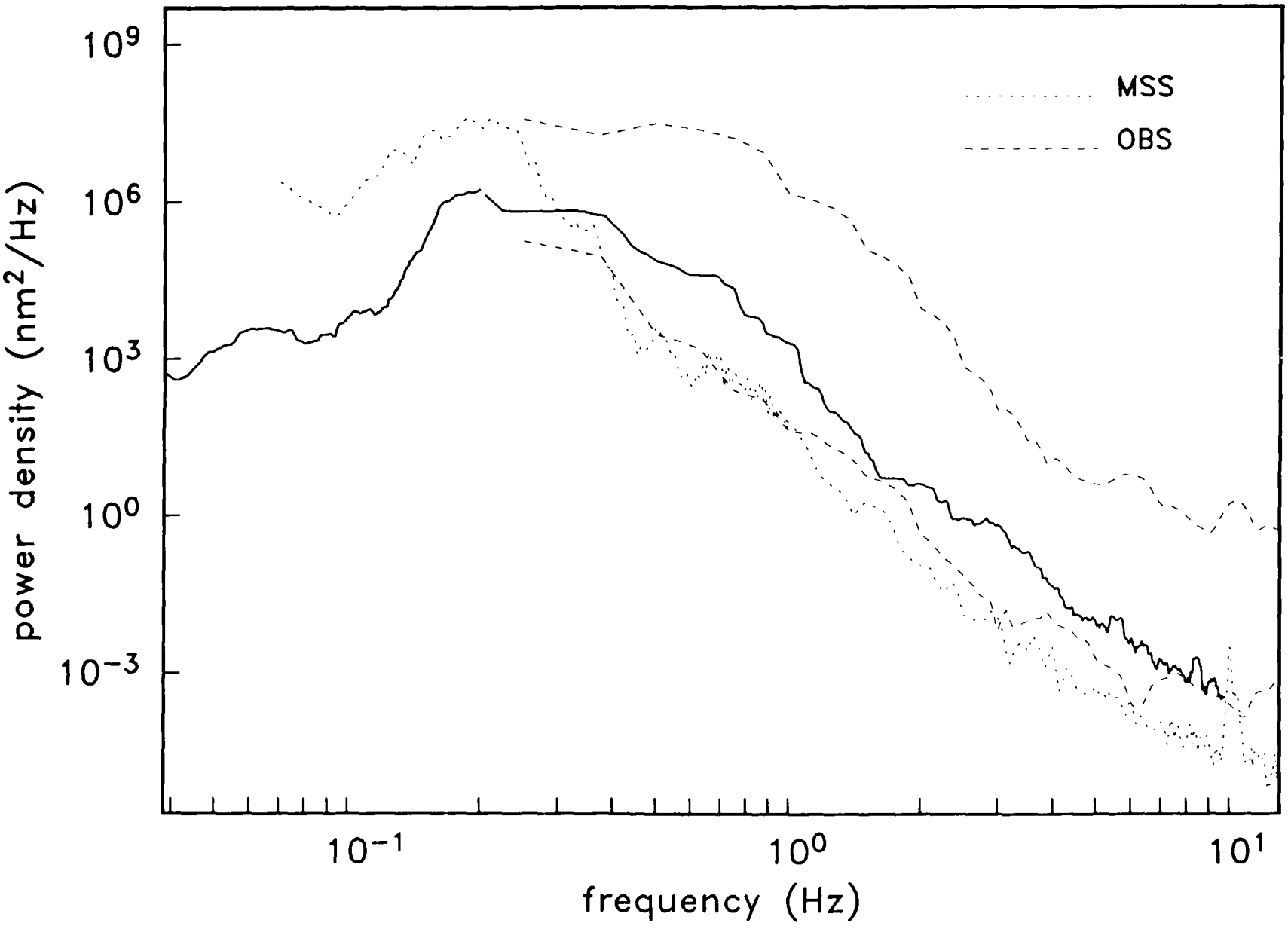
GUMO VERTICAL DISPLACEMENT JANUARY 12, 1976
MSS
OBS
power density (nm²/Hz)
10⁹
10⁶
10³
10⁰
10⁻³
10⁻¹
10⁰
10¹
frequency (Hz)

Figure 5

CHAPTER 2

SEISMIC BROADBAND SIGNAL AND NOISE LEVELS ON AND WITHIN THE SEAFLOOR AND ON ISLANDS.

Michael A.H. Hedlin

Jean-Francois Fels

Jonathan Berger

John A. Orcutt

Dalia Lahav

Institute of Geophysics and Planetary Physics (A-025)

Scripps Institution of Oceanography, La Jolla CA, 92093

Published in the Proceedings of a Workshop on Broad-Band Downhole Seismometers in the Deep Ocean, W.H.O.I., Woods Hole, MA, April 26-28, 1988.

ABSTRACT

Ambient noise levels recorded on and beneath the seafloor are compared with the signal levels expected at an epicentral range of 30° from events ranging in M_W from 5.0 to 9.5. The results indicate that at this range events with M_W as low as 5.5 should be detectable by sensors on the seafloor in the Pacific. Because of lower ambient noise levels present in the Atlantic and beneath the seafloor in the Pacific, events with M_W as low as 5.0 should be detectable in these locations.

Noise level data collected by three land-based IDA/IRIS sensors (RPN, ESK and PFO) ranging in distance from 1 to 100 km from the shoreline are compared. Low frequency noise levels (below 50 mHz) are not sensitive to this distance although at frequencies above 50 mHz noise levels are clearly inversely proportional to the distance from the shoreline. At 250 mHz noise power spectral levels drop 40 dB as the observation point varies from 1 to 100 km from the coast.

INTRODUCTION

It is obvious that the global coverage which land based seismometers provide is limited since 71% of the Earth's surface is covered by water. A much more uniform coverage is feasible if instruments can be deployed on the seafloor in environments with signal-to-noise ratios comparable to those available on land. Many technical deployment problems have been overcome during the past 30 years as seismologists have deployed seismometers on and beneath the sea floor. A previous paper (Hedlin and Orcutt, 1989) has already dealt with the question of the relative noise levels on land and the seafloor. It was concluded that over the frequency band from 40 mHz to 10 Hz the ocean bottom and island noise levels are comparable. In this paper we look more deeply into the acceptability of seafloor noise levels by comparing them with signal levels expected from earthquakes of varying sizes at an epicentral range of 30°.

Although seafloor sites could potentially provide a uniform global coverage, island seismic stations still play an important role in the global seismographic network since they provide a means for deploying sensors in oceans relatively inexpensively and with relative ease. In this paper we will also examine the dependence of island and continental noise levels on the distance from the shoreline.

THE DATA

The sub-seafloor noise level data were collected by the Marine Seismic System (MSS) in February of 1983 during the Scripps' Ngendei Expedition and the noise analysis was originally published by Adair et al (1986). The MSS was deployed at 23.8° S, 165.5° W in DSDP drill hole 595b (leg 91), 124 meters below the sediment-water interface and 54 meters into the basement. The MSS data were obtained from short (40 samples/s) and mid-period (4 samples/s) channels with time series which were roughly 13 and 128 seconds long respectively. To reduce the variance of the power spectral estimates, the short and mid-period curves are based on the average of 10 spectra. The Ocean Bottom Seismometer (OBS) noise level bounds were computed from 25 noise level estimates obtained from data collected at the locations and dates detailed

in table 1. Each individual estimate was made after stacking from 3 to 125 noise level curves although the individual time series collected were too short to obtain high resolution at frequencies approaching 0.2 Hz. Both MSS and OBS power estimates have been corrected for instrument response. The MSS and OBS instruments are discussed in detail in Adair et al (1986) and Orcutt et al (1987).

The data for the high-frequency seafloor pressure spectra were collected on two separate occasions. The Pacific data were collected in May 1988 during the Scripps' Nachos Expedition 350 km west of San Diego in 3850 m of water. A low frequency hydrophone (Cox et al, 1984) mounted on the side of an OBS was sampling at 32 samples/s and the recorder collected 15 minute records. The 28,800 point time series were divided into 30% overlapping 8192 point windows. Each series was Hanning tapered prior to Fourier transformation and then corrected for the instrument response. The final spectral estimate was obtained from a stack of the resulting spectra. The Atlantic seafloor pressure spectrum was computed from data collected by the Woods Hole Oceanographic Institution during the HEBBLE expedition in October of 1985. The HEBBLE pressure data were collected by a long period transducer (Cox et al, 1984) deployed at 4820 m depth over the Nova Scotia Rise. The hydrophone data were sampled at one sample/s during 6 hr time periods each day. To compute the power spectral estimate, the data were treated in a similar manner as the Atlantic high frequency data, the only difference being that 4π prolate windows, rather than Hanning windows, were used to taper each sub-sequence.

The land-based data were collected exclusively at IDA/IRIS stations. Low (1 sample/s) and high frequency (20 samples/s) spectral estimates have been merged to provide the broadband spectra in figure 3. Each spectrum is the result of stacking, in the frequency domain, several spectral estimates calculated from distinct portions of the original noise sample. The very low frequency seafloor pressure data were obtained from figure 6 of Filloux (1980).

COMPARISON OF SEAFLOOR SIGNAL AND NOISE LEVELS

Figure 1 illustrates three seafloor pressure power spectra spanning the band from 0.7 μHz to 20 Hz. The solid and finely-dashed curves represent data collected in the Pacific while the data for the lower power, coarsely-dashed curve were collected in the Atlantic. Power spectral levels in the lowest band, from 0.7 μHz to 20 mHz, decrease monotonically at 25 dB/decade except in the band from 10 to 200 μHz where several tidal lines are recorded. The microseism band in both spectra is dominated by the double frequency microseism peaks above 200 mHz. Between the microseism peaks and 2 Hz, power spectral levels decrease at 40 dB/decade.

In figure 2 the high-frequency data in Figure 1 have been converted to acceleration units and superimposed on curves which illustrate the acceleration expected at an epicentral range of 30° from earthquakes spanning a range of magnitudes. OBS and MSS data have been plotted as well. The conversion from pressure to amplitude was made using a simple acoustic plane wave relationship assuming vertical incidence of seismic energy and continuity of vertical traction and displacement. Although the validity of this conversion is clearly restricted, we expect that the predicted accelerations are probably realistic estimates. The validity of the noise levels can only be verified through experimentation. This figure is very encouraging and indicates that with the exception of the noisiest OBS sites all events with M_W of 5.5 or greater lead to motions above the expected noise levels at a range of 30°. Such earthquakes or explosions should be detectable with seafloor sensors. Using hydrophones deployed in the Atlantic and the MSS buried in the substrate beneath the Pacific, where ambient noise levels appear to be somewhat lower, earthquakes with M_W as low as 5.0 should be detectable at a range of 30°. This conclusion is consistent with the results of Orcutt and Jordan (1985). Using data collected by the MSS during the Ngendei Expedition they found that no events with m_b less than 5.1 were detected at ranges greater than 30°. At lesser distances, where high frequency signals propagate through the high-Q lithospheric waveguide, they found that the detection threshold was far lower. Shallow-focus events at distances on the order of 15° with m_b as low as 3.7 could be detected by the MSS. At the noisiest sites,

depending on the frequency band of interest, the smallest events detectable range in size from M_W of 6 to 8.

THE DEPENDENCE OF LAND-BASED NOISE LEVELS ON THE DISTANCE FROM THE SHORELINE

Figure 3 shows power spectra of noise data obtained from the IRIS/IDA seismographic stations on Easter Island (RPN), one km from the coastline, at Eskdalemuir (ESK), 40 km from the Irish Sea and at Piñon Flat (PFO), some 100 km from the California coast. The dashed lines show the level of minimum and maximum ambient noise at quiet continental locations. The high frequency portion of the spectrum for the RPN station was derived from data collected during the most noisy period experienced during a one-year period; it should be taken as representative of the maximum high frequency noise at an island site. The spectra demonstrate that for periods longer than the microseisms, there is only a small decrease in noise as distances to the coastline increase. Island stations should provide relatively low noise data in this frequency range. At frequencies higher than the microseisms, there is considerable reduction in noise as the distance from the coastline increases. At 250 mHz the noise levels drop 40 dB. Factors such as coastal shoaling, barrier reef coverage, and surf conditions can be expected to cause large variations in the ambient noise in this frequency range.

CONCLUSION

It appears that most locations on the seafloor are sufficiently quiet to permit the detection of moderate-sized earthquakes and explosions at teleseismic ranges. This result is particularly encouraging in view of the need for an increased uniformity of the global coverage of seismic sensors.

The acceptability of island sensor deployments depends on the frequency band of interest and on the distance of the sensor from the shoreline (and thus the size of the island). It appears that low frequency (below 50 mHz) noise levels are insensitive to the distance of the sensor from the shoreline. However, in high-frequency studies it appears that sites on large islands relatively far from the shoreline will have superior noise levels.

ACKNOWLEDGMENTS

We would like to express our appreciation to Spahr Webb for providing us with the Atlantic hydrophone data in advance of publication, and J. H. Filloux for the low-frequency Pacific data.

REFERENCES

Adair, R.G., Orcutt, J.A., Jordan, T.H., 1986, Preliminary Analysis of Ocean-Bottom and Sub-Bottom Microseismic Noise during the Ngendei Experiment, Init. Repts. of DSDP, 88/91, 357-375.

Cox, C.S., Deaton, T., Webb, S.C., 1984, A Deep Sea Differential Pressure Gauge, Journal of Atmospheric and Oceanic Technology, 1, 237-246.

Filoux, J.H., 1980, Pressure Fluctuations on the Open Ocean Floor Over a Broad Frequency Range: New Program and Early Results, Journal of Physical Oceanography, 10, 1959-1971.

Hedlin, M.A.H. and Orcutt, J.A., 1989, A Comparative Study of Island, Seafloor and Sub-Seafloor Ambient Noise Levels, Bulletin of the Seismological Society of America, 79, 172-179.

Orcutt, J.A. and Jordan, T.H., 1985, MSS and OBS data from the Ngendei Experiment in the Southwest Pacific, The Vela Program, A Twenty-Five Year Review of Basic Research, 758-770.

Orcutt, J.A., Moore, R.D., Jordan, T.H., 1987, Description and Performance of the Scripps Ocean Bottom Seismographs during the Ngendei Experiment, Initial Reports of the Deep Sea Drilling Project, 88/91, 347-356.

TABLE AND FIGURE CAPTIONS

Table 1. The geographic coordinates and dates at which the OBS noise samples used in this study were collected.

Figure 1. Noise power spectral density in pressure units for three seafloor sensors. The data for the solid and finely-dashed curves were collected in the Pacific Ocean, off the Coast of California (in 3850 m of water) and off the Gulf of California (at 3210 m depth) respectively. The data for the coarsely-dashed curve were collected in the Atlantic at the Nova Scotia Rise in 5000 m of water.

Figure 2. Acceleration amplitudes expected at an epicentral range of 30° from earthquakes ranging in Mw from 5.0 to 9.5. The data for the light-solid curve were collected in the Pacific Ocean, off the coast of California at 3850 m depth. The two heavy-solid curves represent the extreme noise level bounds detected at 25 sites in the Pacific (see table 1). The frequently dashed curve represents the noise level recorded by the Marine Seismic System deployed during the southwest Pacific Ngendei Expedition. The data for the infrequently dashed curve were collected in the Atlantic at the Nova Scotia Rise in 5000 m of water. The amplitudes plotted are 1.25 times the RMS values over 1/3 octave bandwidths.

Figure 3. Noise recordings made on an island (RPN-Easter Island) compared with measurements made on continental sites located near the ocean (ESK-Eskdalemuir; PFO-Piñon Flat (Observatory). Note that the high frequency content of the microseism noise decreased as the distance from the shore increases. The amplitude of the microseism peak also decreases in the same sense as the high frequencies.

Table 1 OBS data

NUMBER OF SAMPLES	LATITUDE	LONGITUDE	DATE
6	41° 30' N	127° 20' W	JUN 1976
2	16° 0' N	145° 0' W	OCT 1977
1	29° 30' N	122° 0' W	OCT 1977
3	18° 0' N	145° 20' W	JAN 1976
8	16° 30' N	100° 30' W	JUN 1977
4	20° 50' N	109° 6' W	APR 1979
1	23° 48' S	165° 30' W	FEB 1983

Figure 1

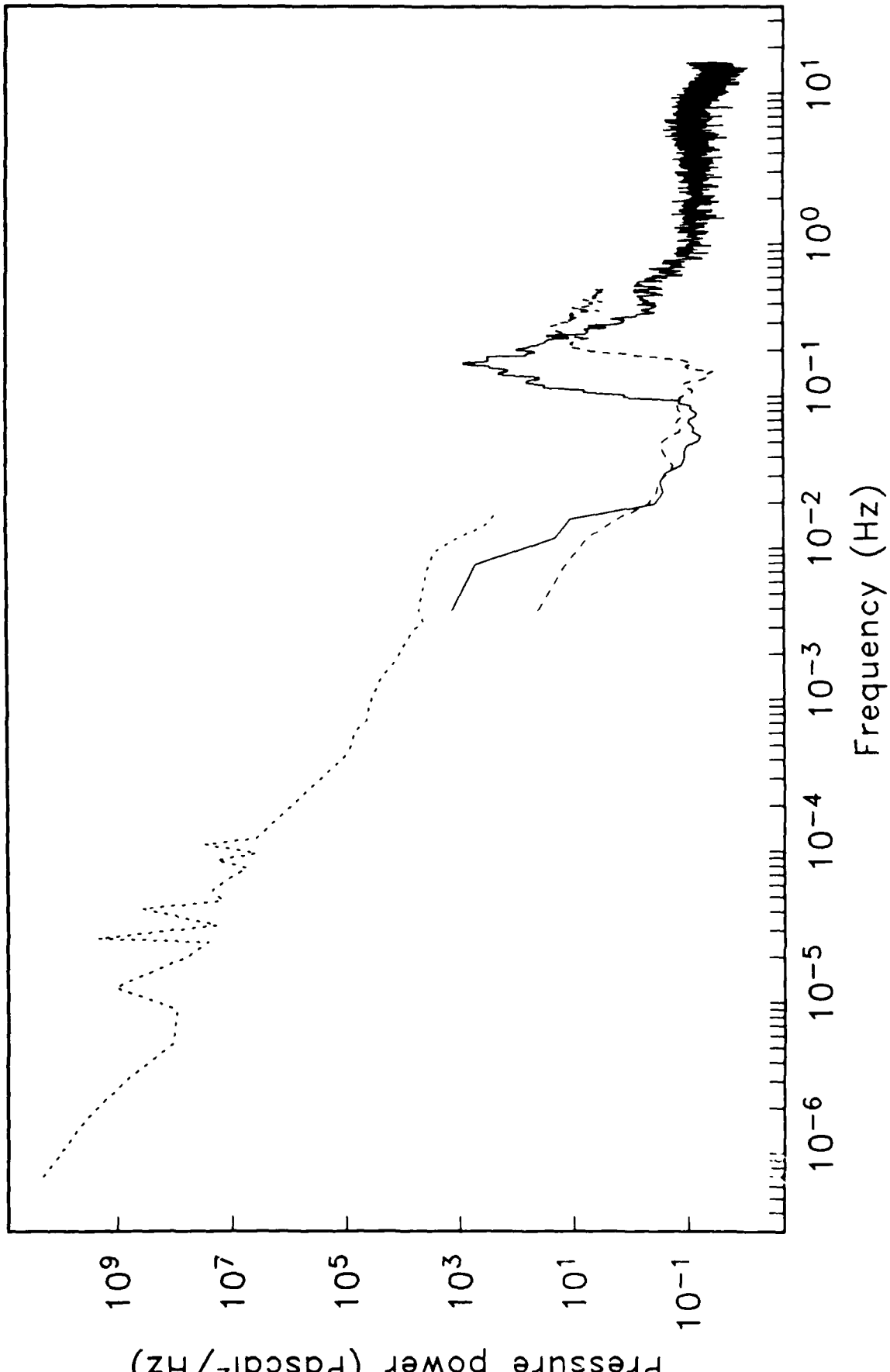
Pressure power (Pascal²/Hz)
10⁹
10⁷
10⁵
10³
10¹
10⁻¹
10⁻⁶
10⁻⁵
10⁻⁴
10⁻³
10⁻²
10⁻¹
10⁰
10¹
Frequency (Hz)

Figure 2

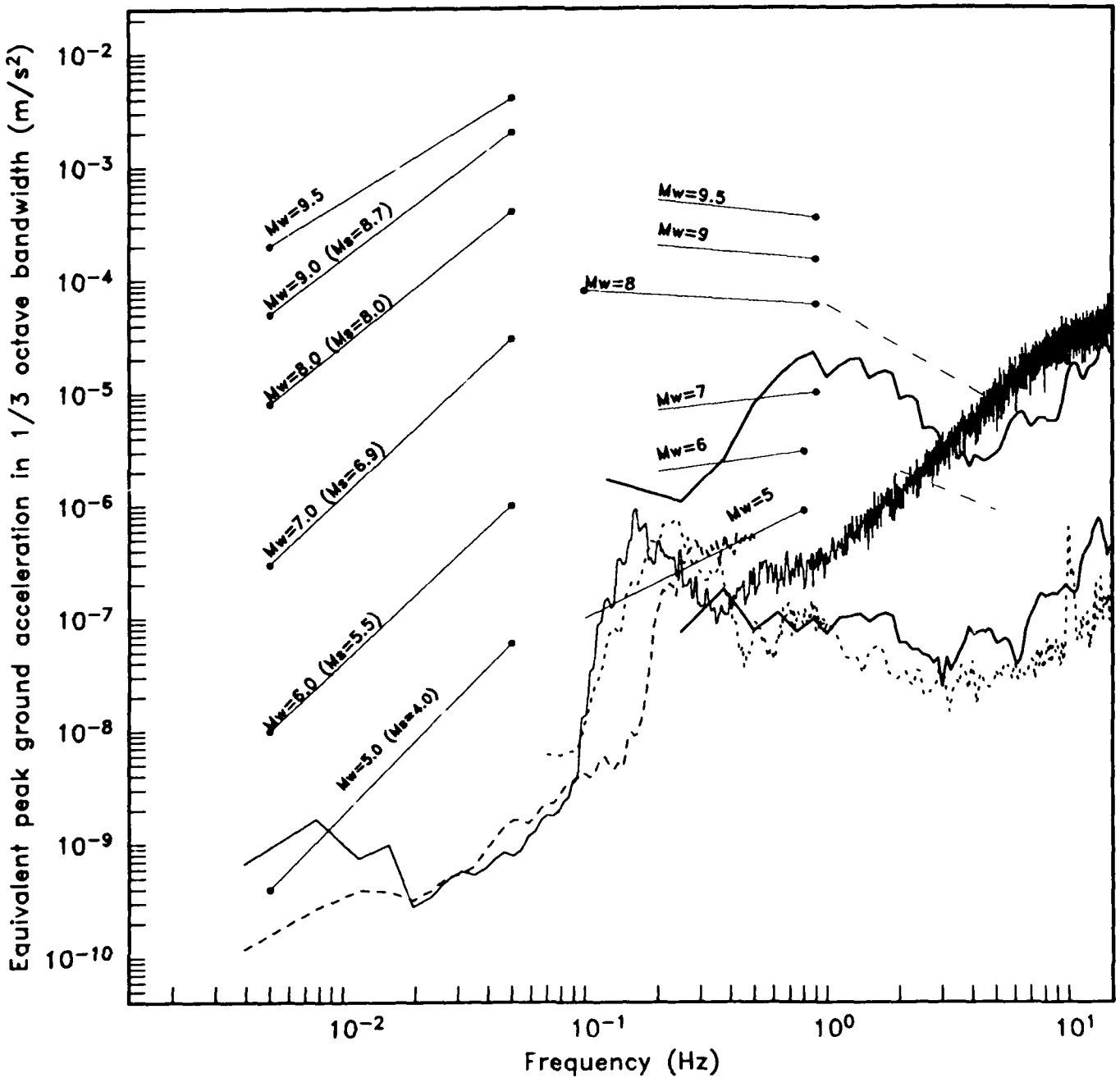
Equivalent peak ground acceleration in 1/3 octave bandwidth (m/s²)
10⁻²
10⁻³
10⁻⁴
10⁻⁵
10⁻⁶
10⁻⁷
10⁻⁸
10⁻⁹
10⁻¹⁰
Mw=9.5
Mw=9.0 (Ms=8.7)
Mw=8.0 (Ms=8.0)
Mw=7.0 (Ms=6.9)
Mw=6.0 (Ms=5.5)
Mw=5.0 (Ms=4.0)
Mw=9.5
Mw=9
Mw=8
Mw=7
Mw=6
Mw=5
10⁻²
10⁻¹
10⁰
10¹
Frequency (Hz)

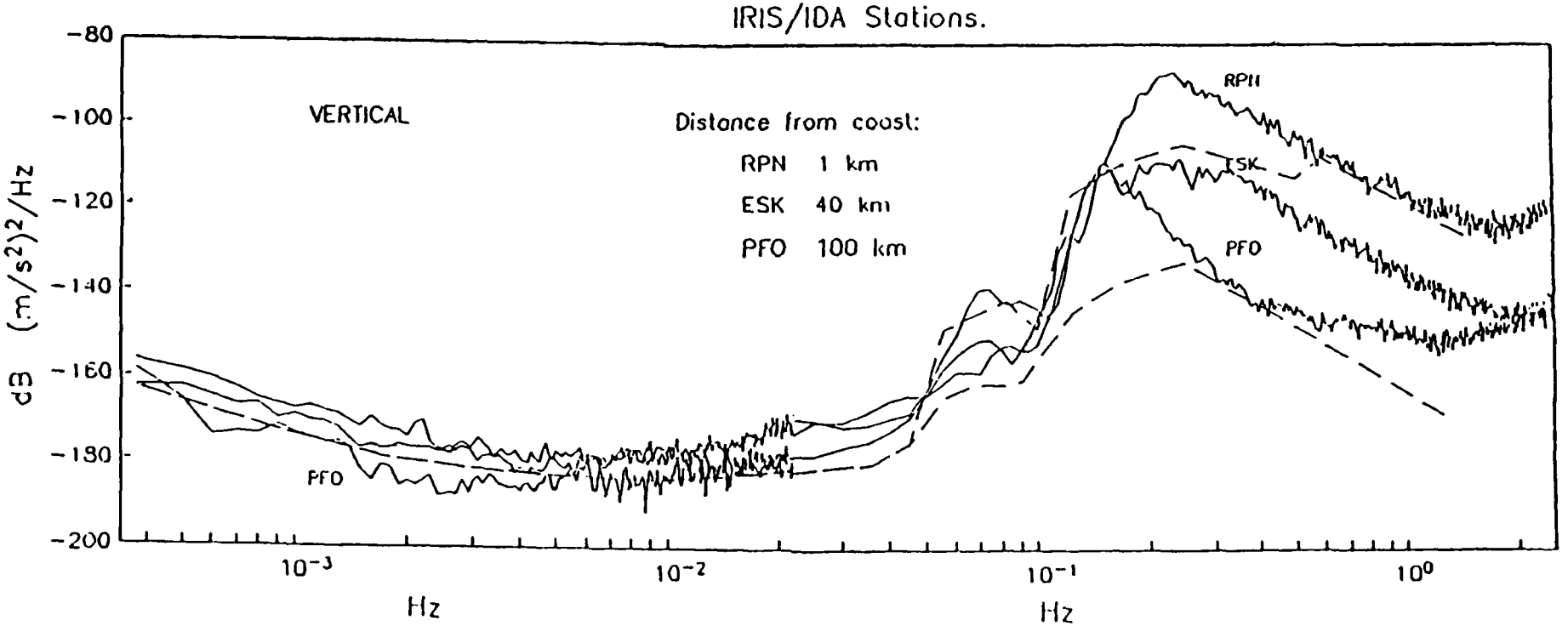
IRIS/IDA Stations.
VERTICAL
Distance from coast:
RPN 1 km
ESK 40 km
PFO 100 km
RPN
ESK
PFO
PFO
dB (m/s²)²/Hz
-80
-100
-120
-140
-160
-180
-200
10⁻³
10⁻²
10⁻¹
10⁰
Hz
Hz

Figure 3

CHAPTER 3

THE TIME-FREQUENCY CHARACTERISTICS OF QUARRY BLASTS AND CALIBRATION EXPLOSIONS RECORDED IN KAZAKHSTAN U.S.S.R.

Michael A. H. Hedlin

J. Bernard Minster

John A. Orcutt

Institute of Geophysics and Planetary Physics (A-025),

Scripps Institution of Oceanography,

University of California at San Diego, La Jolla CA 92093

accepted for publication in the Geophysical Journal

SUMMARY

In this paper we consider two fundamentally different processes that can be responsible for the organization of energy in seismic coda into discrete time-independent frequency bands. One process involves the resonance of energy in low velocity horizons and the other requires the interaction of time offset wavefields produced by sub-events within multiple-event mine explosions (ripple-fired quarry blasts).

We examined data collected by high frequency seismometers in Kazakhstan U.S.S.R. and observed regular time-independent spectral modulations in coda resulting from events strongly suspected to be Soviet quarry blasts, but not in the coda from single event calibration explosions detonated at similar ranges. We conclude these modulations are a source effect and due to ripple-firing. This modulation is independent of the source-receiver azimuth and we infer that the spatial array of sub-shots in each event must be small. We demonstrate that simple linear superposition theory can be used to reproduce effectively the spectral modulation observed in real quarry blasts.

On the basis of these observations we attempt to discriminate between the two types of events using a spectral pattern-based algorithm that seeks time-independent features. We consider the detrimental effect that resonant energy in low velocity horizons can have on the successful application of our algorithm.

INTRODUCTION

In theory any process that introduces a regular repetition into a seismic wavetrain will impress upon the spectrum of that energy a regularly spaced modulation. Superposed regular modulations were observed in spectra computed from Pn and Sn coda collected in the S.W. Pacific in 1983 during Scripps' Ngendei expedition. These were explained by Sereno and Orcutt (1985 a and b) as being due to the resonance of energy in the water and sedimentary columns near the receiver. This mechanism has provided an elegant alternative explanation to the scattering theory previously held by many as the dominant source of coda generation in the oceanic lithosphere.

We have recently observed very similar spectral modulation in data collected in the Soviet republic of Kazakhstan in 1987. This data set includes calibration events, where the source-time function is presumably relatively simple, and many other regional events, a large fraction of which are likely mine explosions. This unusual spectral modulation is only observed in the latter events and thus we suspect that it is not a propagation effect, as was the case in the Ngendei data set. For example, Baumgardt and Ziegler (1988) discuss a commonly used technique in mining known as ripple-firing. In this practice a number of sub-explosions are staggered in time and space to reduce ground motions in areas proximal to the mine as well as to enhance the fracturing of the rock. The most plausible explanation of the spectral modulation we observe in the Soviet data is that it is a source effect which stems from the highly repetitive nature of ripple-fired mine explosion source-time functions.

Although the physics behind these two types of modulations is fundamentally different, the effect they have on the spectra of the recorded energy is strikingly similar. We predict mathematically that both processes are capable of impressing a time-independent modulation on the spectra of seismic wavefields.

We feel the problem of discriminating ripple-fired mine explosions (quarry blasts) from underground nuclear explosions has become increasingly important and deserves close scrutiny. As discussed by Stump and Reamer (1988), a reduced Threshold Test Ban Treaty would bring the magnitude of the largest allowable nuclear explosions down to that of large "engineering"

explosions otherwise known as quarry blasts. The problem of discriminating quarry blasts from other events is not a new one, and has been investigated by several other authors. Aviles and Lee (1986) considered quarry blasts and earthquakes on the west coast of the United States and found they had success in discriminating between the two types of events by computing ratios of the spectral energy at 1.5 and 12 Hz. They found quarry blasts to be relatively deficient in high frequency energy and proposed a preferred attenuation of high frequency energy near the quarry blast source by near-surface fractures. Although this method may be valid in the western U.S. it seems that its success would be highly dependent on mining practice and the geology of the region in which the discriminant is being used. As we discuss later, the ratios of power in any two frequencies is highly dependent on the geometry and timing of the sub-shots in the quarry blast sequence.

Many authors have performed cepstral analyses of multiple source events. The cepstrum, which is the Fourier transform of the log of the spectrum (Tribolet, 1979), is sensitive to regular spectral modulation in the coda of multiple source events. Baumgardt and Ziegler (1988) showed that cepstra of ripple-fired sources display power highs at certain times dependent on the timing of the shots in the quarry blast sequence. A weakness of studies which employ the cepstrum for discrimination purposes is that simple events (earthquakes and single shot explosions) can possess significant cepstral structure. The cepstra computed by Baumgardt and Ziegler (1988) from the coda of some earthquakes illustrate this point. The problem of discrimination becomes somewhat arbitrary when it must be decided how much structure is sufficient to identify an event as a quarry blast.

Gupta et al (1984) attempted to discriminate between single and multiple-event explosions and earthquakes and explored several methods which were based on the expected differences between the distribution of energy in Pg and Lg phases at a variety of frequencies. The expected differences they discussed were mainly due to the proximity of explosions to the free surface and their omnidirectionality (resulting in their relative inability to generate SH energy). They found that each of the proposed discriminants taken separately had a high failure rate and thus it was necessary to combine all of them into a multivariate discriminant. They observed large differences in the Pg and Lg

phases excited by two proximal nuclear explosions and attributed the wide variability in their results to the sensitivity of the Pg and Lg phases to near source effects.

We feel that a successful discriminant must be relatively independent of the variability of seismic phases, of mining practice and geologic setting. In this paper we suggest that the property that best distinguishes multiple-shot explosions from all other seismic events is the persistence through time of prominent spectral features in the onsets and coda produced by these complex events. We propose a time versus frequency pattern-based discriminant which seeks long-lived spectral features in seismic coda. The concept of exploiting the time-independence of the spectral modulation induced by ripple-firing the source is not entirely new and was previously suggested by Bell (1977).

SPECTRAL MODULATIONS IN SEISMOGRAMS

Sereno and Orcutt (1985b) demonstrate the significant influence of low velocity horizons in the oceanic environment on coda duration and amplitude. This layer resonance enriches the spectrum of the coda at certain equispaced eigenfrequencies, determined by the layer thickness and velocity. Considering a relatively simple case in which a wavelet w(t) is reverberating in a single low velocity surface layer, the linear sum of all reverberations x(t) equals:

$$x(t) = w(t) * \left[\frac{1}{T} \mathrm{III}\left(\frac{t}{T}\right) \cdot e^{-\alpha|t|} \cdot H(t) \cdot e^{-i\pi t/T} \right] \qquad (1)$$

The time between successive reverberations is represented by T and to a good approximation equals the two-way vertical travel time in the horizon. The "shah" function is tapered exponentially to simulate the effect of attenuation and is multiplied by the Heaviside step function to exclude any acausal energy. The final exponential is required by the π phase shift incurred by reflection at the free surface.

By Fourier transforming the preceding equation the authors found that the spectrum of the original wavelet is multiplied by an infinite set of staggered tapering functions which decay at a rate controlled by and proportional to the attenuation parameter α. The amplitude spectrum of the sum of wavelets is given by:

$$|\tilde{X}(f)| = |\tilde{W}(f)| \cdot \left| \text{III}(fT + \frac{1}{2}) * \left[\frac{\alpha - i2\pi f}{(\alpha^2 + 4\pi^2 f^2)} \right] \right| \qquad (2)$$

The thicker - or equivalently, the slower - the horizon the more closely spaced the spectral highs will be. In the simple case where one horizon is responsible for the bulk of the resonance and the receiver is a significant distance from the source (so that the incident energy has high phase velocity) the period of the modulation observed on vertical or horizontal component sensors is largely independent of time in the coda (Hedlin, Orcutt and Minster, 1988). Sereno and Orcutt (1985b) point out that in situations where two or more different modulations are superposed, either due to more than one resonating horizon or the combination of compressional and shear resonance in the same horizon, the interference of the competing modulations can produce time-dependent behavior, most likely manifested as an evolution to lower frequency content as time progresses.

We now consider the theory underlying a distinctly different origin of spectral modulation, one originating at the source rather than through propagation. We consider a simple model of a ripple-fired mine explosion (quarry blast) in which all sub-shots occur at the same point in space and are offset from each other by equal time spans T. In addition we assume that all wavelets produced by each sub-shot w(t) are identical and superpose linearly. Approaching the problem in the manner of Sereno and Orcutt (1985b) we can compute the seismogram x(t) produced by the entire suite of sub-shots by convolving the wavelet (coda) produced by each identical sub-explosion by the finite duration "shah" function:

$$x(t) = w(t) * \left[\frac{1}{T} \text{III}(\frac{t}{T}) \cdot B(\frac{t}{D}) \right] \qquad (3)$$

The shah function is multiplied by the boxcar function B(t) which lasts D seconds, the duration of the entire suite of sub-shots in the quarry blast. By Fourier transforming (3) we find that the spectrum of the entire seismogram equals that of an individual shot multiplied by an infinite set of equispaced "sinc" functions.

$$\tilde{X}(f) = \tilde{W}(f) \bullet \left[\text{III}(fT) * \frac{\sin(\pi f D)}{\pi f} \right] \tag{4}$$

Although the physics behind the two processes that lead to modulations are fundamentally different, the mathematics that describe them at this simple level are extremely similar. The principal difference between the two models arises from the shah function which convolves the starting wavelet and is truncated by the boxcar describing the abrupt beginning and end of the quarry blast source. In the Pn propagation problem the overall modulation arises from a smoother function which reflects the loss of energy due to attenuation. Figure 1 displays the modulation caused by linearly superposing the wavelets produced by 1 to 5 sub-shots located at the same point in space and delayed 100 ms from each other. The amplification at the preferred frequencies equals the number of sub-shots. The degree to which the energy is confined to the preferred frequencies is directly dependent on the duration of the quarry blast set. By inspection of equation (4) one can see that the smaller the spacing between successive shots, the more broadly spaced the modulation in the frequency domain will be. The frequency spacing is equivalent to the inverse of the shot spacing and, as is displayed in figure 1, a 100 ms spacing results in a frequency spacing of 10 Hz. In this idealized case the modulation is independent of time.

More general mine explosions, involving arbitrary offsets in time, can be simulated in a similar manner. The theory has been dealt with by Baumgardt and Ziegler (1988) but is similar to that described above provided the scatter of offset times is not too great. Again linear superposition is assumed.

$$x(t) = \sum_{i=1}^{n} w(t-T_i) \qquad (5)$$

The absolute time of each of the n sub-events (relative to the first event) equals T_i. After Fourier transformation we find that the amplitude spectrum of the sum of wavelets equals:

$$\tilde{X}(f) = \tilde{W}(f) \cdot \left[\left(\sum_{i=1}^{n} \cos(2\pi f T_i) \right)^2 + \left(\sum_{i=1}^{n} \sin(2\pi f T_i) \right)^2 \right]^{\frac{1}{2}} \qquad (6)$$

The energy from one sub-event is multiplied by a sum of sines and cosines, and is still organized preferentially into time-independent frequency bands provided that the scatter of time delays from a constant value is not too great. Figure 2 displays the modulation pattern expected from an event consisting of 50 sub-shots. The time delays between adjacent events are distributed normally with a mean value of 63 ms and a variance of 6.3 ms. The power is concentrated near the simply predicted frequencies of 16, 32 and 48 Hz, although as the frequency of the overtone increases so does the scatter. This model is undoubtedly more realistic than the first. Although the mining engineers may want their sub-shots to adhere to a regular time-spacing there may be considerable deviation from this in practice (Stump and Reamer, 1988). Using high speed photographic observations of the sub-shot blast times in quarries in the eastern U.S. the authors observed that deviations between the intended and actual times were as high as 34%. In addition, no true quarry blast consists of a number of discrete events all located at the same point in space. True quarries employ a spatial array of sub-shots in blasting. These spatial offsets are equivalent to apparent offsets in time that depend on the slowness of the energy being considered and the azimuth from the mine to the receiver. They will, along with the true scatter, introduce a deviation from a regular time spacing but will not altogether destroy the organization of the energy into time-independent bands provided that the shot array dimensions are not too great. Although this is quite easily dealt with (Smith, 1989), as will

be discussed later it appears that we do not need this refinement to interpret the events we examine in this study.

THE DATA SET

The data used for this study were collected in 1987 in the Soviet republic of Kazakhstan roughly 200 km from the Semipalatinsk underground nuclear test site. Three receiver sites were established in the spring of 1987 in a triangular array near the towns of Bayanaul, Karkaralinsk and Karasu (see figure 3). The local crust varies in thickness from roughly 40 km (near Karasu) to 50 km near Karkaralinsk and Bayanaul (Balyaevsky et al, 1973; Leith, 1987). All three sites were installed on granitic intrusions of Permian to Triassic age and consisted of surface and borehole instruments (deployed at 99, 66 and 101 meters respectively). Although establishing the receivers on granitic outcrops should have eliminated the problem of near receiver reverberations, the site at Karasu was clearly contaminated by an anomalous site response (Eissler et al, 1988) and the data from this site have been excluded from this study.

Teledyne Geotech 54100 seismometers sampling at 250 s^{-1} with a flat response to velocity between 0.2 and 100 Hz were deployed in each of the boreholes (Berger et al, 1987) . The surface data used in this study were collected by GS-13 seismometers deployed in shallow vaults, which were also sampled at 250 s^{-1}. These instruments have a flat response to ground velocity between 1 and 80 Hz. All seismometers recorded data only after triggering.

Three calibration events detonated in September of 1987 provide the only well constrained events in this data set. They varied in size from 10 (events 1 and 3) to 20 tons (event 2) and ranged from 157 to 254 km from the receivers (see figure 1). Unlike events 1 and 3, event 2 was not fully contained underground. These events were estimated by Eissler et al (1988) to have equivalent seismic moments on the order of 10^{12} to 10^{13} Nm. Since event 3 was detonated at the same site as event 1 and occurred simultaneously with the arrival of a teleseism originating in the MacQuarie Islands, it has not been used in this study.

The region surrounding the seismic network experiences a low level of seismicity (Leith, 1987) and is considered to be tectonically stable. We believe that the bulk of the events recorded during the operation of the network are man-made and are likely mine explosions. The events considered in this paper range from 105 to 264 km from the receivers. Compelling support for the identification of one of these events (event i, figure 3; table 1) as a quarry blast comes from a French SPOT photo provided by Dr. Cliff Thurber at the State University of New York, Stony Brook. The photo of the area surrounding event i, and a number of other proximal events not discussed in this paper, clearly shows four open pit mines. All events other than the calibration shots were located by Cliff Thurber (Thurber et al, 1988) using the method described by Bratt and Bache (1988).

All spectral estimates displayed in this paper have been computed using an adaptive multi-taper algorithm described by Thompson (1982). The spectral leakage that plagues all estimates, especially the highly-colored spectra which we encountered in this study, is dealt with in an effective manner by employing several tapers that minimize the leakage from outside a pre-specified bandwidth. Secondly, the analysis of the time dependence of the energy in the coda requires the computation of spectra from short time series which, especially at the times of onsets, are particularly non-stationary. Park, Lindberg and Vernon (1987) demonstrated the multi-taper method is superior in this situation to conventional single taper algorithms because it employs several tapers that do not overemphasize the data at the center of the time series and discard significantly less data than conventional single-taper algorithms.

DATA ANALYSIS

Since we are looking for the presence or absence of time-independent banding, we have found it useful to calculate frequency-time displays of seismograms, known as sonograms in acoustics (Markel and Gray, 1976), because they preserve the time dependence information.

It is logical to begin the analysis with an event about which we know a great deal. The calibration event Chemex 2 was a 20 T explosion detonated at 50.00° N, 77.34° E at a depth of 17 m in a mining tunnel drilled through granite (see

table 1). The vertical component seismogram for this event recorded at high gain by the GS-13 seismometer and the corresponding sonogram are displayed in figure 4. The velocity seismogram has been decimated to one point in 16 (retaining the maximum and minimum amplitudes), and is otherwise unfiltered. The spectral estimates in this and all subsequent figures are of the acceleration amplitude plotted on a linear scale. Each spectral estimate consists of a weighted sum of 7 sub-estimates computed using a time-bandwidth product of 4. Each estimate has been computed from two seconds of data (i.e. 500 samples), padded to 4 seconds with zeros. A fairly broadband compressional onset occurs 27 seconds after the event. At this range (157 km) we expect that the onset energy has traveled solely within the crust. A relatively narrow band, high amplitude shear onset arrives at 48 seconds followed roughly 10 seconds later by a small amplitude surface wave packet. The most striking feature of this sonogram is that the energy is clearly not organized into time-independent frequency bands but, with the exception of the onsets, is distributed fairly randomly.

We strongly suspect that event c (figure 3) is a ripple-fired mine explosion. It was recorded by the same seismometer and processed in exactly the same manner as Chemex 2 and is displayed in figure 5. The sonograms for this event and Chemex 2 are strikingly different. The energy is clearly organized into time-independent bands regularly spaced at roughly 6 Hz. Considering the regularity of the modulation, it seems reasonable to accept, for now, the initial, simplest, quarry blast model discussed above. A simple calculation thus suggests that this event consisted of a number of sub-events spaced on the order of 167 ms from each other. The actual number of sub-events involved is not as simply assessed since the estimation involves using the falloff rates of the spectral peaks which are much more difficult to compute.

These time-independent bands are observed in virtually all the unidentified events. The primary difference between them is the period of this modulation along the frequency axis. A third event's sonogram, (event i in figure 3, located 105 km from Bayanaul) is displayed in figure 6. The broader spectral spacing (df = 16 Hz) suggests a more closely grouped set of sub-shots separated by roughly 63 ms.

In order to enhance the time-independent modulation we remove the large scale structure caused by the compressional and shear onsets as well as the high frequency spectral falloff. We have found that an effective method involves differencing two versions of each original spectral estimate. As figure 7 illustrates we compare a relatively unsmoothed version with one that resolves only the large scale structure in order to extract the regular modulation. In practice, when analyzing the events considered in this paper, the smoothed versions were obtained by simply convolving the original spectral estimates with boxcar functions spanning 2.5 and 1.0 Hz. We represent all regions of the sonogram matrix where the local power is high relative to the more regional average power by a value of +1 (denoted as white in this and all subsequent figures) and where it is low by a -1 (black). In this manner the bulk of the magnitude information is discarded and the true sonogram matrix is "flattened" to a very simple, yet informative, binary matrix.

The binary matrix representing the first 35 seconds following the compressional onset of event Chemex 2 recorded at Bayanaul to a frequency of 35 Hz is displayed in figure 8. Aside from the suggestion of time-independent structure in the vicinity of 5 Hz, the energy is distributed more or less randomly. It seems intuitively reasonable that a single source explosion should give rise to a coda in which the energy is distributed randomly as a function of frequency and time if the dominant coda generation mechanism involves the scattering of energy by a random distribution of randomly sized inhomogeneities. This example suggests that layer resonance, proposed by Sereno and Orcutt (1985a) as the dominant source of coda in the oceanic lithosphere, plays only a supporting role in generating seismic coda in this region of the continental crust. We contrast this result with the coda produced by event c (figure 9) which displays obvious time-independent spectral modulation.

We examined a fourth event (event d in figure 3) to find that the regular modulation is not restricted to the vertical component. Indeed, as figure 10 reveals, the modulation appears to be quite independent of the component of displacement. Only the vertical and radial components are shown, but the transverse component is nearly identical. This observation lends support to

the hypothesis that the time-independent spectral modulation is a source and not a propagation effect. This observation is not unique to this event but appears to be shared by all events other than the calibration shots.

The quarry blast spectral modulation is not only independent of component but appears to be independent of the azimuth from the source to the receiver as well as source-receiver range. In figure 11 we compare the vertical component modulation of event d as recorded at Bayanaul (at a range of 159 km and a back azimuth of 268°) and Karkaralinsk (at a range of 217 km and a back azimuth of 317°). The independence of azimuth suggests that the array of sub-shots comprising event d may be very small. The apparent time offsets caused by spacing the sub-shots become significant when the array is large and as discussed earlier these apparent offsets have an azimuthal dependence.

To constrain the probable dimensions of a typical quarry blast we employ the formula of Smith (1989) to equate true spatial offsets with apparent time offsets δT_i^a

$$\delta T_i^a = p \sqrt{\delta X_i^2 \sin^2\theta + \delta Y_i^2 \cos^2\theta} + \delta T_i \qquad (7)$$

Each sub-event occurs at point $(\delta X_i, \delta Y_i)$ in space and at time δT_i. The energy under consideration travels at a slowness of p s km^{-1} along an azimuth from the source to the receiver of θ degrees. To permit a crude calculation we adopt an array consisting of just two shots. We simplify the calculation by aligning the X and Y axes parallel and perpendicular to the line joining the shots respectively. To use this equation, we must first estimate the dependence of the modulation pattern on source to receiver azimuth. In general it is true in this dataset that little difference in the modulation period associated with any single event can be discerned between the recordings made at Karkaralinsk and Bayanaul. Thus, for a crude estimate of the likely source dimensions we model a typical event (d, figure 10) with sub-shots arranged spatially to give rise to the maximum possible azimuthal dependence of the spectral modulation when observed at these two stations. We will realize the maximum possible change in modulation period between Bayanaul and Karkaralinsk if we place this dipolar shot array so that the normal to the line joining the shots lies

exactly half way between the two receivers. Using elementary error analysis, and knowing that $\delta T = 1/\delta F$ (where δT is the time offset and δF is the spacing of adjacent peaks in the frequency domain) we find that the change in δT (or $\delta^2 T$) required by a change in the modulation spacing ($\delta^2 F$) is given by:

$$\delta^2 T = - \frac{\delta^2 F}{(\delta F)^2} \tag{8}$$

If we observe n cycles in the frequency span of ΔF Hz in one recording of an event, and in $\Delta F \pm dF$ Hz in another recording then

$$\delta^2 T = - \frac{ndF}{(\Delta F)^2} \tag{9}$$

Combining equations (7) and (9) we find that

$$\delta X = - \frac{ndF}{(\Delta F)^2 p \left[\sin(\theta_1) - \sin(\theta_2) \right]} \tag{10}$$

where δX is the inferred shot spacing and θ_1 and θ_2 are the azimuths to Bayanaul and Karkaralinsk (and equal +24.6° and -24.6° respectively). In figure 11 we observe 11 cycles present in a frequency band of 30 ± 1 Hz in both the recordings of this event. Thus, using equation (10), and considering a typical crustal ray with a slowness of 1/7 s km^{-1} we infer a shot spacing of 100 m or less. Clearly many assumptions have been made in this calculation so it should be regarded as a crude estimate at best. We have no a-priori information on what blasting techniques (shot geometry and timing) the Soviet mining engineers employ in their quarry blasts. Combining this fact with the observations that the spectral modulations are regular in frequency and independent of time and source-receiver azimuth it seems inappropriate to attempt a more sophisticated modeling by allowing spatial offsets. We can adequately model these Soviet quarry blasts by employing either of the two models proposed earlier in this paper.

Assuming linear superposition (and the first quarry blast model), it is a simple matter to synthesize a quarry blast by linearly superposing a Green's function upon itself after offsetting by a delay time prior to each addition. By chance it turns out that Chemex 2 is at nearly the same distance from Bayanaul as is

event d, and thus it is eligible for use as a "Green's function" if lateral variations of crustal structure are small. This observed rather than synthesized Green's function has the obvious drawback of being produced by a significantly larger source than a likely sub-event in a typical quarry blast, so that its corner frequency will be lower. This shouldn't be a significant problem since, as Evernden, Archambeau and Cranswick (1986) note, the Sharpe explosion model (Sharpe, 1942), predicts the corner frequency of a tamped explosion of this size to be 30 to 35 Hz. This is approximately the upper frequency limit in all binary sonograms considered in this study. The usefulness in general of such a Green's function is limited because it is only available at a small number of ranges (defined by the offsets between the two events and the two receivers). It has the distinct advantage vis-a-vis synthetics that the propagation transfer function is nearly exact (assuming horizontal layers). By taking the vertical component of motion from Chemex 2 observed at Bayanaul (figure 4) and stacking it upon itself twice after offsetting each successive trace by 133 ms, we obtain the "synthetic" quarry blast displayed in figure 12. The binary sonogram corresponding to a synthetic quarry blast consisting of 3 shots offset by 382 ms, displayed in figure 13, compares well with the actual binary sonogram computed from event d. Although non-linear effects must clearly occur during a quarry blast, simple linear theory can be very effective in reproducing the observed modulation. In principle, we can time an observed ripple fired quarry blast repetition rate with this method. In this case we have illustrated a likely offset time (382 ms) for event d.

DISCRIMINATION BETWEEN SINGLE AND MULTIPLE SHOT EXPLOSIONS

The method described above of reducing sonograms to binary matrices provides simple patterns that allow visual discrimination between quarry blasts and simpler events (single event explosions and perhaps earthquakes). Clearly there are a number of mathematical operations we can employ to reduce these matrices to scalars which reflect the presence or absence of time-independent spectral banding. Two methods seem promising at this time but have not yet been developed. One involves the comparison of three component binary matrices by performing a 3 way cross-correlation. As discussed above the quarry blast modulation is a source effect and is not

dependent on the recorded component. We expect a relatively high cross-correlation between the three components of recorded motion resulting from a quarry blast relative to that computed from simpler events. In an alternate method the 2-dimensional Fourier transform of the binary sonogram matrix is computed. We expect the presence or absence of time-independent modulation would be reflected in the time axis DC power levels, those events with time-independent modulation should have relatively high levels. For the present purposes, however, we feel it is sufficient to recognize simply that distinct time versus frequency pattern differences between quarry blasts and calibration explosions exist. By comparing individual columns in the binary sonogram matrices calculated from single and multiple-event explosions we can assess the enhanced discrimination potential of binary sonogram matrices over that of single spectral estimates. In figure 8 many of the columns possess a regular modulation comparable to that seen in single columns computed from the coda resulting from a quarry blast (for example figure 9). Individual spectral estimates computed from even simple single event explosions can have significant regular modulation and thus distinguishing between these and more complex multiple-event explosions using single spectra is expected to be difficult. The profound differences between these two types of events becomes obvious when many spectra offset from each other in time are computed. The persistence of spectral features through time in the coda of multiple source events, but not single source events, is what sets them apart.

A weakness of this discriminant and indeed any algorithm which seeks to separate quarry blasts from other events on the basis of their unusual spectral color is that time-independent spectral modulation can be acquired during propagation. The binary sonogram matrix of Chemex 2 recorded at Bayanaul possesses a faint but undeniable time-independent structure at about 5 Hertz. Comparison of this figure with the binary sonogram computed from Chemex 2 recorded at Karkaralinsk reveals that the two stations have recorded essentially the same patterns. The same exercise performed on the Chemex 1 recordings at Bayanaul and Karkaralinsk revealed faint but strikingly similar time-independent patterns distinct from the Chemex 2 patterns. These features are most likely a source effect since similar patterns have sources, not receivers, in common. Since the Chemex events are known to be single source events, the most plausible explanation is that the patterns are due to

reverberations occurring in a shallow, near source horizon. Although these time-independent effects are faint they are worth considering further. Reverberations can occur at any time during propagation from the source to the receiver, but the two points at which the effects are going to be most noticeable and most likely is near the source and near the receiver. These are the only two points at which the recorded body wave energy is most likely to encounter a low velocity horizon. Prior to using the discriminant, we are proposing that a receiver must be shown to be free of reverberations by recording single event explosions. If the site is able to record these events with no time-independent effects then it is eligible for this type of work. Fortunately the Chemex events have not produced significant time-independent structure (the high frequency overtones have not developed), but they do indicate that it may be possible to disguise a single event explosion as a quarry blast by detonating it in a low velocity horizon.

A second problem exists when events have been recorded at a time of high noise levels, especially when the events are small and/or distant and when spectral spikes exist in the noise. Prominent features in ground or instrumental noise can emerge from the signal after the onset and be misinterpreted as time-independent features due to the source, especially if more than one harmonic is present. To combat this problem it is necessary to obtain and analyze pre-event noise samples to permit the identification of time-independent features in the coda that are really due to noise. In this study, all time-independent features attributed to the source are seen on both the Karkaralinsk and Bayanaul records. It is also true that while signal spectra between the two receivers have high coherence, the pre-event noise spectra do not.

In practice it is clearly desirable that more than one station be used when attempting to discriminate quarry blasts from simpler events. As discussed earlier, if the quarry blast sub-shot array is not infinitely small we expect the modulation pattern to show an azimuthal dependence. There are certain array geometries, for example linear arrays, that will produce, at certain source-receiver azimuths, negligible apparent time offsets between the sub-shots and thus little or no time-independent spectral structure. It is extremely unlikely that a second receiver simultaneously recording this event at a different

azimuth will also have such a problem. None of the quarry blasts we have examined show evidence for such azimuthal effects.

CONCLUSIONS

We have observed a significant difference between events which consist of a number of sub-explosions closely grouped in space and time and simpler, single explosion, events. The former type of event (a quarry blast) possesses a distinctive time-independent spectral structure that can be easily explained assuming linear superposition of the wavefields produced by each of the sub-events. The latter type of source does not cause a regular organization of the energy and thus the distribution of energy in the coda is controlled by the propagating medium. The observed randomness of this energy as a function of frequency and time suggests that the dominant mechanism of coda generation in this region of the continental crust involves scattering by small scale inhomogeneities. We conclude these two types of events can be most effectively distinguished from each other by exploiting the expected differences in the time- and frequency-evolution of energy in the onsets and coda. We propose a time versus frequency pattern-based discriminant.

Although we have no a-priori information on the mining practice employed by the Soviet quarry blast engineers we infer regular offsets in time and small spatial array dimensions by observing that the modulations are regular in frequency and independent of time and source-receiver azimuth.

In the future we will expand this analysis to include earthquakes and explosions in other regions. We expect we can demonstrate the independence of the algorithm on mining practice and geologic setting. We hope to extend the pattern-based discriminant by reducing the binary sonogram matrices to scalars which reflect the presence or absence of time-independent modulation.

ACKNOWLEDGMENTS

We thank Dr. Cliff Thurber at the State University of New York, Stony Brook for his helpful review and comments and for providing us with the satellite

photos and event locations. We also express our appreciation to Dr. Alan Chave, currently at AT & T Bell Laboratories, for supplying us with the multi-taper algorithm that was used to compute spectral estimates. This research was sponsored by the Defense Advanced Research Projects Agency (DARPA) / Air Force Geophysical Laboratory (AFGL) under Contracts No. F19628-87-K-0013 and F19628-88-K-0044. The Kazakh stations were installed and operated by the Institute of Physics of the Earth of the Soviet Academy of Sciences and the Natural Resources Defence Council. We thank the team of scientists who set up these stations.

REFERENCES

Aviles, C. A. & Lee, W. H. K., 1986. Variations in Signal Characteristics of Small Quarry Blasts and Shallow Earthquakes. *EOS, Trans. of the American geophys Union*, **67**, 1093.

Balyaevsky, N. A., Borisov, A. A., Fedynsky, V. V., Fotiadi, E. E., Subbotin, S. I. & Volvovsky, I. S., 1973. Structure of the Earth's Crust on the Territory of the U. S. S. R.. *Tectonophys.*, **20**, 35-45.

Baumgardt, D. R. & Ziegler, K. A., 1988. Spectral Evidence for Source Multiplicity in Explosions: Application to Regional Discrimination of Earthquakes and Explosions. *Bull. seism. Soc. Am.*, **78**, 1773-1795.

Bell, A. G. R., 1977. A Digital Technique for Detection of Multiple Seismic Events. *EOS, Trans. of the American geophys.Union*, **57**, 444.

Berger, J., Eissler, H.K., Vernon, F.L., Nersesov, I.L., Gokhberg, M.B., Stolyrov, O.A. & Tarasov, N.D., 1987. Studies of High-Frequency Seismic Noise in Eastern Kazakhstan. *Bull. seism. Soc. Am.*, **78**, 1744-1758.

Bratt, S. R. & Bache, T. C., 1988. Locating Events With a Sparse Network of Regional Arrays. *Bull. seism. Soc. Am.*, **78**, 780-798.

Eissler, H.K., Tarasov, N.T., Zhuravlev, V., Thurber, C.H., Vernon, F.L., Berger, J. & Nersesov, I.L., 1988. High-Frequency Seismic Observations of Chemical Explosions of Known Location and Yield in Eastern Kazakhstan, U.S.S.R.. *Submitted to the J. geophys. Res.*

Evernden, J. F., Archambeau, C. B. & Cranswick, E., 1986. An Evaluation of Seismic Decoupling and Underground Nuclear Test Monitoring Using High-Frequency Seismic Data. *Reviews of geophys.* **24**, 143-215.

Gupta, I. N., Burnetti, J. A., Wagner, R. A. & Marshall, M., 1984. Discrimination between Quarry Blasts, Nuclear Explosions and Earthquakes. *Unclassified AFTAC/TG-DARPA DoD report*, - TGAL-TR-84-1.

Hedlin, M. A. H., Orcutt, J. A. & Minster, J. B., 1988. A Comparative Study of High Frequency Signal and Noise in Oceanic and Continental Environments. *Paper presented at the 10th annual AFGL/DARPA seism. Res. Symp.*

Leith, W., 1987. Geology of NRDC seismic stations in Eastern Kazakhstan, U.S.S.R.. *U.S.G.S. Open-File Report* 87-597.

Markel, J. D. & Gray, A. H. Jr., 1976. *Linear Prediction of Speech*, Springer-Verlag, Berlin Heidelberg New York.

Park, J., Lindberg, C. R. & Vernon, F. L., 1987. Multitaper Spectral Analysis of High-Frequency Seismograms. *J. geophys. Res.*, **92**, 12675-12684.

Sereno, T. J. Jr., 1986. The Propagation of High Frequency Seismic Energy Through Oceanic Lithosphere. *Ph.D. Thesis*, University of California.

Sereno, T. J. Jr. & Orcutt, J. A., 1985a. Synthetic seismogram modelling of the oceanic Pn phase. *Nature*, **316**, 246-248.

Sereno, T. J. Jr. & Orcutt, J. A., 1985b. Synthesis of Realistic Oceanic Pn Wave Trains. *J. geophys. Res.*, **90**, 12755-12776.

Sharpe, J. A., 1942. The production of Elastic Waves by Explosion Pressures, I. Theory and Empirical Field Observations. *Geophysics*, **7**, 144-154.

Smith, A. T., 1989. High-Frequency Seismic Observations and Models of Chemical Explosions: Implications for the Discrimination of Ripple-Fired Mining Blasts. *Submitted for publication in the Bull. seism. Soc. Am.*

Stump, B. W. & Reamer, S. K., 1988. Temporal and Spatial Source Effects from Near-Surface Explosions. *Paper presented at the 10th annual AFGL/DARPA seism. Res. Symp.*

Thompson, D. J., 1982. Spectrum Estimation and Harmonic Analysis. *IEEE Proc.*, **70**, 1055-1096.

Tribolet, J. M., 1979. *Seismic Applications of Homomorphic Signal Processing.* Prentice-Hall Signal Processing Series.

Thurber, C. H., Eissler, H., Berger, J., Zhuravlev, V. & Tarasov, N., 1988. Location of Regional Explosions and Earthquakes with the NRDC-Soviet Academy of Sciences Seismic Network in Kazakhstan. *EOS, Trans. of the American geophys.Union*, **69**, 1332.

FIGURE CAPTIONS

Figure 1. Spectral modulations predicted for events consisting of 1 to 5 sub-shots spaced evenly at 100 ms.

Figure 2. Spectral modulation predicted for an event consisting of 50 sub-shots. The offset times are distributed as a Gaussian with a mean of 63 ms and a variance of 6.3 ms.

Figure 3. Receiver and event Geography.

Figure 4. Seismogram resulting from chemex 2 recorded at a range of 157 km by the vertical surface seismometer at Bayanaul and corresponding sonogram.

Figure 5. Seismogram resulting from event c recorded at a range of 264 km by the vertical surface seismometer at Bayanaul and corresponding sonogram.

Figure 6. Seismogram resulting from event i recorded at a range of 105 km by the vertical surface seismometer at Bayanaul and corresponding sonogram.

Figure 7. Original spectral estimate and two versions, one relatively unsmoothed and the other relatively highly smoothed. This figure is intended to illustrate the means by which we reduce each spectral estimate to a "binary spectral estimate". The regions of locally high power are represented by a +1 (white). Regions deficient in power are represented by a -1 (black).

Figure 8. Vertical component binary sonogram matrix corresponding to chemex 2 recorded at Bayanaul. The first 25 seconds of coda after the compressional onset are represented in this and all subsequent figures.

Figure 9. Vertical component binary sonogram matrix corresponding to event c recorded at Bayanaul.

Figure 10. Binary sonogram matrices representing the vertical (a) and radial (b) components of displacement recorded at Bayanaul from event d.

Figure 11. Vertical component binary sonogram matrices corresponding to event d recorded at Bayanaul (a) and Karkaralinsk (b).

Figure 12. (a) Time series and sonogram corresponding to chemex 2 recorded at Bayanaul. (b) Time series and sonogram representing a "synthetic" quarry blast involving 3 shots spaced in time by 133 ms.

Figure 13. (a) Vertical component binary sonogram matrix corresponding to a synthetic quarry blast consisting of 3 sub-events spaced in time by 382 ms. (b) Vertical component binary sonogram matrix corresponding to event d recorded at Bayanaul.

Table 1. Event Locations			
Event	Latitude	Longitude	Origin Time
	(°N)	(°E)	year/day/h:m:s
CH2	50.000	77.340	87/245/09:27:04.950
EVC	49.333	72.667	87/135/10:35:00.2
EVD	50.742	73.275	87/141/09:16:43.3
EVI	51.760	75.572	87/146/08:33:26.5

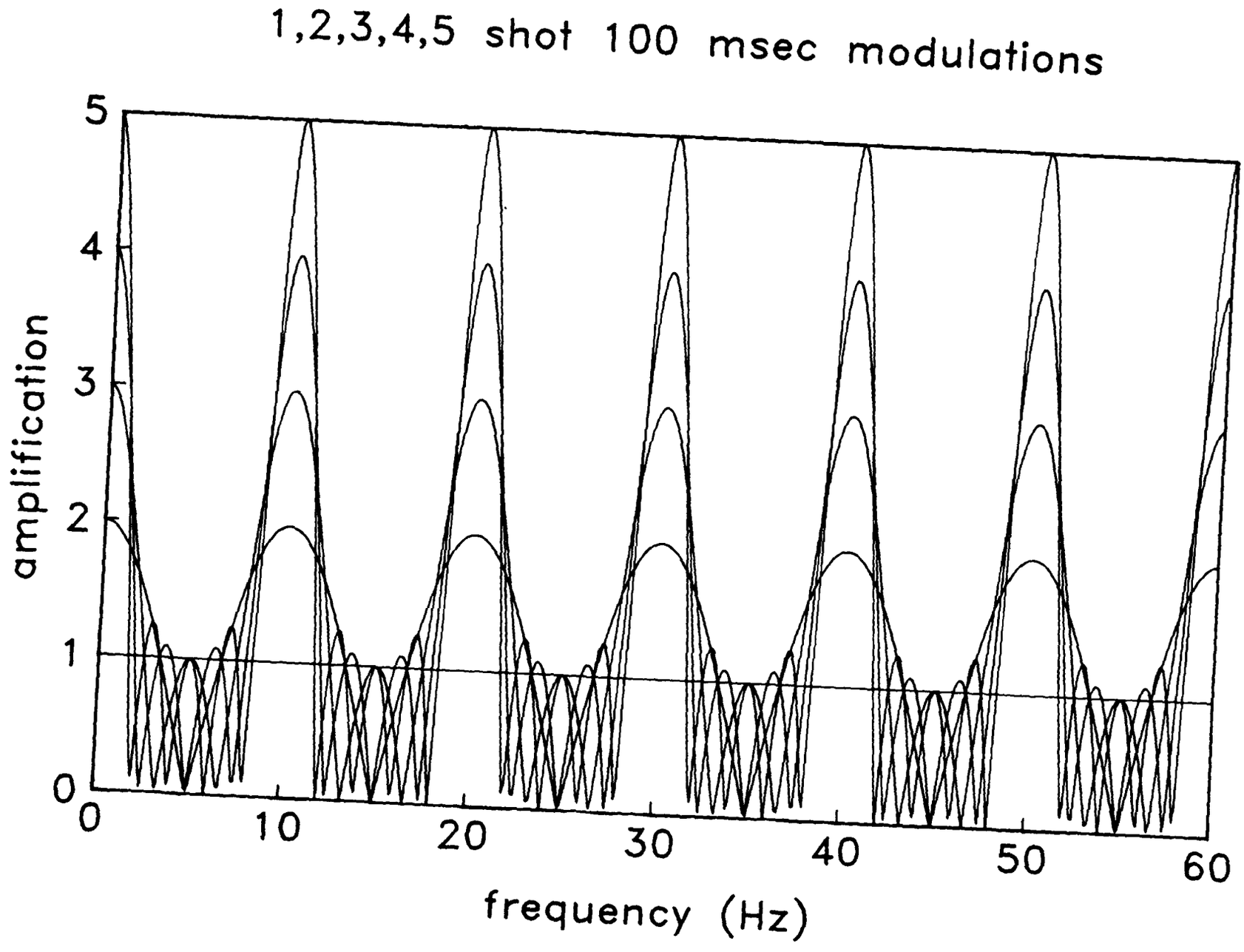
1,2,3,4,5 shot 100 msec modulations
amplification
0
1
2
3
4
5
0
10
20
30
40
50
60
frequency (Hz)

Figure 1

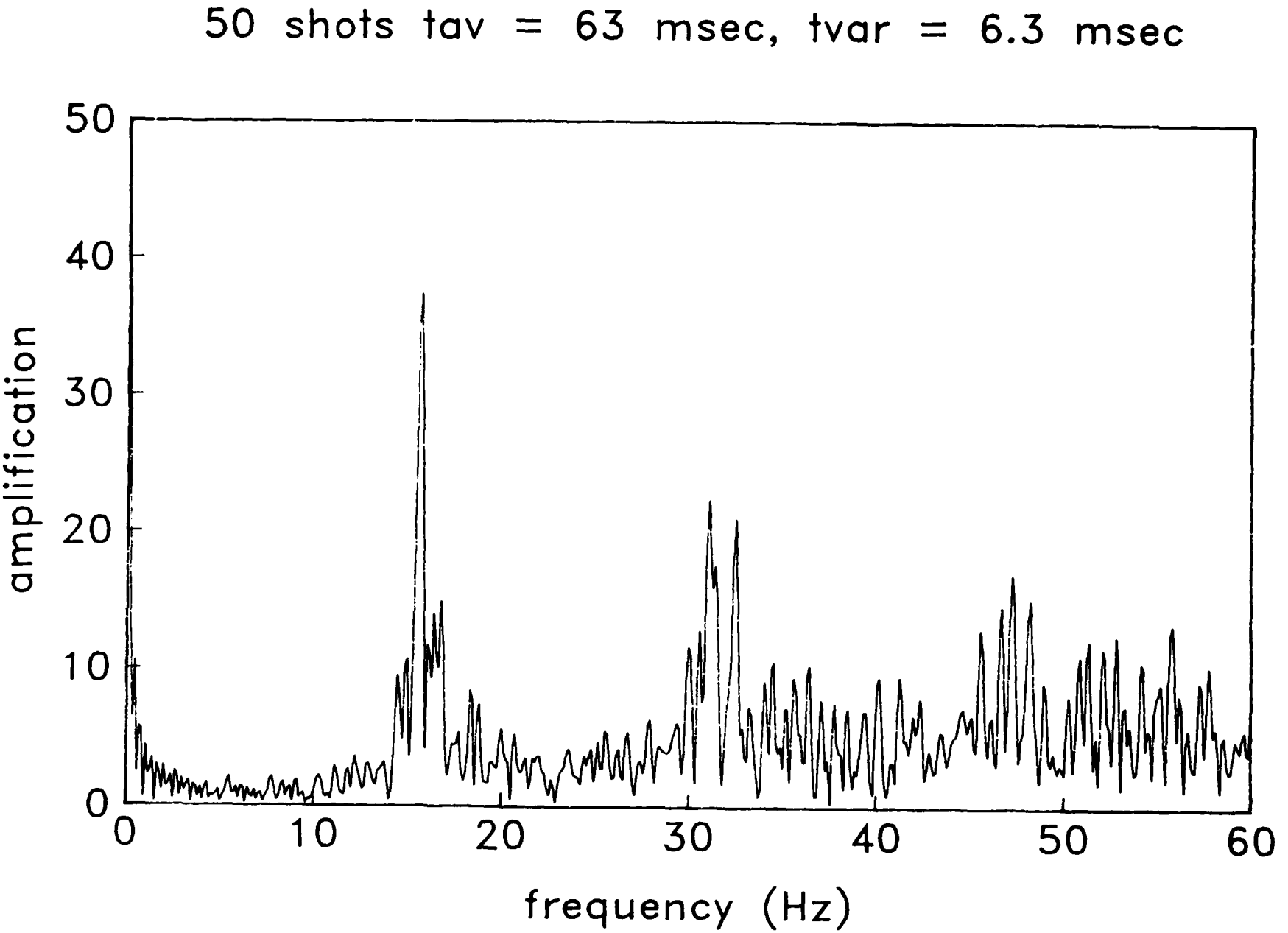
50 shots tav = 63 msec, tvar = 6.3 msec
amplification
0
10
20
30
40
50
0
10
20
30
40
50
60
frequency (Hz)

Figure 2

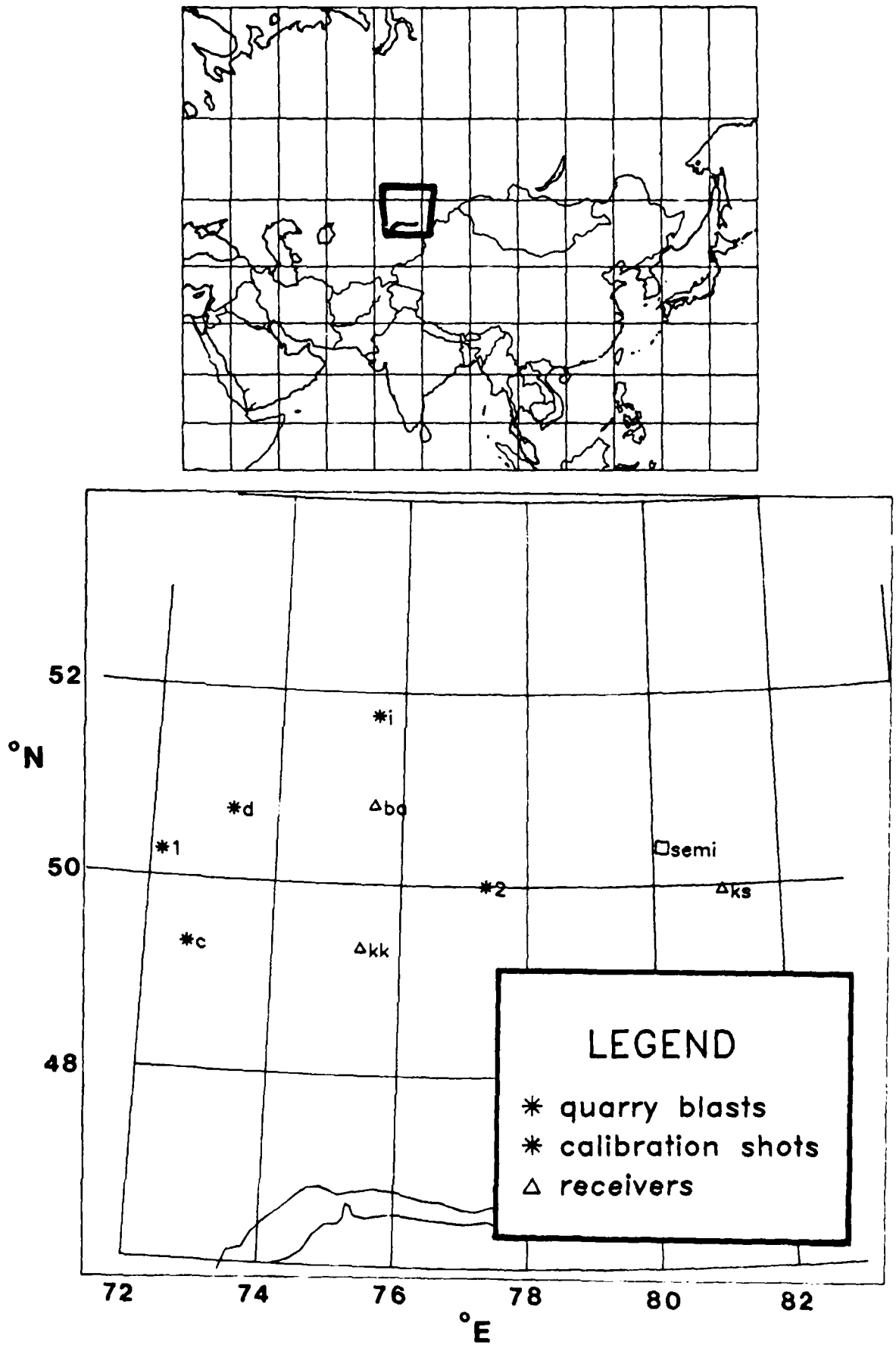
52
°N
50
48
*i
*d
△bq
*1
□semi
*2
△ks
*c
△kk
72
74
76
78
80
82
°E
LEGEND
* quarry blasts
* calibration shots
△ receivers

Figure 3

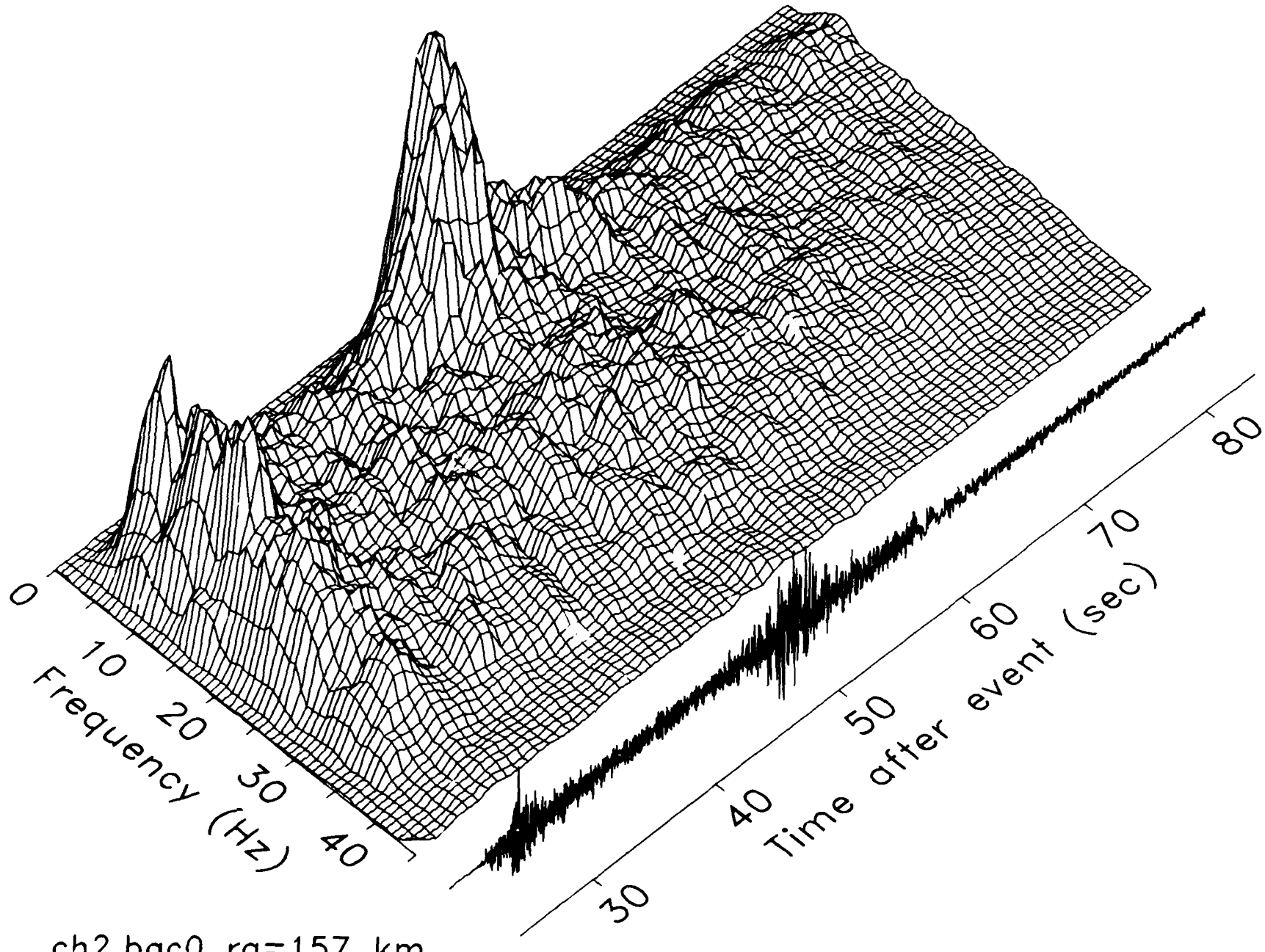
0
10
20
30
40
Frequency (Hz)
30
40
50
60
70
80
Time after event (sec)
ch2.bac0 rg=157 km

Figure 4

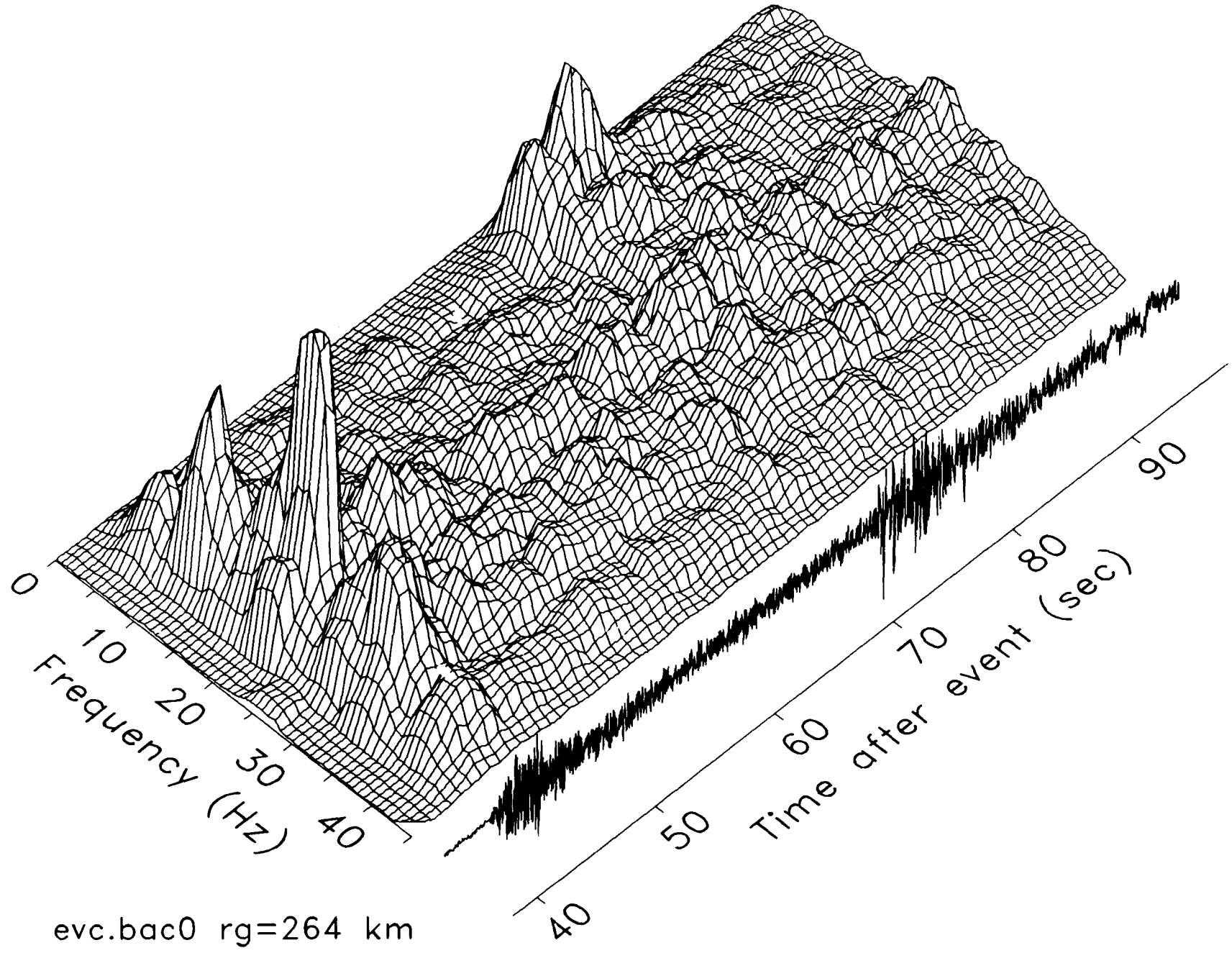
0
10
20
30
40
Frequency (Hz)
40
50
60
70
80
90
Time after event (sec)
evc.bac0 rg=264 km

Figure 5

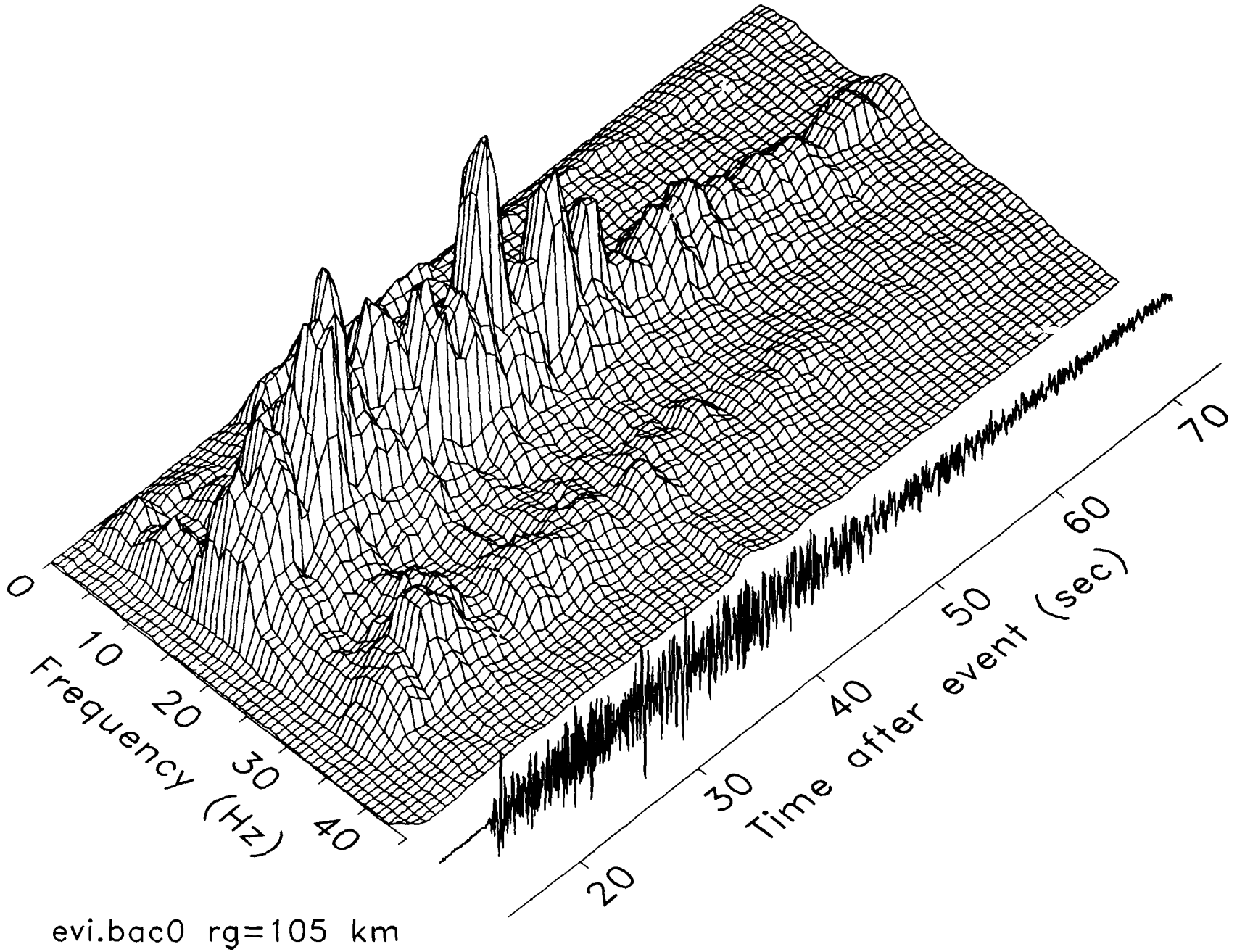
0
10
20
30
40
Frequency (Hz)
20
30
40
50
60
70
Time after event (sec)
evi.bac0 rg=105 km

Figure 6

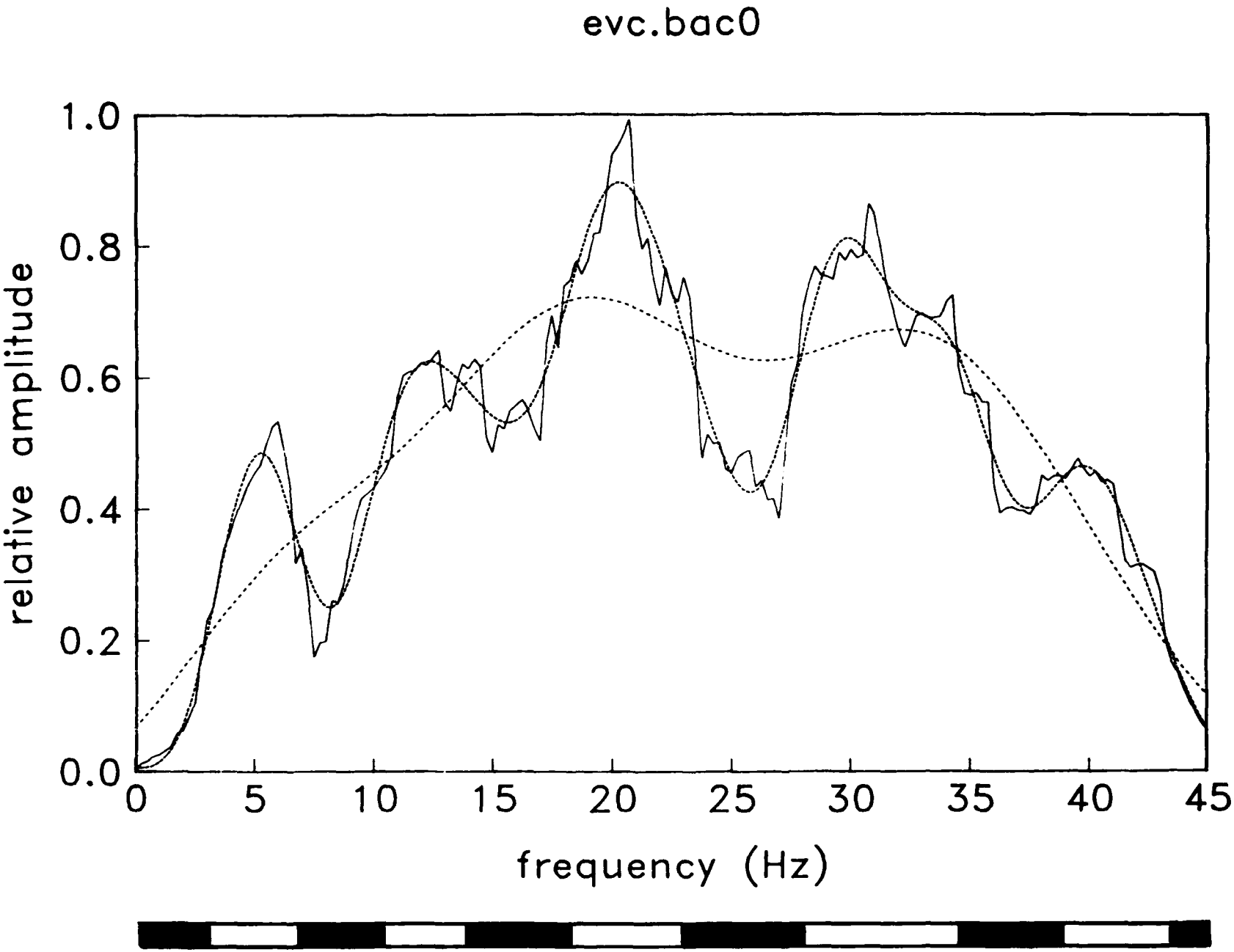
evc.bac0
relative amplitude
1.0
0.8
0.6
0.4
0.2
0.0
0
5
10
15
20
25
30
35
40
45
frequency (Hz)

Figure 7

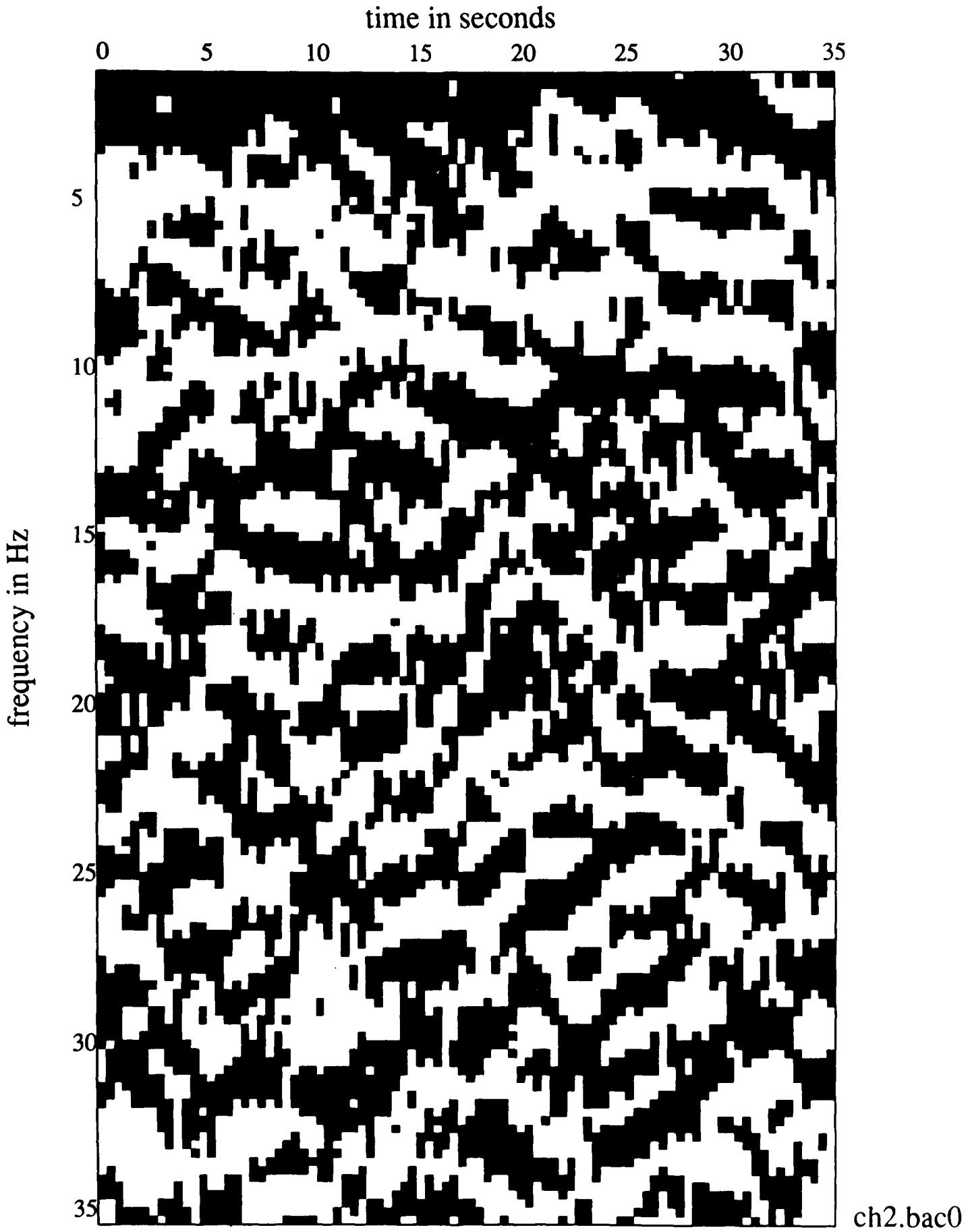
time in seconds
0
5
10
15
20
25
30
35
frequency in Hz
5
10
15
20
25
30
35
ch2.bac0

Figure 8

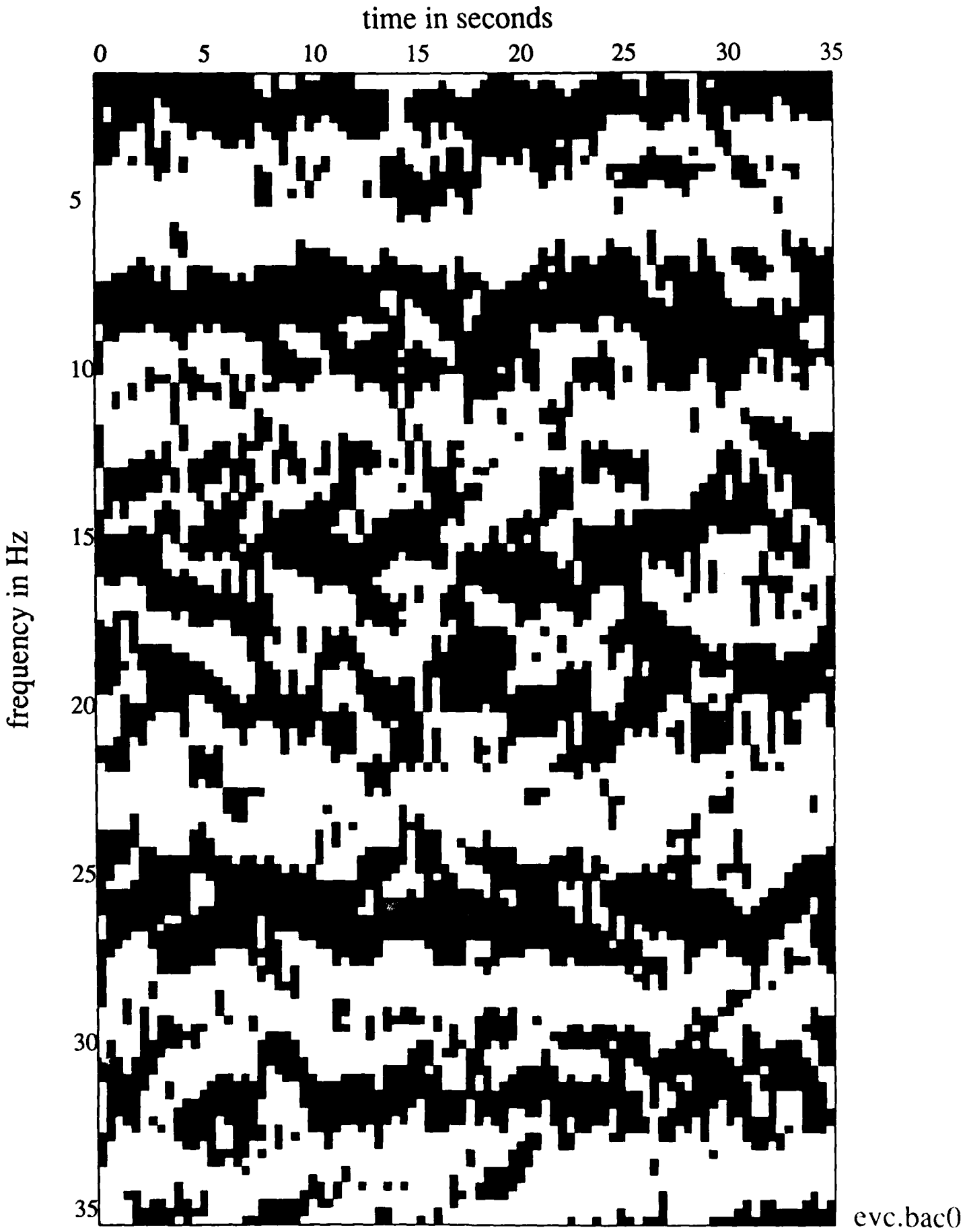
time in seconds
0
5
10
15
20
25
30
35
frequency in Hz
5
10
15
20
25
30
35
evc.bac0

Figure 9

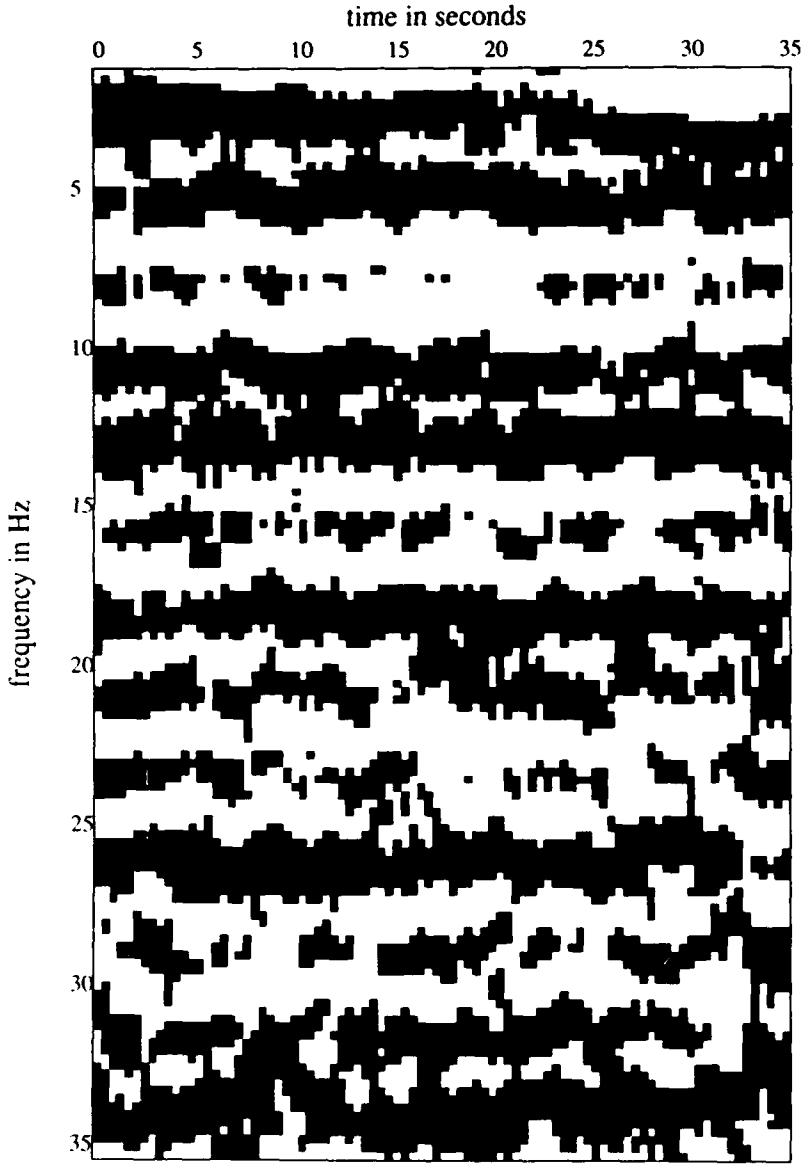
time in seconds
0
5
10
15
20
25
30
35
frequency in Hz
5
10
15
20
25
30
35
evd.bac0

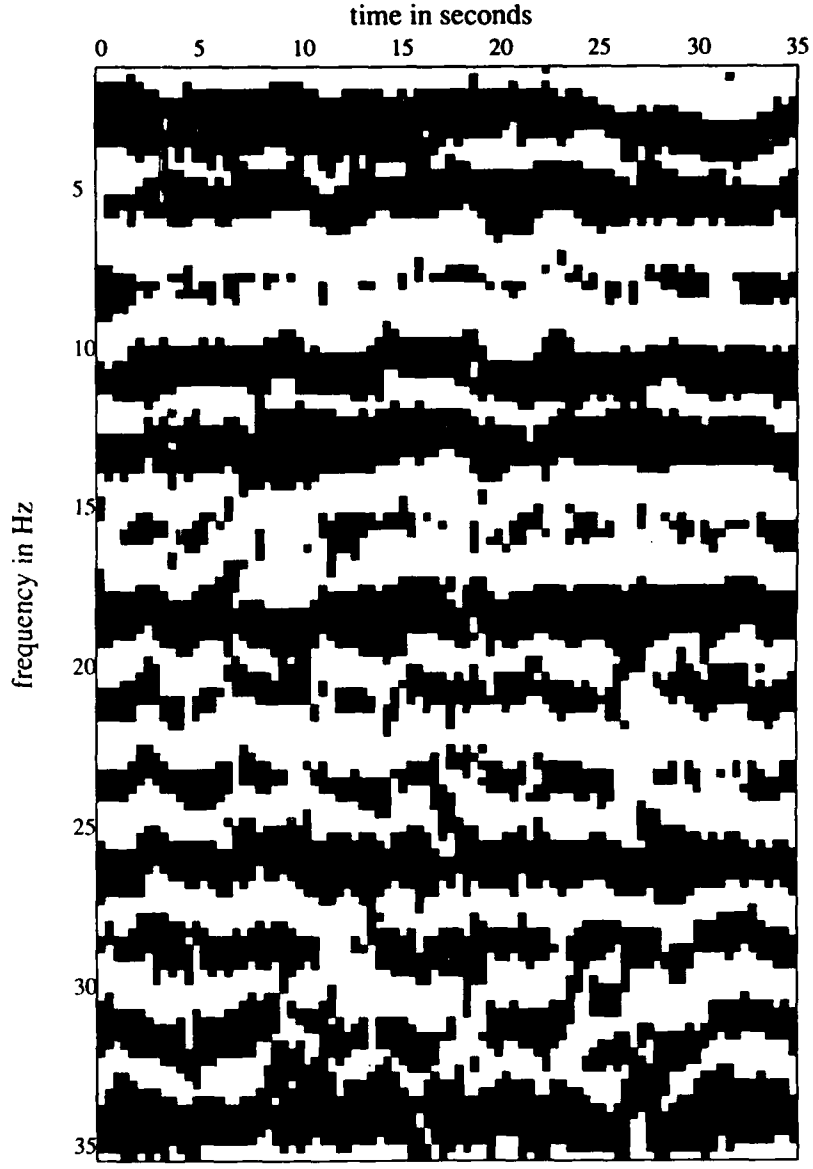
time in seconds
0
5
10
15
20
25
30
35
frequency in Hz
5
10
15
20
25
30
35
evd.bacr

Figure 10

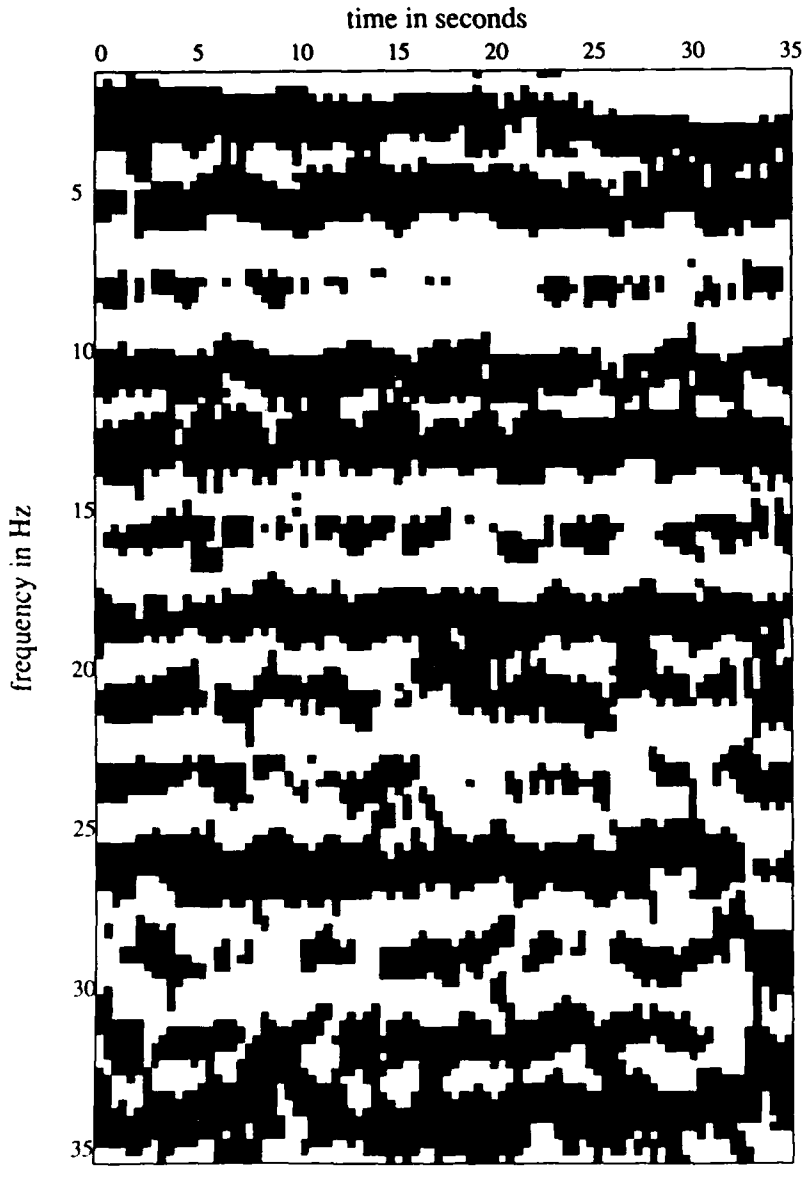
time in seconds
0 5 10 15 20 25 30 35
frequency in Hz
5 10 15 20 25 30 35
evd.bac0

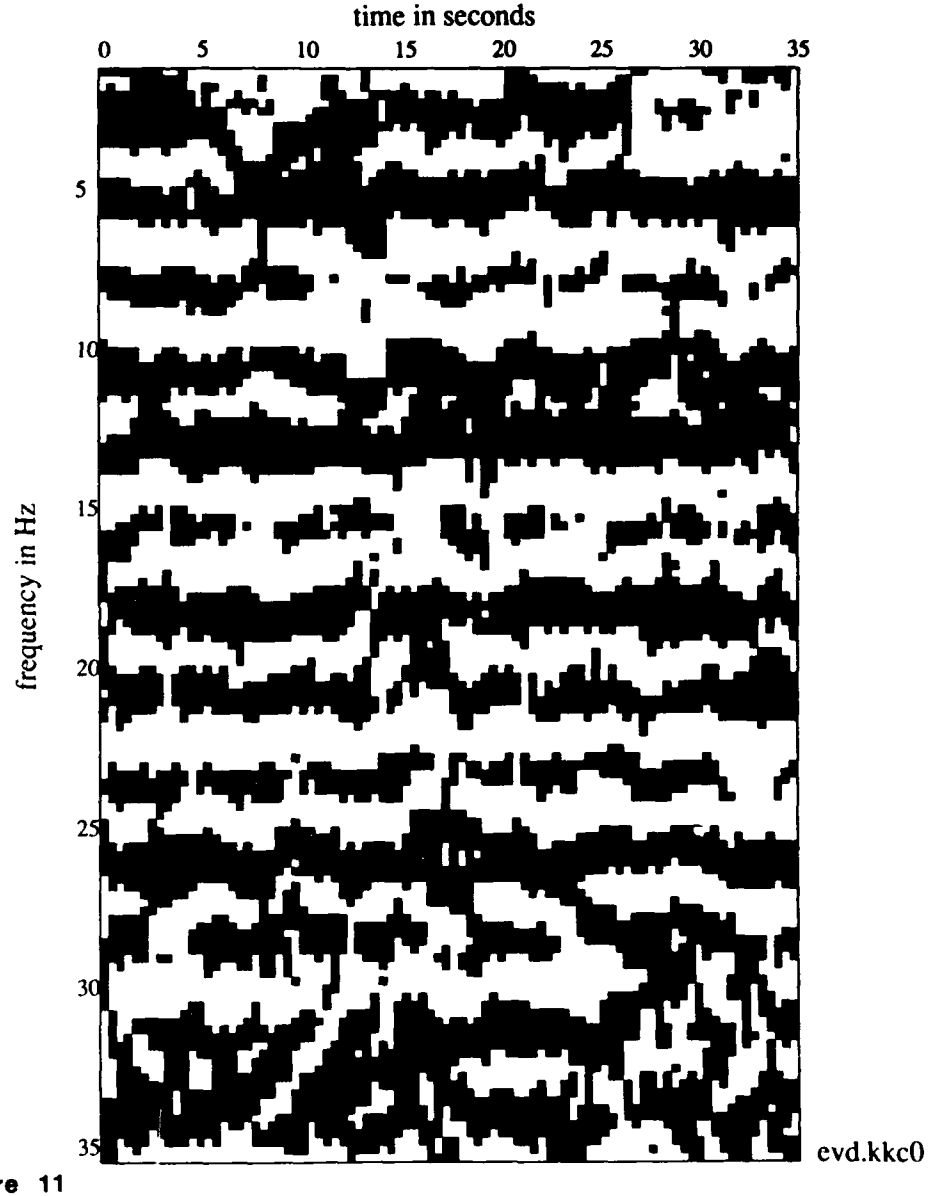
time in seconds
0 5 10 15 20 25 30 35
frequency in Hz
5 10 15 20 25 30 35
evd.kkc0

Figure 11

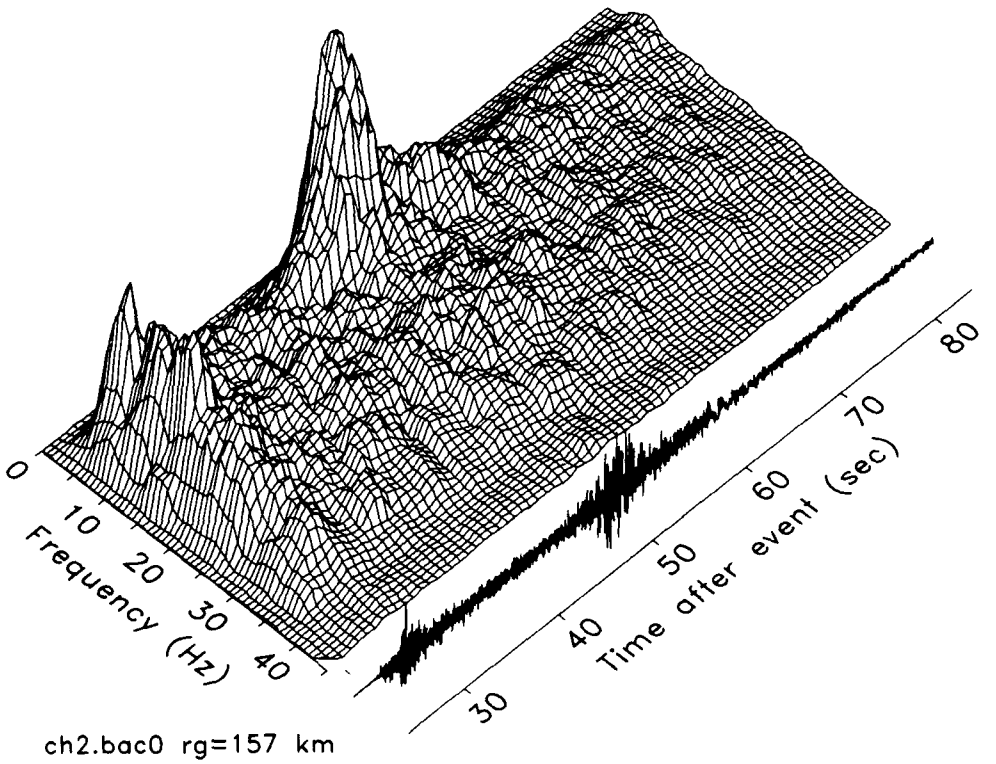

ch2.bac0 rg=157 km

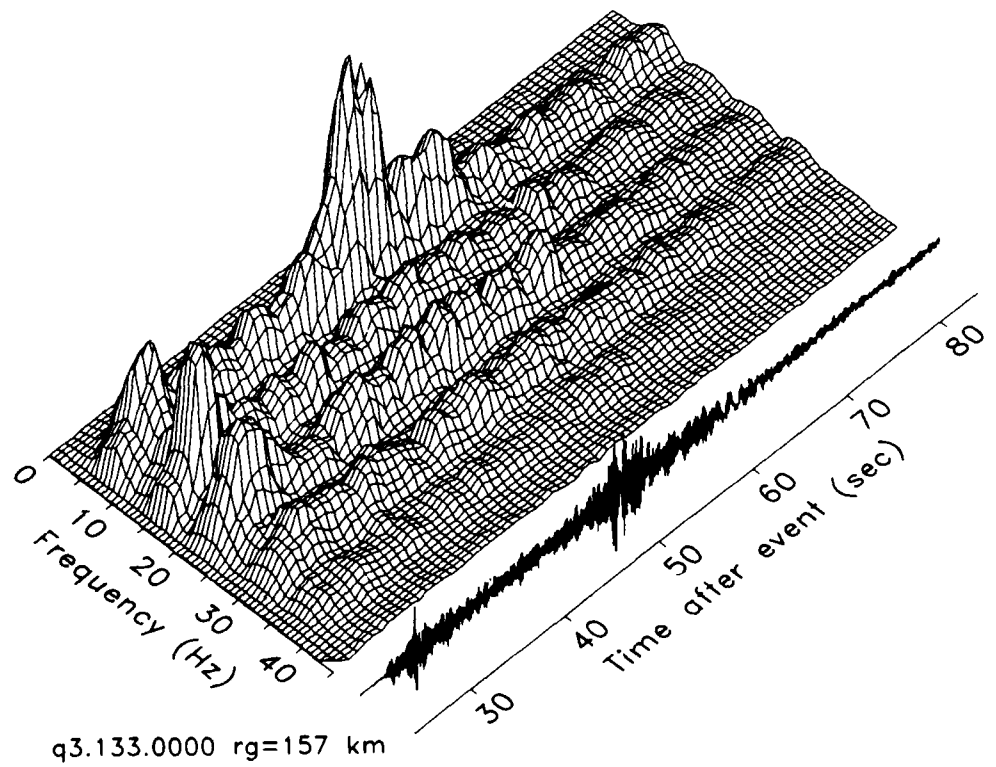

q3.133.0000 rg=157 km

Figure 12

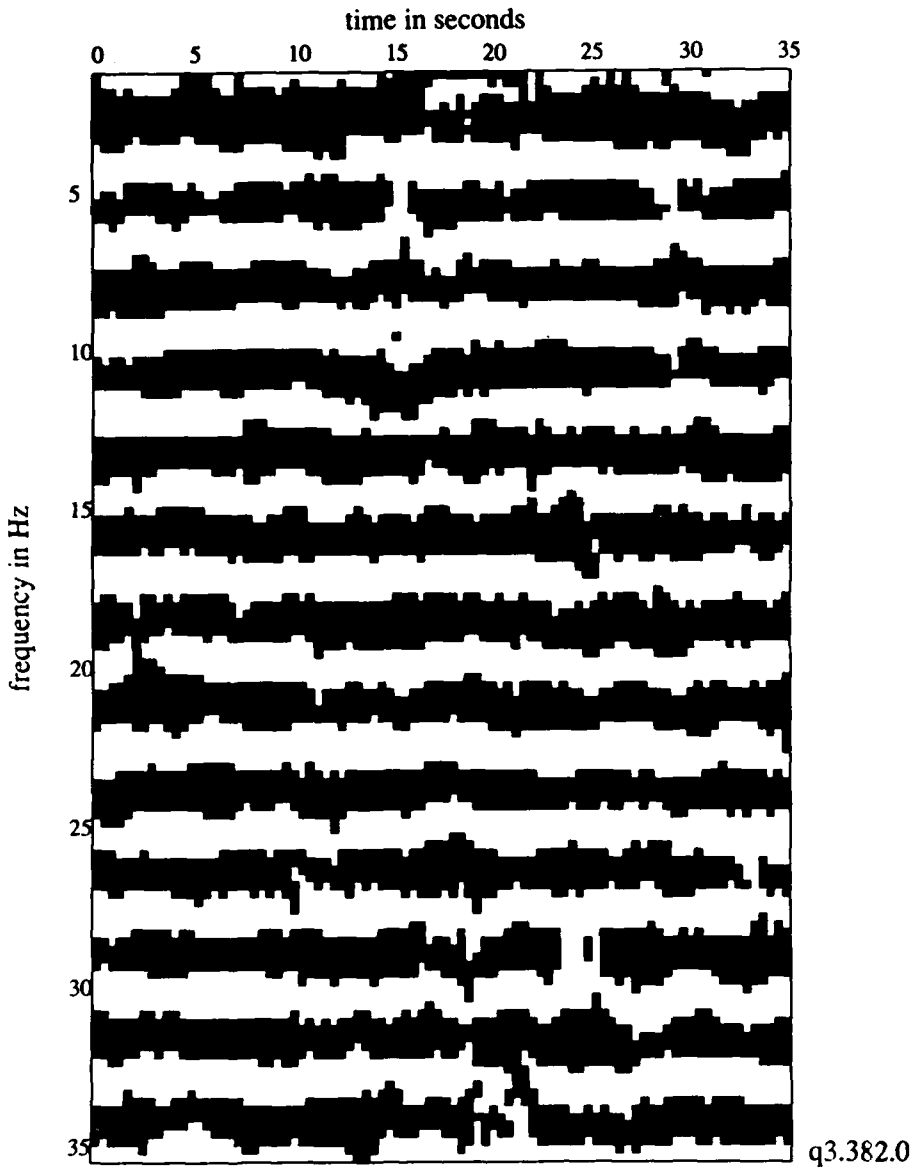
time in seconds
0 5 10 15 20 25 30 35
frequency in Hz
5 10 15 20 25 30 35
q3.382.0

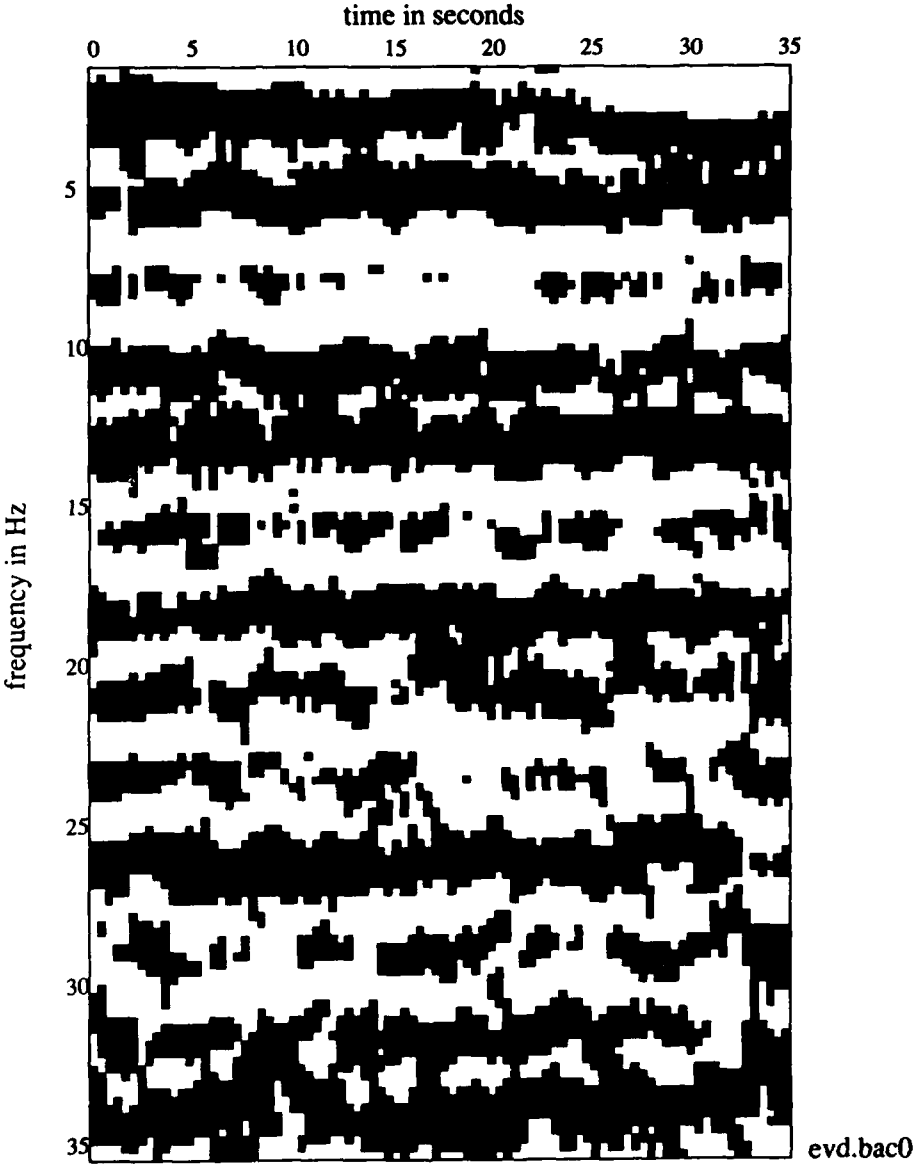
time in seconds
0 5 10 15 20 25 30 35
frequency in Hz
5 10 15 20 25 30 35
evd.bac0

Figure 13

CHAPTER 4

THE TIME-FREQUENCY CHARACTERISTICS OF QUARRY BLASTS, EARTHQUAKES AND CALIBRATION EXPLOSIONS RECORDED IN SCANDINAVIA AND KAZAKHSTAN U.S.S.R.

Michael A.H. Hedlin

John A. Orcutt

J. Bernard Minster

Harold Gurrola

Institute of Geophysics and Planetary Physics (A-025)

Scripps Institution of Oceanography, La Jolla CA, 92093

prepared for the 1989 DARPA/AFGL Seismic Research Symposium

OBJECTIVE

The primary objective of this study is to develop an algorithm that will routinely discriminate between ripple-fired mine explosions (events that consist of several sub-explosions closely grouped in space and time) and all other seismic events (including earthquakes and single-event explosions). To develop the algorithm and test its independence from local mining practice and geologic setting we have selected two independent data sets (data collected by the NORESS array in southern Norway and by sensors deployed in Kazakhstan U.S.S.R.). To assess the relative value of these two data sets for this type of work we have conducted a comparative analysis of ambient noise levels at these two sites.

SUMMARY

A commonly used technique in mining practice, known as ripple-firing, involves the detonation of a number of sub-explosions offset from each other by small distances and times. The intent of this procedure is to enhance fracturing of the rock and reduce ground motion in areas proximal to the mine. The observation has been made by several researchers (Smith, 1989, Stump and Reamer, 1988, Baumgardt and Ziegler, 1988) that such events tend to give rise to seismic coda possessing highly colored spectra. That is, spectra enriched in power at certain preferred frequencies and depleted in power at other frequencies.

This spectral color is certainly due to the interaction of the time-offset wavefields produced by each sub-explosion. The manner in which the wavefields interact is not known, and undoubtedly is largely non-linear, however we feel that simple linear theory is sufficient to describe the most obvious result, specifically the pronounced spectral modulation. Briefly, the regular repetition and superposition of similar seismic motions in the time domain leads to regular amplification and suppression of power in the frequency domain. Furthermore, as is demonstrated by Hedlin et al (1989) in the limit where all sub-explosions occur at the same point in space, the spectral features are independent of time in the coda. Because we predict that ripple-fired events should give rise to pronounced, time-independent, spectral features, we have found it useful to calculate frequency-time displays of the seismograms, known as sonograms.

In figure 1 we display the vertical component time series, and sonogram, of a 20 T single-event calibration explosion detonated and recorded in Kazakhstan U.S.S.R. in 1987. The recording was made by a GS-13 seismometer sampled at 250 s^{-1} and deployed at the surface near the town of Bayanaul. The energy in the coda from this event is distributed fairly randomly as a function of frequency and time. There is no evident organization of the energy into time-independent bands. In figure 2 we show the result of the same processing techniques applied to an unidentified event that occurred 264 km from the station. The spectra of this event are distinctly modulated and furthermore the

energy is very clearly organized into time-independent bands. We strongly suspect that this event was a ripple-fired quarry blast.

We have found it useful to suppress the large scale structure provided by the compressional and shear onsets as well as the high frequency spectral falloff and thus enhance any time-independent features that may be present by comparing two versions of each spectral estimate. As figure 3 illustrates we compare a relatively unsmoothed version of the original spectral estimate with one that is heavily smoothed. We represent all regions of the sonogram matrix where the local power is high relative to the *regional* power by a value of +1 (denoted as white for display purposes) and where it is low by a -1 (black). In this manner we discard the bulk of the magnitude information and "flatten" the original sonogram matrix to a very simple, yet informative, binary matrix. In figures 4 and 5 we display the binary sonogram matrices corresponding to the originals displayed in figures 1 and 2 respectively. This method of reducing sonogram matrices to binary form provides simple patterns that allow visual discrimination between mine explosions and single-event explosions.

To extend this work we have examined data collected by the NORESS array in southern Norway. Our goal was to discover whether earthquakes can be as easily distinguished from mine blasts as single-event explosions. We also wanted to determine if the algorithm would be successful in a different geologic setting and in an area of different mining practice than present in central Asia. We have concentrated our efforts thus far on events known to either be earthquakes or mine explosions. The NORESS array data have a distinct advantage over the Kazakh data since typically 30 sensors simultaneously record each event. The obvious disadvantage is that the array data are only digitized at 40 s^{-1} and thus cannot resolve spectral features above 20 Hz. In figure 6 we display the sonogram of a presumed earthquake which occurred 454 km from the array. This display has been produced by stacking the amplitude spectra from each of the 24 vertical channels after converting each spectrum to binary form and assuming infinite phase velocity. The compressional onset occurs at 12 seconds. As expected, little structure can be discerned other than the microseismic noise below 2 Hz. Figure 7 was computed from the coda produced by a Blasjo mine explosion which occurred

302 km from the array. The compressional onset occurs at 15 seconds and is followed by a very obvious time-independent banding. The time-independent structure present prior to the onset is due to long lived spectral lines in the noise and does not correlate with the spectral features present in the coda.

In figures 8 and 9 we display the ambient noise levels present at the high-frequency element of the NORESS array (site NRF0 ; sampling at 125 s^{-1}) and in the boreholes at the Kazakh sites near the towns of Bayanaul and Karkaralinsk. All seismometers recorded the vertical component of velocity and were deployed at 60, 66 and 99 meters depth respectively. The noise levels are represented by three curves which illustrate the average and 95% confidence limits of acceleration power. Above 1 to 2 Hz the Kazakh noise levels are generally slightly (up to 10 dB) higher. The apparent rise in power above 40 Hz at the NORESS array is probably not natural but due to digitization noise. Below 1 to 2 Hz the NORESS noise levels are significantly higher than in central Asia. Although these curves do not extend across the entire microseism band, the suggestion is that microseismic noise levels are higher in Norway than in central Asia. This seems intuitively reasonable given the relative proximity of the NORESS array to an ocean. This appears to be a long-range extension of the observation made by Hedlin et al (1988) that microseismic noise levels appeared to be inversely correlated with the distance from the shoreline in the range of 1 to 100 km.

CONCLUSIONS AND RECOMMENDATIONS

We observe significant differences between ripple-fired mine-explosions and earthquakes and single-event explosions. The close grouping in space and time of several sub-explosions appears to be responsible for the impression of prominent time-independent spectral modulation on the frequency spectrum of the resultant coda.

We plan to extend further the pattern-based discriminant by reducing the binary sonogram matrices to scalars which reflect the presence or absence of time-independent modulation.

It appears that lower microseismic noise levels will be realized at sites far removed from large bodies of water.

REFERENCES

Baumgardt, D. R. & Ziegler, K. A., 1988. Spectral Evidence for Source Multiplicity in Explosions: Application to Regional Discrimination of Earthquakes and Explosions. *Bull. seism. Soc. Am.*, **78**, 1773-1795.

Hedlin, M. A. H., Fels, J. F., Berger, J., Orcutt, J. A. & Lahav, D., 1989, Seismic Broadband Signal and Noise Levels on and Within the Seafloor and on Islands, *Proceedings of a Workshop on Broad-Band Downhole Seismometers in the Deep Ocean, W.H.O.I., Woods Hole, MA, April 26-28, 1988.*

Hedlin, M. A. H., Minster, J. B. & Orcutt, J. A., 1989, The Time-Frequency Characteristics of Quarry Blasts and Calibration Explosions Recorded in Kazakhstan U.S.S.R., *Accepted for publication in the Geophysical Journal.*

Smith, A. T., 1989. High-Frequency Seismic Observations and Models of Chemical Explosions: Implications for the Discrimination of Ripple-Fired Mining Blasts. *Submitted for publication in the Bull. seism. Soc. Am.*

Stump, B. W. & Reamer, S. K., 1988. Temporal and Spatial Source Effects from Near-Surface Explosions. *Paper presented at the 10th annual AFGL/DARPA seism. Res. Symp.*

FIGURE CAPTIONS

Figure 1. Seismogram resulting from a single-event calibration explosion recorded at a range of 157 km by the vertical surface seismometer at Bayanaul and corresponding sonogram.

Figure 2. Seismogram resulting from a suspected mine-explosion recorded at a range of 264 km by the vertical surface seismometer at Bayanaul and corresponding sonogram.

Figure 3. Original spectral estimate and two versions, one relatively unsmoothed and the other relatively highly smoothed. This figure is intended to illustrate the means by which we reduce each spectral estimate to a "binary spectral estimate". The regions of locally high power are represented by a +1 (white). Regions deficient in power are represented by a -1 (black).

Figure 4. Vertical component binary sonogram matrix corresponding to the single-event calibration explosion recorded at Bayanaul (refer to figure 1). The first 35 seconds of coda after the compressional onset are represented in this and the following figure.

Figure 5. Vertical component binary sonogram matrix corresponding to the suspected mine-explosion recorded at Bayanaul.

Figure 6. Vertical component sonogram matrix corresponding to a presumed earthquake recorded at the NORESS array.

Figure 7. Vertical component sonogram matrix corresponding to a Blasjo mine explosion recorded at the NORESS array.

Figure 8. The average and 95% confidence limits of ambient noise levels recorded at the NORESS array and near the town of Bayanaul in Kazakhstan, U.S.S.R.

Figure 9. The average and 95% confidence limits of ambient noise levels recorded at the NORESS array and near the town of Karkaralinsk in Kazakhstan, U.S.S.R.

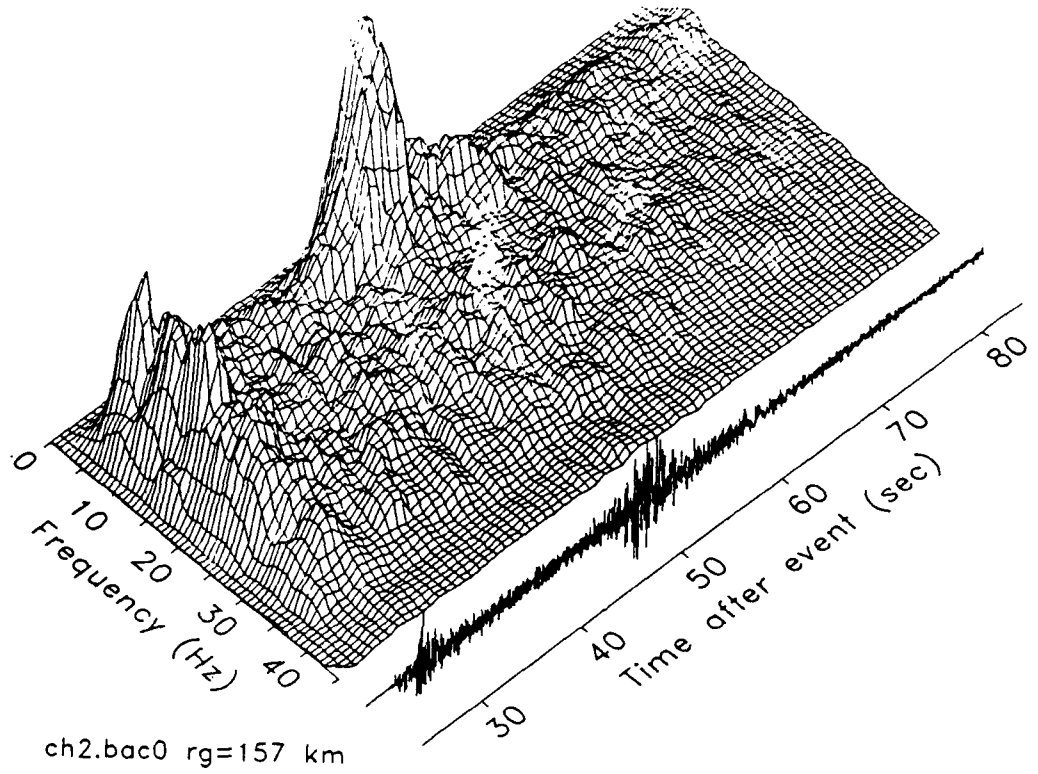

Figure 1. Seismogram resulting from a single-event calibration explosion recorded at a range of 157 km by the vertical surface seismometer at Bayanaul and corresponding sonogram.

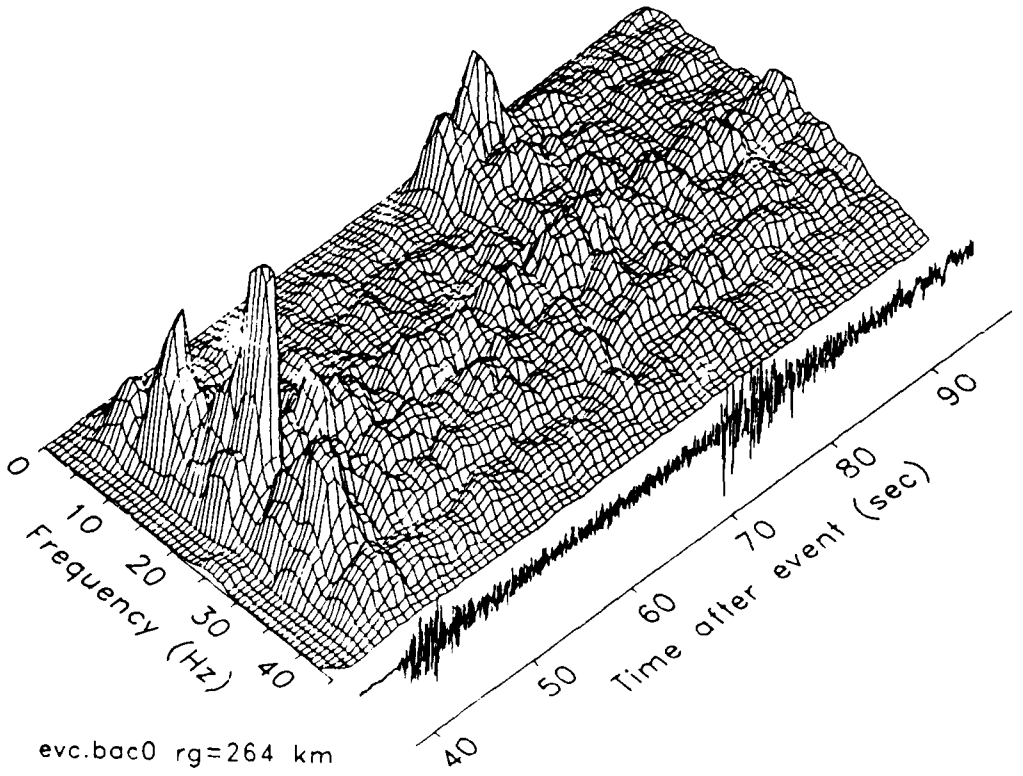

Figure 2. Seismogram resulting from a suspected mine-explosion recorded at a range of 264 km by the vertical surface seismometer at Bayanaul and corresponding sonogram.

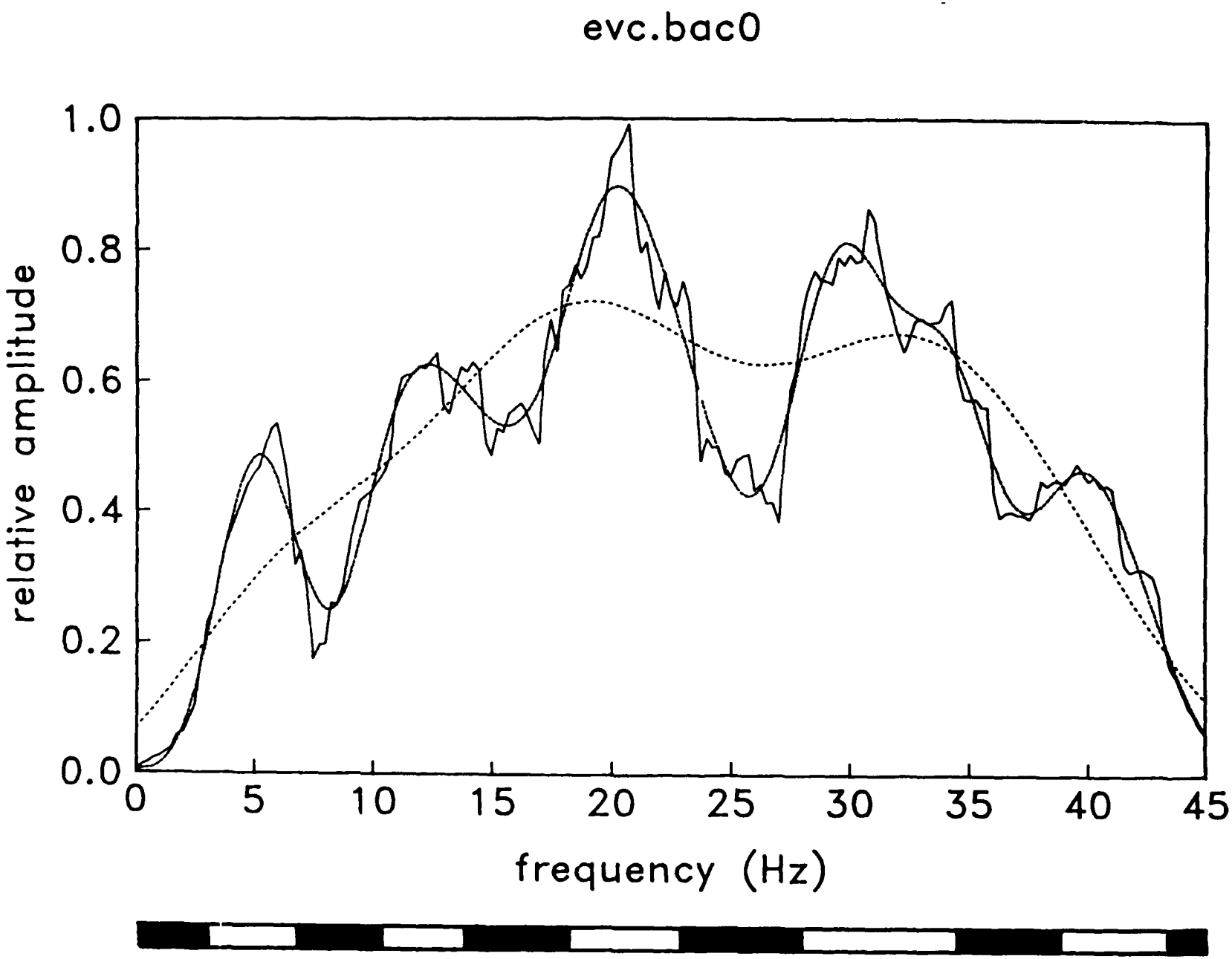

Figure 3. Original spectral estimate and two versions, one relatively unsmoothed and the other relatively highly smoothed. This figure is intended to illustrate the means by which we reduce each spectral estimate to a "binary spectral estimate". The regions of locally high power are represented by a +1 (white). Regions deficient in power are represented by a -1 (black).

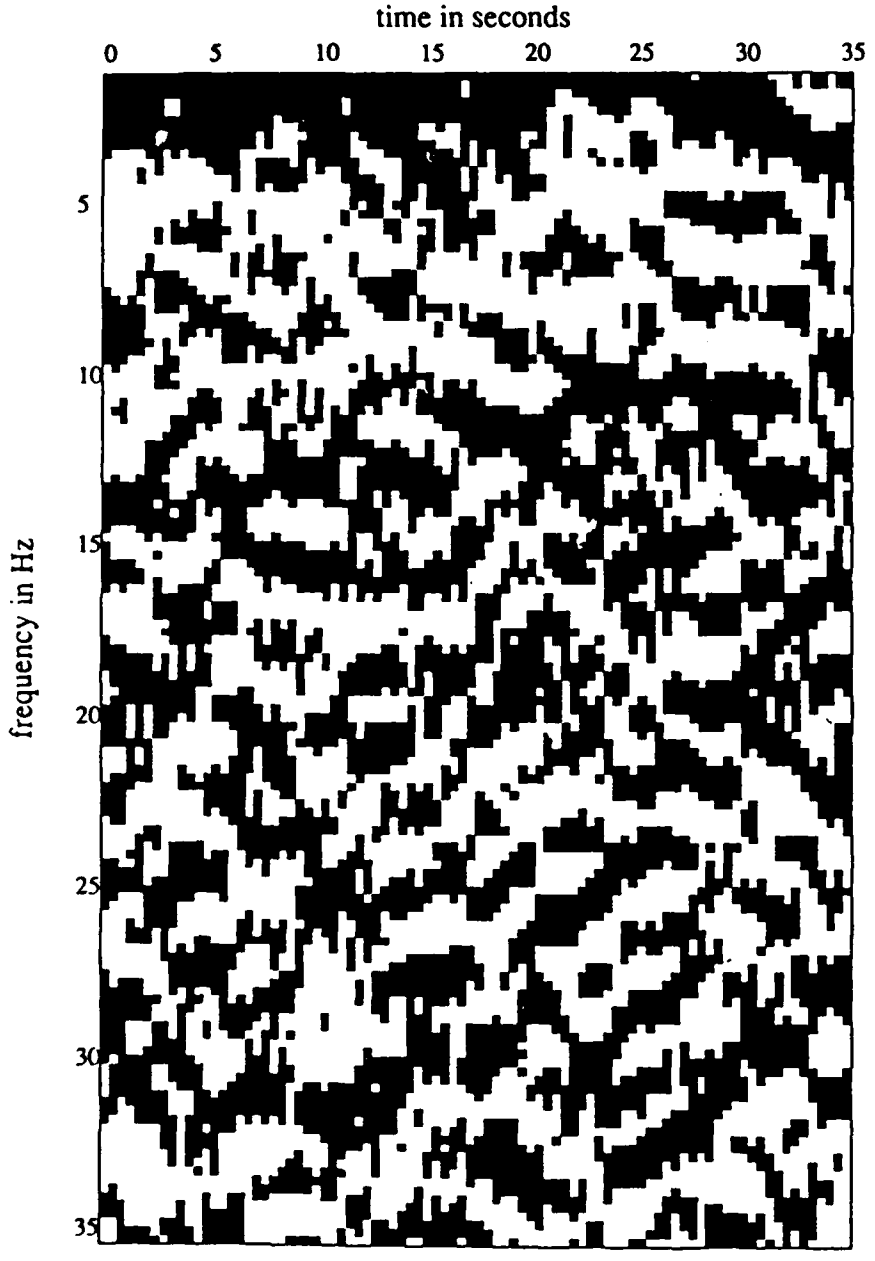

Figure 4. Vertical component binary sonogram matrix corresponding to the single-event calibration explosion recorded at Bayanaul (refer to figure 1). The first 35 seconds of coda after the compressional onset are represented in this and the following figure.

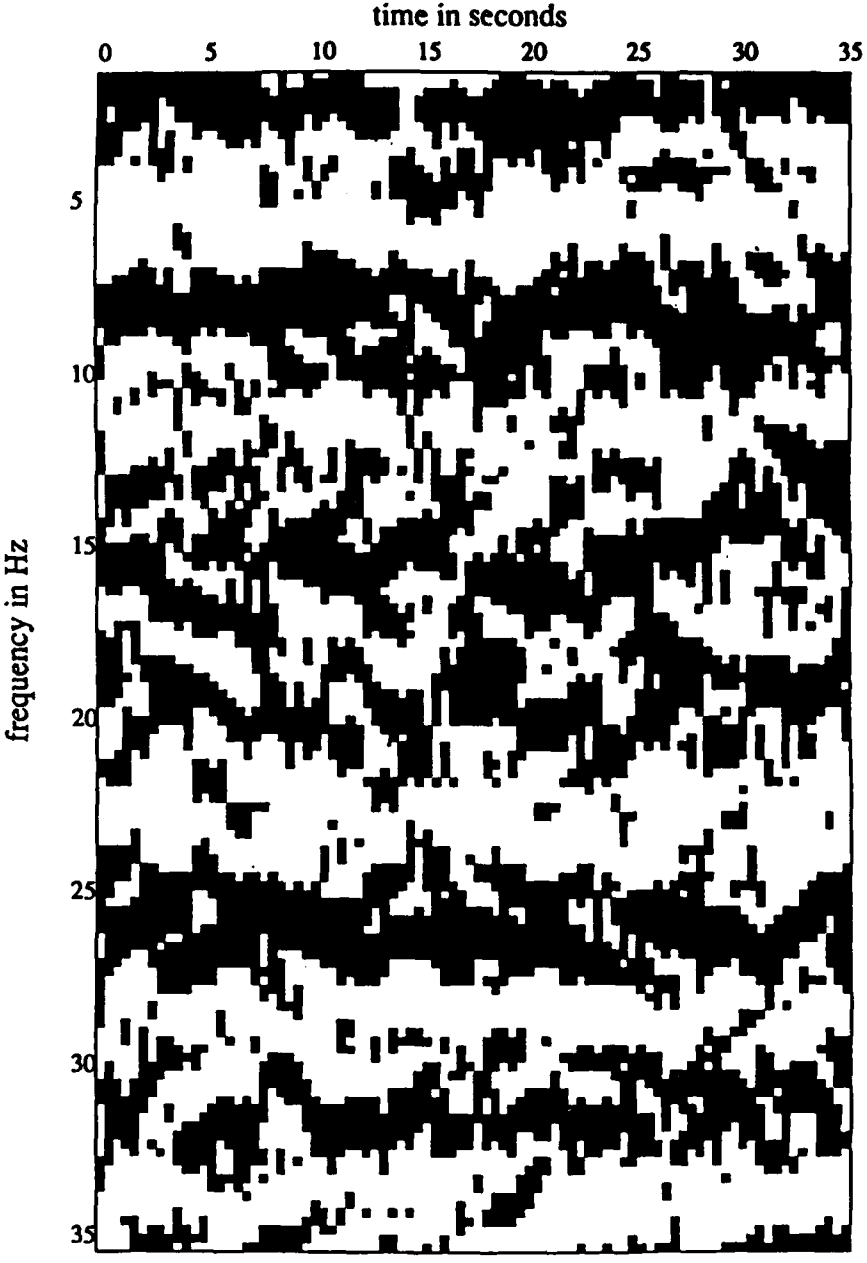

Figure 5. Vertical component binary sonogram matrix corresponding to the suspected mine-explosion recorded at Bayanaul.

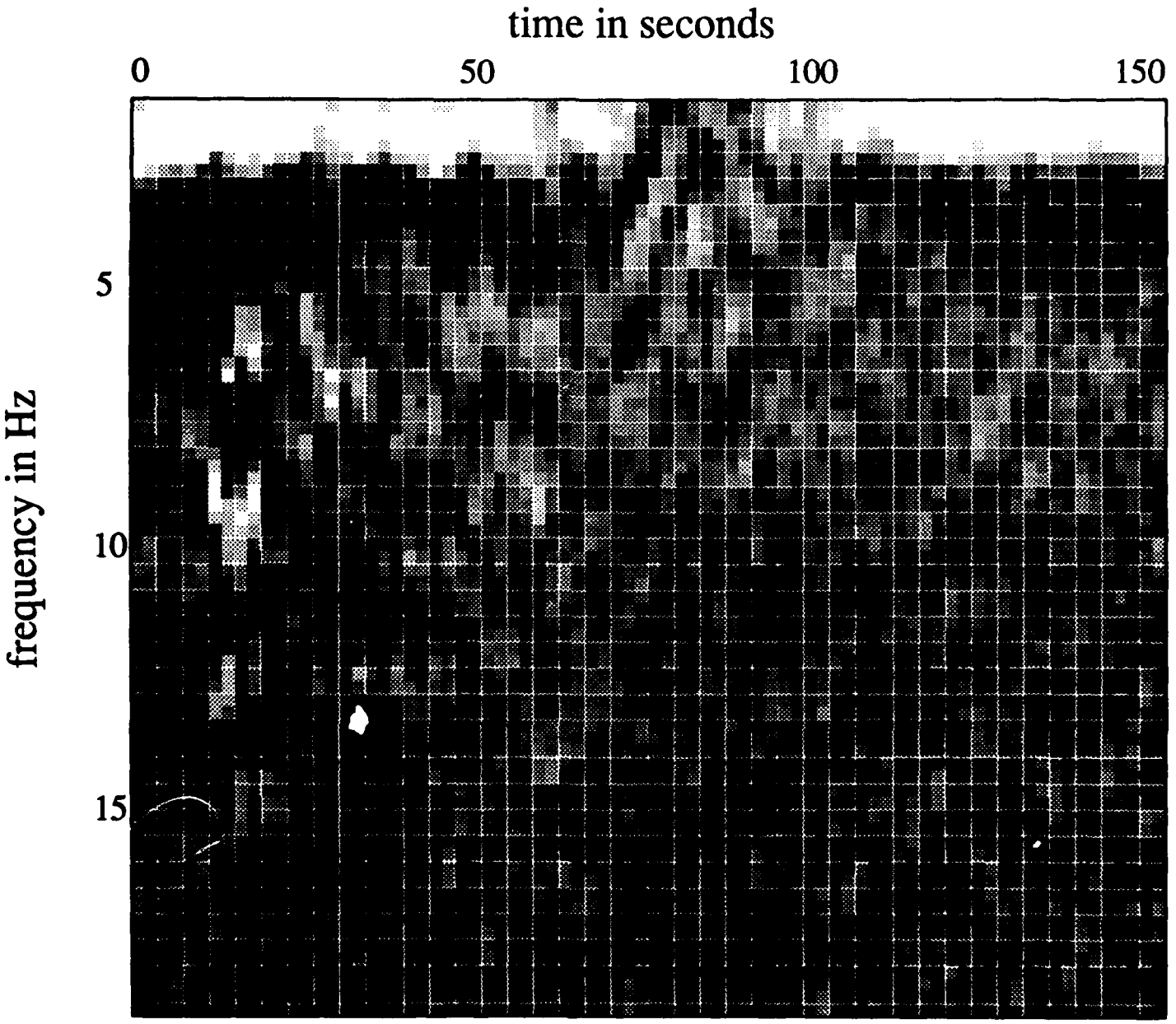

Presumed earthquake 0422 - 454 km from NORESS

Figure 6. Vertical component sonogram matrix corresponding to a presumed earthquake recorded at the NORESS array.

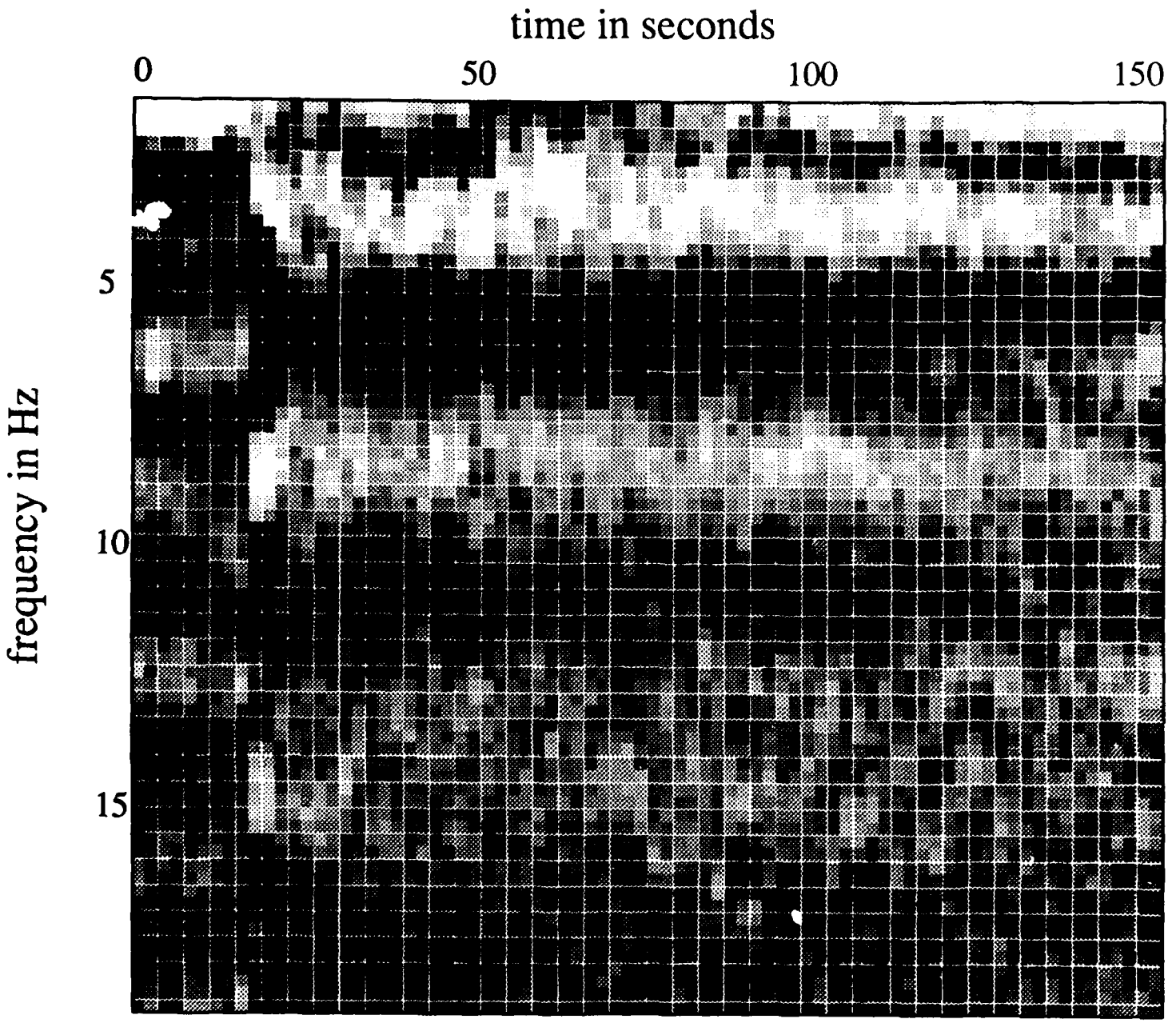

Figure 7. Vertical component sonogram matrix corresponding to a Blasjo mine explosion recorded at the NORESS array.

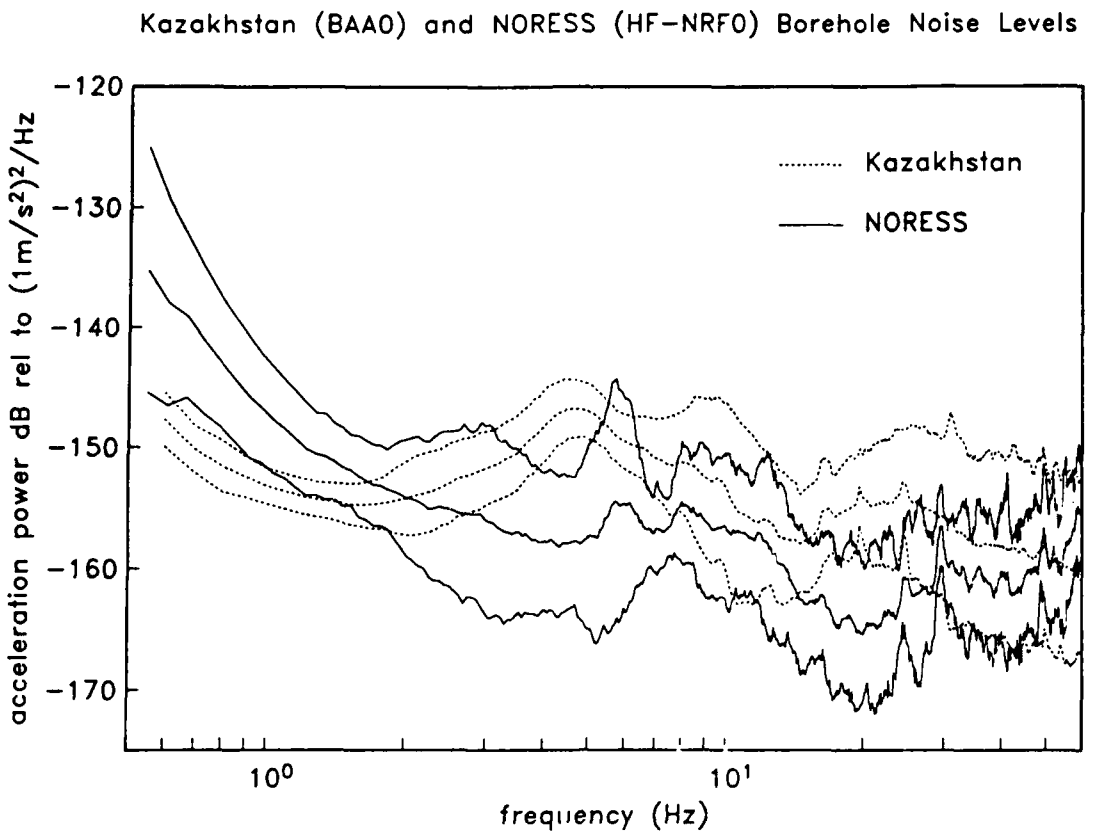

Figure 8. The average and 95% confidence limits of ambient noise levels recorded at the NORESS array and near the town of Bayanaul in Kazakhstan, U.S.S.R.

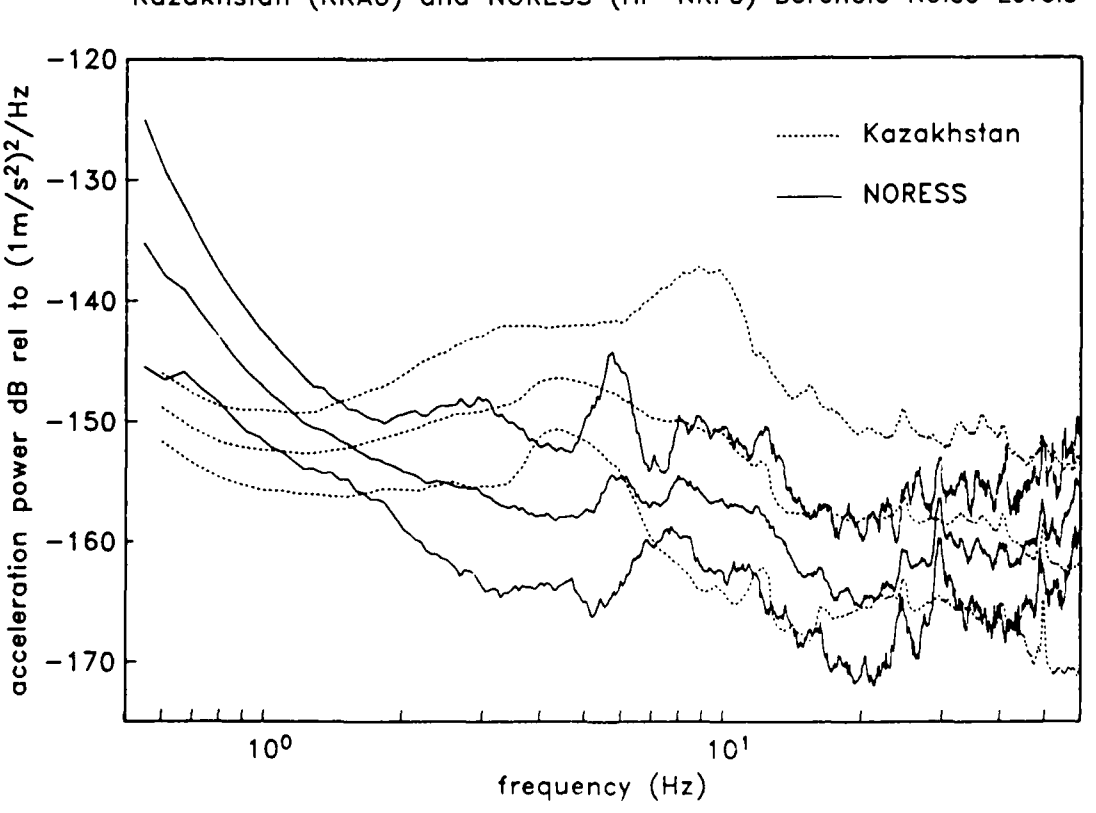

Figure 9. The average and 95% confidence limits of ambient noise levels recorded at the NORESS array and near the town of Karkaralinsk in Kazakhstan, U.S.S.R.

CHAPTER 5

THE SPECTRAL CHARACTERISTICS OF SEISMIC CODA RECORDED BY OCEAN BOTTOM SEISMOMETERS AND HYDROPHONES

Michael A.H. Hedlin and John A. Orcutt

Manuscript in preparation for submission to the Geophysical Research Letters

ABSTRACT

We observe significant modulation in spectra computed from seismic coda recorded by seafloor seismometers and hydrophones deployed in the S.W. Pacific and in the Wake Island Hydrophone array. These modulations are consistent with those present in synthetic spectra, generated using an Earth model consisting of homogeneous layers, and consistent with the locations of spectral peaks we predict using simple layer resonance theory. Our observations agree with those made by Sereno and Orcutt (1985 a,b) and are consistent with their model of coda generation by layer resonance.

INTRODUCTION

For years researchers have recorded seismic energy that has propagated through the oceanic lithosphere. Distinguishing features of this energy are that high frequencies are retained at teleseismic ranges from the source (Walker et al, 1978). In addition long coda are observed following the compressional and shear onsets (Walker et al, 1983). It is widely accepted that this energy remains within the oceanic lithosphere (Sereno, 1986); however, the mechanism by which the seismic coda is generated has not been established. Richards and Menke (1983) and Menke and Chen (1984) propose that scattering by small scale inhomogeneities is an effective mechanism for the generation of long coda. Recently an alternative theory was proposed by Sereno and Orcutt (1985a,b). They suggest that resonance of energy in the water column and underlying, low velocity, sediment layer is sufficient to generate the long coda observed. A likely feature of coda produced by such a mechanism is that is should possess a spectral scalloping, or regular modulation in the frequency domain, produced by the superposition of resonant phases in time. The objective of this paper is to reproduce the results of Sereno and Orcutt (1985a,b) by observing this spectral scalloping.

RESONANCE THEORY

The theory behind the generation of seismic coda by layer resonance was developed by Sereno and Orcutt (1985b) and thus only a terse description is given here. The authors demonstrate the significant influence of low velocity horizons in the oceanic environment on coda duration and amplitude. This layer resonance enriches the spectrum of the coda at certain equispaced eigenfrequencies, determined by the layer thickness and velocity. Considering a relatively simple case in which a wavelet w(t) is reverberating in a single low velocity surface layer, the linear sum of all reverberations x(t) equals:

$$x(t) = w(t) * \left[\frac{1}{T} III\left(\frac{t}{T}\right) \cdot e^{-\alpha|t|} \cdot H(t) \cdot e^{-i\pi t/T} \right] \qquad (1)$$

The time between successive reverberations is represented by T and, to a good

approximation, equals the two-way vertical travel time in the horizon. The "shah" function is tapered exponentially to simulate the effect of attenuation and is multiplied by the Heaviside step function to exclude any acausal energy. The final exponential is required by the π phase shift incurred by reflection at the free surface.

By Fourier transforming the preceding equation the authors found that the spectrum of the original wavelet is multiplied by an infinite set of staggered tapering functions which decay at a rate controlled by and proportional to the attenuation parameter a. The amplitude spectrum of the sum of wavelets is given by:

$$|\tilde{X}(f)| = |\tilde{W}(f)| \cdot \left| \text{III}(fT + \frac{1}{2}) * \left[\frac{\alpha - i2\pi f}{(\alpha^2 + 4\pi^2 f^2)} \right] \right| \qquad (2)$$

The thicker - or equivalently, the slower - the horizon the more closely spaced the spectral highs will be.

In the Oceanic setting there are two low velocity strata, the water column and the underlying sediment layer. It is resonance in these horizons that Sereno and Orcutt (1985a,b) invoked in their explanation of the origin of the significant Pn and Sn coda. It is modulations from these resonances that we seek in the real and synthetic data sets considered below as we attempt to confirm their conclusions.

DATA SETS

The model proposed by Sereno and Orcutt (1985a,b) to explain the propagation of the Pn phase, and the development of long coda, was established primarily using data collected by Ocean Bottom Seismometers (OBS's) and Hydrophones. This data set was collected during Scripps' Ngendei expedition in the South-West Pacific in 1983 (Orcutt et al, 1987). In this paper we compare the results of this experiment with those of an independent data set collected by near-seafloor sensors in the Wake Island Hydrophone (WIH) array (McCreery, 1987). We have obtained recordings of 70 teleseismic events made by this array. One advantage of this data set is that each event is simultaneously recorded by several (usually 5) seafloor sensors and thus we can gain a limited

improvement in signal to noise ratios by stacking in the time-domain. The slight disadvantage is that the sensors are deployed in the water column. We investigate the feasibility of testing a crustal propagation model using sensors uncoupled from the seafloor and we compare synthetic seismograms computed with receivers in both the water column and the underlying sediment layer. We have used the Wavenumber Integration algorithm for this purpose (Luco and Apsel, 1983; Apsel and Luco, 1983). This algorithm requires that the Earth be modeled as a stack of homogeneous layers. It is able to include all phases resulting from the interaction of the propagating wavefield with all interfaces in the model and the free surface. It is thus ideal as a tool to predict the likely features of coda generated simply by layer resonance. We have used the constant Q Ngendei model proposed by Sereno (1986). This model is distinguished by a 5.5 km thick water column and a low velocity (α=1.6 km/s, β=0.116 km/s) 70 m thick sediment layer.

SYNTHETIC RESULTS

We have computed synthetic Green's functions corresponding to a lateral offset between the source and receivers of 1000 km. To carry out the actual computation two separate sources, each consisting of vertical and horizontal point forces, were located at the sediment/water interface and 0.5 m above the interface in the water column. The receiver was located at 15 km depth. Using reciprocity we obtain the response to a source buried at 15 km when observed at the shallower depths (Shaw and Orcutt, 1984). These receiver locations enable us to predict the relative abilities of hydrophones and seafloor seismometers for sensing the resonance of energy in the sediment layer and water column.

In figure 1 we display the vertical normal stresses due to a vertical point force (Σ_{zz0}) at both receiver depths. We expect this Green's function should be strongly influenced by the propagation of high phase velocity compressional energy. Frequency and time representations of these functions are displayed in the upper and lower halves of the figure respectively. The portions of the time series used in computing the spectra are indicated by horizontal bars in the lower figures. The spectral estimates, computed using a multi-taper algorithm (Thompson, 1982), consist of the sum of 5 sub-estimates, computed

using a time-bandwidth product of 3.0. The upper and lower spectra, corresponding to the receivers at 5.5495 and 5.5000 km depth respectively, both are dominated by a regular modulation with a spacing of 0.136 Hz. This modulation was explained by Sereno (1986) as being due to the resonance of acoustic energy in the water column. The predicted eigenfrequencies corresponding to this resonance are indicated by the vertical dashed lines. There is a striking correlation between synthetically computed and predicted spectral peaks. It is clear that this Green's function is strongly influenced by the resonance of acoustic energy in the water column. By examining the time series there is clearly a periodicity of roughly 7 seconds (the two way travel time of acoustic energy in the water column) following the onset of Pn energy about 125 seconds after the event. From this exercise we conclude that sensors on the seafloor, and above in the water column, should be sensitive to the resonance of acoustic energy in the water column.

In figure 2 we display the same Green's function, however the time-window considered was shorter (20 sec) and restricted to the time immediately following the Pn onset. We expect that this Green's function should also be influenced by compressional energy resonance in the sediment layer. The spectra and time series in this figure are arranged in the same manner as those in figure 1, however the spectral estimates were made using 7 sub-estimates computed using a time-bandwidth product of 4.0. We observe a broad power high centered close to the eigenfrequency predicted for the resonance of compressional energy in the sediment layer. The spectral rolloff occurring above 8 Hz is due to the taper applied when converting the green's functions from the frequency domain to the time domain and is not due to resonance. The predicted frequency spacing of this modulation is 11.4 Hz and thus the synthetics computed to a nyquist frequency of only 9 Hz only illustrates the first, broad, spectral peak.

In figure 3 we illustrate the same results for the vertical normal stress due to a horizontal point force (Σ_{zz1}). We expect this Green's function should be greatly influenced by radial particle motion and thus should be strongly dependent on the resonance of shear energy in the sediment layer. We have indicated the frequencies of the predicted spectral peaks by the dashed vertical lines in the upper half of the figure (the frequency spacing is 0.83

Hz). We have computed spectra from 90 seconds of the Sn coda. The lower spectrum was computed from the receiver located at the sediment/water interface. As expected it is strongly influenced by shear wave, sediment layer, resonance. The green's function in the water column, just 0.5 m above, is clearly oblivious to this resonance. The spectrum is influenced by acoustic, water layer, resonance and little else. By inspection of the Green's functions in the time-domain, the water multiples are obvious in the water column but much inter-multiple energy due to sediment layer resonance, that is present in the lower time series, is absent. We believe there is a simple explanation for this. In figure 4 we display the modulus of the transmission coefficient for upward traveling energy, converting from shear to compressional propagation at the sediment/water interface. Although the transmission coefficient is a monotonically increasing function of ray parameter, it remains below 0.007 over the range of slownesses we expect to dominate the Pn and Sn coda (0.12 to 0.35 s/km). As one would intuitively expect, considering the particle motions involved, shear energy does not readily convert to compressional energy at the boundary between these low velocity horizons. We conclude that the WIH dataset is inappropriate when seeking evidence of shear wave resonance in the sediment layer and we do not consider it further.

RECORDED RESULTS

We now consider actual coda recorded by the Wake Island Hydrophones and the Ocean Bottom Seismometers and Hydrophones deployed during the Ngendei expedition. In figure 5 we display the spectra and time series corresponding to an event roughly 1000 km from the receivers. We indicate by the dashed vertical lines the predicted eigenfrequencies corresponding to compressional energy resonating in the sediment layer (assuming a net π phase shift between successive multiples). The lower spectrum, computed from 50 seconds of Pn coda recorded by the vertical component seismometer (pictured at the bottom), displays a clear modulation consistent with the prediction at frequencies below 40 Hz (the point at which signal falls into noise). The spectrum computed from the same portion of the Pn coda recorded by the hydrophone displays a similar, though less evident, modulation; however, the positions of the power highs suggest that successive compressional sediment layer multiples are in phase. The power highs are consistent with the second,

solid, set of vertical lines computed assuming no net phase shift. This phenomenon is not restricted to this event but is common to all we have examined that have induced the resonance of compressional energy in the sediment layer. It is possible to induce compressional energy resonance in the sediment layer by introducing energy from above, or below. As is discussed by Sereno (1986), arrivals from below are followed by an infinite sequence of echos each π phase shifted from its immediate neighbors in time. The cumulative modulus of reflection incurred by bouncing at the sediment/water and then the sediment/crust interfaces is, assuming the constant Q Ngendei model, 0.029. The primary arrival (with an amplitude of 1.0) is followed by a second with an amplitude of 0.029, and a third of .00084 and so on - the echos die away quickly. Significant resonances should be induced by downward traveling energy that has reflected at the free surface. The primary downward traveling arrival will pass the sediment water interface and be followed by an echo after the energy reflects at the sediment/crust interface. Energy propagating with a phase velocity of 8.2 km/s undergoes no phase shift either in transmitting into the sediment layer, or by the reflection at the top of the crust, and thus the primary arrival and its echo should be in phase. The resultant spectral modulation will have peaks at multiples of the frequency of the first (see the solid vertical lines in figure 5). The echo should have an amplitude of 0.79 relative to the initial arrival. This form of resonance is nearly truncated after the first echo. All subsequent echos have insignificant amplitudes relative to the first. For this theory to be tenable the observed "anti-correlation" between the hydrophone and seismometer spectra must not be present in the portion of the coda after the Pn onset and before the arrival of the first multiple off the free surface (a span of 7.3 seconds). In figure 6 we look at the vertical component seismometer and hydrophone spectra computed from the initial 6.5 seconds of coda after the Pn onset of an event recorded by OBS karen. Virtually no broad modulation can be discerned in either of these spectra (there is only a slight suggestion of spectral peaks at 5.7 and 17.1 Hz), however there is a clear coincidence of smaller scale spectral features. When we look at the time span from 7.0 to 13.5 seconds after the Pn onset (figure 7) we see that the modulation is much more apparent and a distinct anti-correlation between seismometer and hydrophone spectra is present. In this time span the energy from the free surface has had enough time to return to the seafloor. There is likely a competition between two types

of compressional sediment layer resonances. One that includes an infinite sequence of quickly decaying echos that are π phase shifted from their neighbors, and the other consisting of only a single significant echo that is in phase with the primary arrival. It appears that in the Ngendei dataset the latter form of resonance is dominant at the level of the hydrophone and the former dominates the seismometer - coupled to the sediment layer. In the synthetics it appears that the former type of resonance dominates both the sensor in the water column and the one at the interface.

The event in figure 8 was recorded by the WIH array. It was an event with mb of 6.0 and occurred at a depth of 159 km and a range of 2170 km. The spectra display signal and noise levels and were computed from the portions of the time series delineated by the horizontal bars. The time series obtained from each of the 6 seafloor sensors that recorded this event were stacked while beamforming for the Pn phase. Signal remains above noise in the Pn coda produced by this event to a frequency of 22 to 25 Hz. A subtle, broad, modulation is evident at lower frequencies and corresponds to the eigenfrequencies predicted assuming no net phase shift between successive water multiples. The spacing of these power highs suggests a two way travel time in the sediment layer of roughly 0.15 seconds.

In figure 9 we display the same event pictured in figure 5. We've magnified the frequency scale of the upper half of the figure to illustrate the fine scale modulation consistent with resonance of acoustic energy in the water column (see the vertical dashed lines). Both spectra have a fine modulation; however, the upper spectrum, computed from the hydrophone channel, possesses a more pronounced modulation at this scale. We see a similar result when examining a second event recorded by the WIH array (figure 10). This event was an mb 5.4 earthquake, 33 km deep which occurred at a range of 2057 km from the WIH array.

CONCLUSIONS

We have observed significant spectral modulation present in the coda of events recorded by seafloor seismometers and hydrophones and near-seafloor sensors in the Wake Island Hydrophone array. These modulations are

pronounced and consistent with those present in synthetic spectra in which we know the regular spectral peaks are due to layer resonance only. Our results substantiate the conclusions made by Sereno and Orcutt (1985a,b) that layer resonance is a significant, perhaps dominant, source of coda in the oceanic environment.

ACKNOWLEDGMENTS

We thank Boomer Baumgart at the Center for Seismic Studies for supplying us with the Wake Island Hydrophone data.

REFERENCES

Apsel, R.J. and Luco, J.E., 1983, On the Green's Functions for a Layered Half-Space, Part II, Bulletin of the Seismological Society of America, 73, 931-951.

Luco, J.E. and Apsel, R.J., 1983, On the Green's Functions for a Layered Half-Space, Part I, Bulletin of the Seismological Society of America, 73, 909-929.

McCreery, C.S., 1987, Ambient Infrasonic Ocean Noise and Wind, Hydrophone Investigations of Earthquake and Explosion Generated High-Frequency Seismic Phases, Progress and Forecast Report to the Air Force Office of Scientific Research, 1 May, 1987.

Menke, W. and Chen, R., 1984, Numerical Studies of the Coda Falloff Rate of Multiply Scattered Waves in a Randomly Layered Media, Bulletin of the Seismological Society of America, 74, 1605-1621.

Orcutt, J.A., Moore, R.D., Jordan, T.H., 1987, Description and Performance of the Scripps Ocean Bottom Seismographs during the Ngendei Experiment, Initial Reports of the Deep Sea Drilling Project, 88/91, 347-356.

Richards, P. and Menke, W., 1983, The apparent Attenuation of a Scattering Medium, Bulletin of the Seismological Society of America, 73, 1005-1021.

Sereno, T.J., 1986, The Propagation of High Frequency Seismic Energy Through Oceanic Lithosphere, PhD Thesis, University of California at San Diego, 168 pp.

Sereno, T.J. and Orcutt, J.A., 1985a, Synthetic Seismogram Modelling of the Oceanic Pn Phase, Nature, 316, 246-248.

Sereno, T.J. and Orcutt, J.A., 1985b, Synthesis of Realistic Oceanic Pn Wave Trains, Journal of Geophysical Research, 90, 12755-12776.

Shaw, P. and Orcutt, J.A., 1984, Propagation of PL and Implications for the Structure of Tibet, Journal of Geophysical Research, 89, 3135-3152.

Thompson, D. J., 1982. Spectrum Estimation and Harmonic Analysis. *IEEE Proc.*, **70**, 1055-1096.

Walker, D.A., McCreery, C.S. and Sutton, G.H., 1978, Spectral Analyses of High-Frequency Pn and Sn Phases Observed at Great Distances in the Western Pacific, Science, 199, 1333-1335.

Walker, D.A., McCreery, C.S. and Sutton, G.H., 1983, Spectral Characteristics of High-Frequency Pn,Sn Phases in the Western Pacific, Journal of Geophysical Research, 88, 4289-4298.

FIGURE CAPTIONS

Figure 1. Synthetic Green's functions (Σ_{zz0}) and corresponding frequency power spectra at depths of 5.5495 and 5.5000 km due to a vertical point force buried 15 km at a range of 1000 km. In figures 1,2,3,5,6,7,9 and 10 the upper spectral estimates correspond to the upper time series. In each case the estimates were computed from the portions of the seismograms indicated by the horizontal bars. The spectral estimates were computed using a time-bandwidth product of 3.

Figure 2. Synthetic Green's functions (Σ_{zz0}) and corresponding frequency power spectra at depths of 5.5495 and 5.5000 km due to a vertical point force buried 15 km at a range of 1000 km. The spectral estimates were computed using a time-bandwidth product of 4.

Figure 3. Synthetic Green's functions (Σ_{zz1}) and corresponding frequency power spectra at depths of 5.5495 and 5.5000 km due to a horizontal point force buried 15 km at a range of 1000 km. The spectral estimates were computed using a time-bandwidth product of 3.

Figure 4. The modulus of the transmission coefficient corresponding to the conversion, at the sediment/water interface, of shear energy propagating upward and converting to upward propagating compressional energy.

Figure 5. Power spectral estimates and seismograms corresponding to an earthquake 1000 km from the sensor. The data were collected by an Ocean Bottom Seismometer and Hydrophone deployed in the S.W. Pacific. The vertical dashed and solid lines indicate the predicted locations of spectral peaks due to compressional energy resonance in the sediment layer where successive multiples are phase shifted by π and 0.0 respectively.

Figure 6. In this figure we consider the event displayed in figure 5; however, we only consider the first 6.5 seconds of coda, following the Pn onset, in the spectral estimates. The solid vertical lines indicate the eigenfrequencies associated with the resonance of compressional energy in the sediment layer in which successive multiples are π phase shifted.

Figure 7. In this figure we consider the event displayed in figure 5; however, we only consider the portion of the coda arriving from 7.0 to 13.5 seconds after the Pn phase. The dashed and solid vertical lines indicate the eigenfrequencies associated with the resonance of compressional energy in the sediment layer in which successive multiples are phase shifted by π and 0.0 respectively.

Figure 8. Signal and noise power spectral estimates and seismogram corresponding to an mb 6.0 earthquake which occurred at a depth of 159 km and a range of 2168 km from the Wake Island Hydrophone array. The vertical dashed lines indicate the predicted locations of spectral peaks due to compressional energy resonance in the sediment layer where successive multiples are in phase.

Figure 9. Power spectral estimates and seismograms corresponding to the event displayed in figure 5. The vertical dashed lines indicate the predicted locations of spectral peaks due to compressional energy resonance in the water column.

Figure 10. Power spectral estimate and seismogram corresponding to mb 5.4 earthquake which occurred at a depth of 33 km and a range of 2057 km from the Wake Island Hydrophone array. The vertical dashed lines indicate the predicted locations of spectral peaks due to compressional energy resonance in the water column.

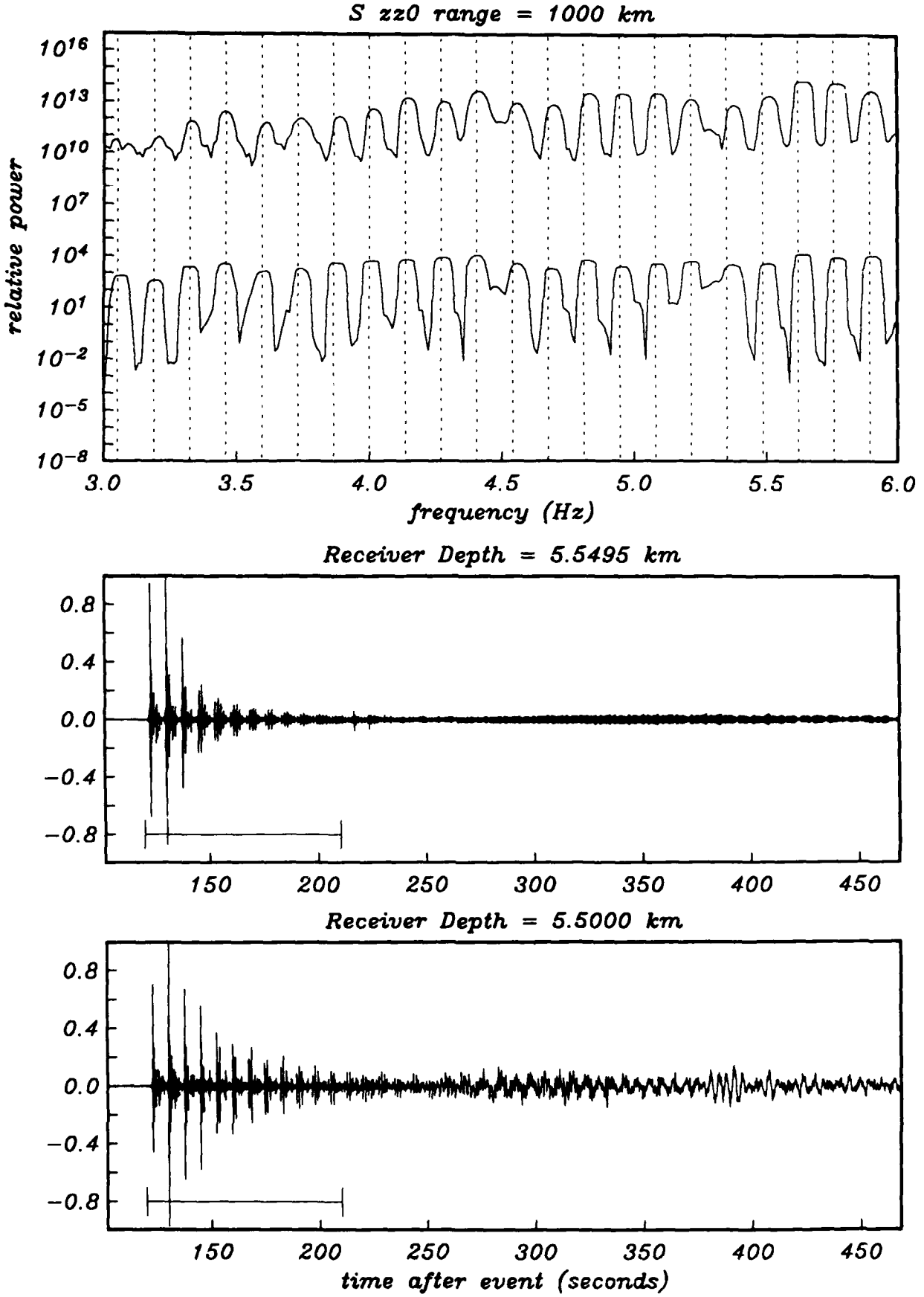
S zz0 range = 1000 km
relative power
frequency (Hz)
Receiver Depth = 5.5495 km
Receiver Depth = 5.5000 km
time after event (seconds)

Figure 1

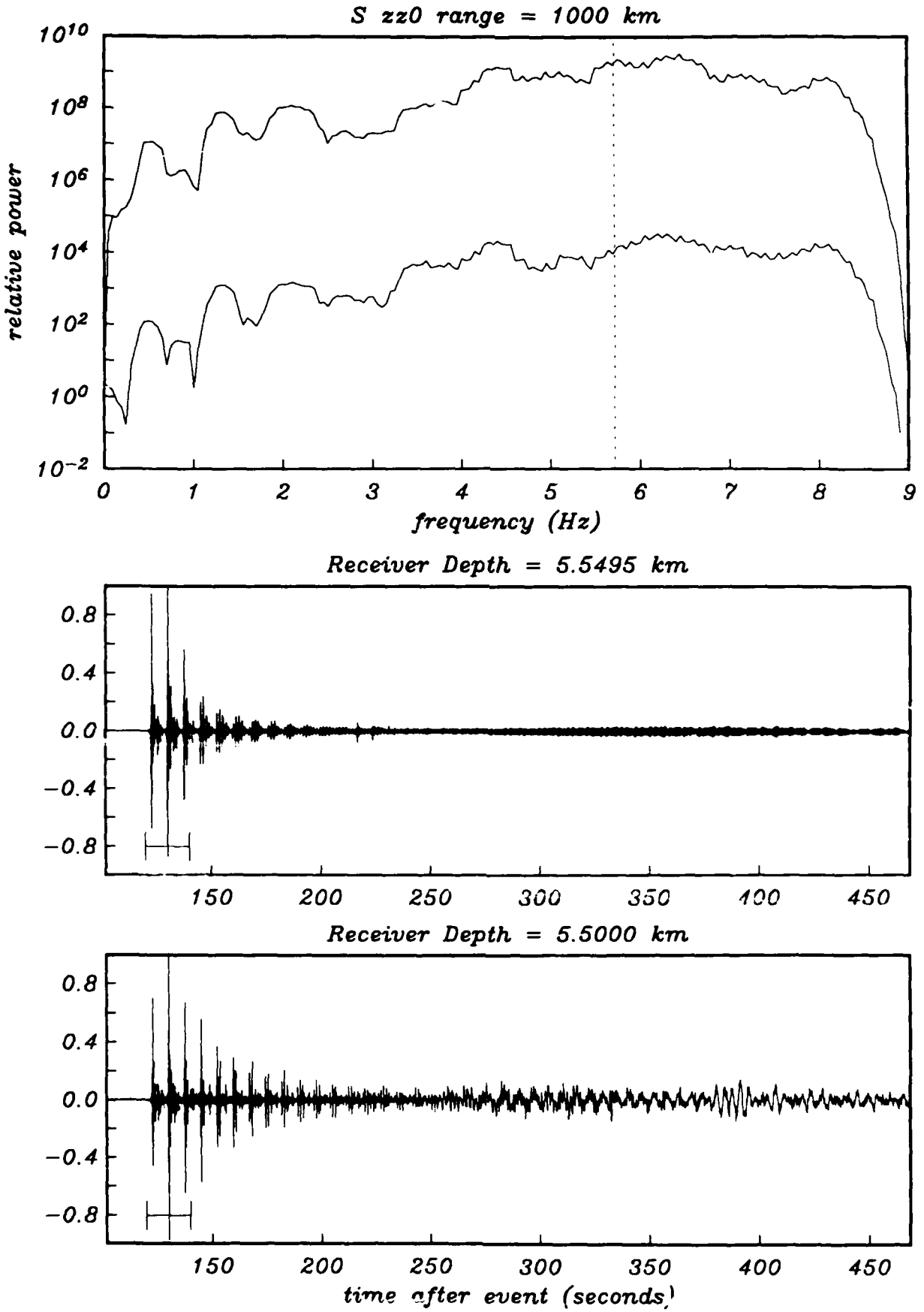
S zz0 range = 1000 km
relative power
frequency (Hz)
Receiver Depth = 5.5495 km
Receiver Depth = 5.5000 km
time after event (seconds)

Figure 2

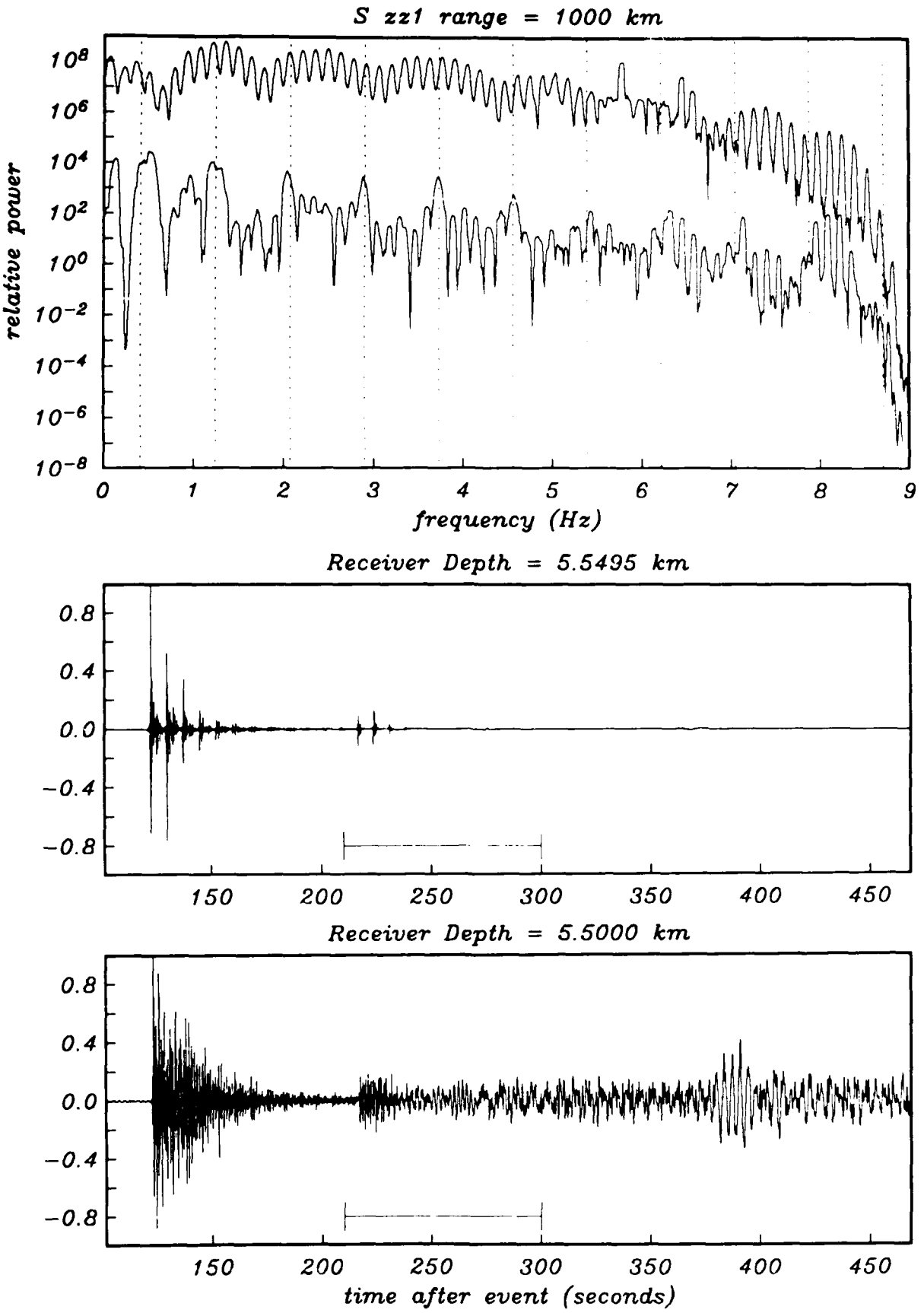
S zz1 range = 1000 km
relative power
frequency (Hz)
Receiver Depth = 5.5495 km
Receiver Depth = 5.5000 km
time after event (seconds)

Figure 3

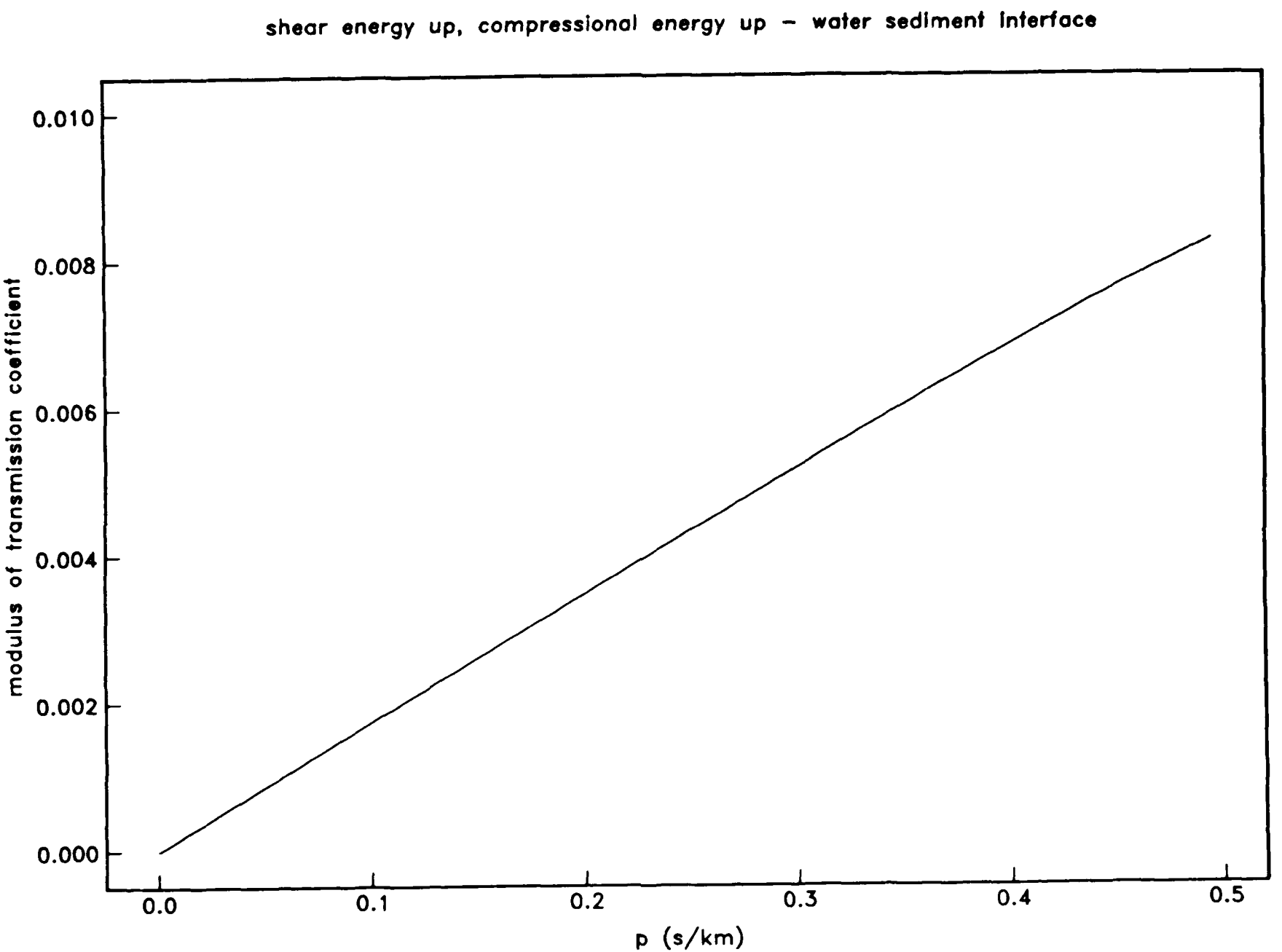
shear energy up, compressional energy up – water sediment interface
modulus of transmission coefficient
0.010
0.008
0.006
0.004
0.002
0.000
0.0
0.1
0.2
0.3
0.4
0.5
p (s/km)

Figure 4

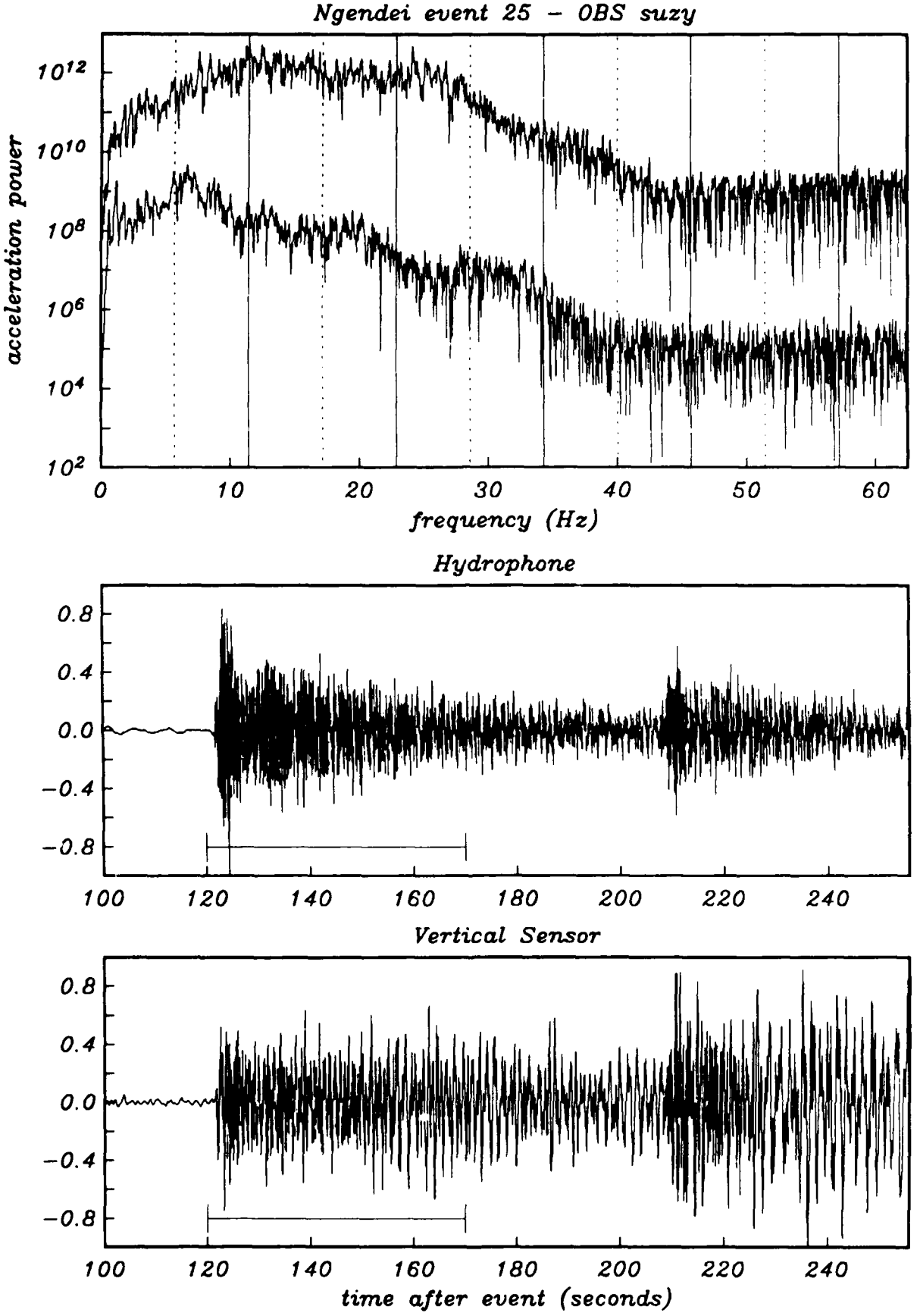
Ngendei event 25 – OBS suzy
acceleration power
10^{12}
10^{10}
10^{8}
10^{6}
10^{4}
10^{2}
0
10
20
30
40
50
60
frequency (Hz)
Hydrophone
0.8
0.4
0.0
−0.4
−0.8
100
120
140
160
180
200
220
240
Vertical Sensor
0.8
0.4
0.0
−0.4
−0.8
100
120
140
160
180
200
220
240
time after event (seconds)

Figure 5

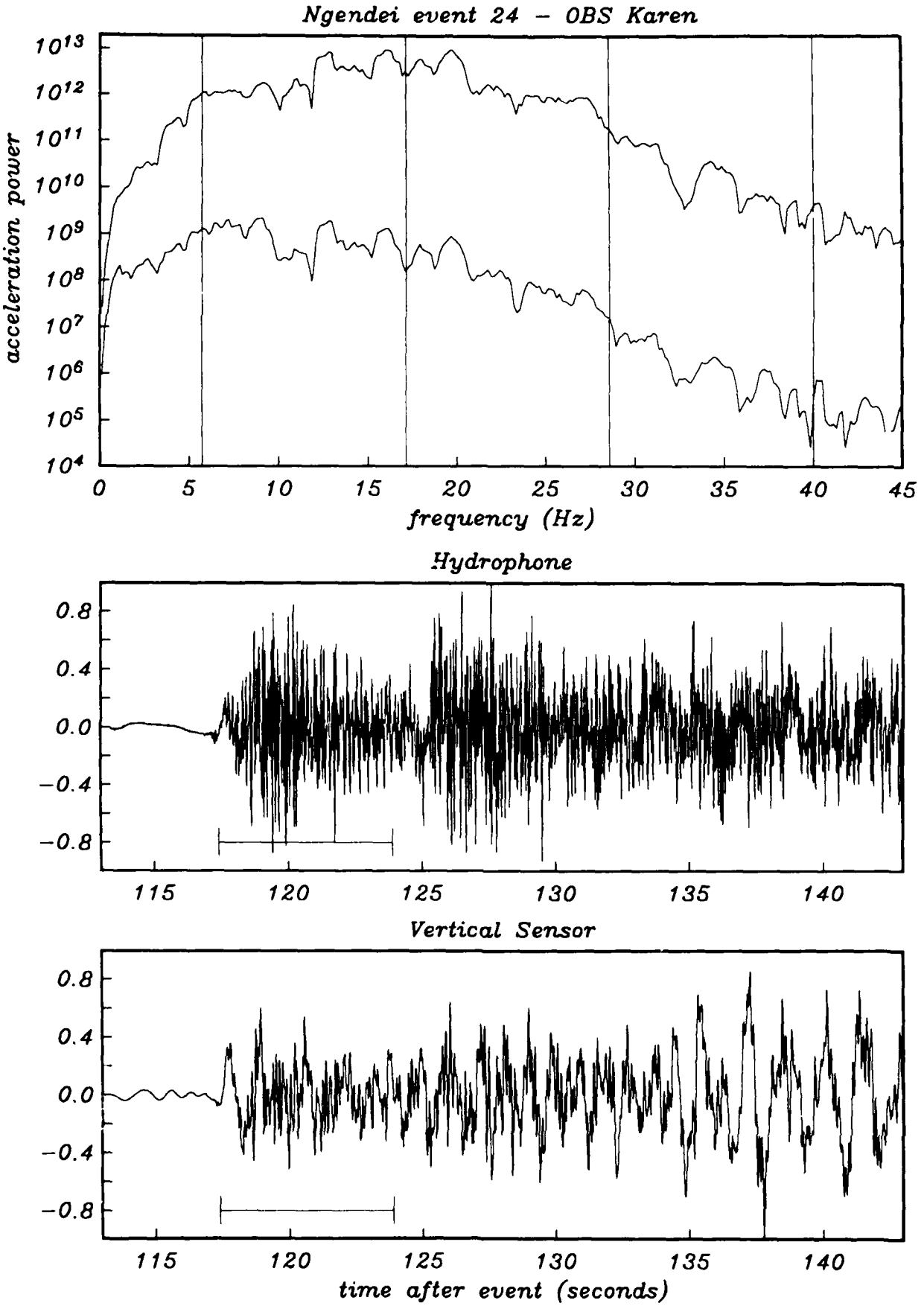
Ngendei event 24 – OBS Karen
acceleration power
10^{13}
10^{12}
10^{11}
10^{10}
10^{9}
10^{8}
10^{7}
10^{6}
10^{5}
10^{4}
0 5 10 15 20 25 30 35 40 45
frequency (Hz)
Hydrophone
0.8
0.4
0.0
−0.4
−0.8
115 120 125 130 135 140
Vertical Sensor
0.8
0.4
0.0
−0.4
−0.8
115 120 125 130 135 140
time after event (seconds)

Figure 6

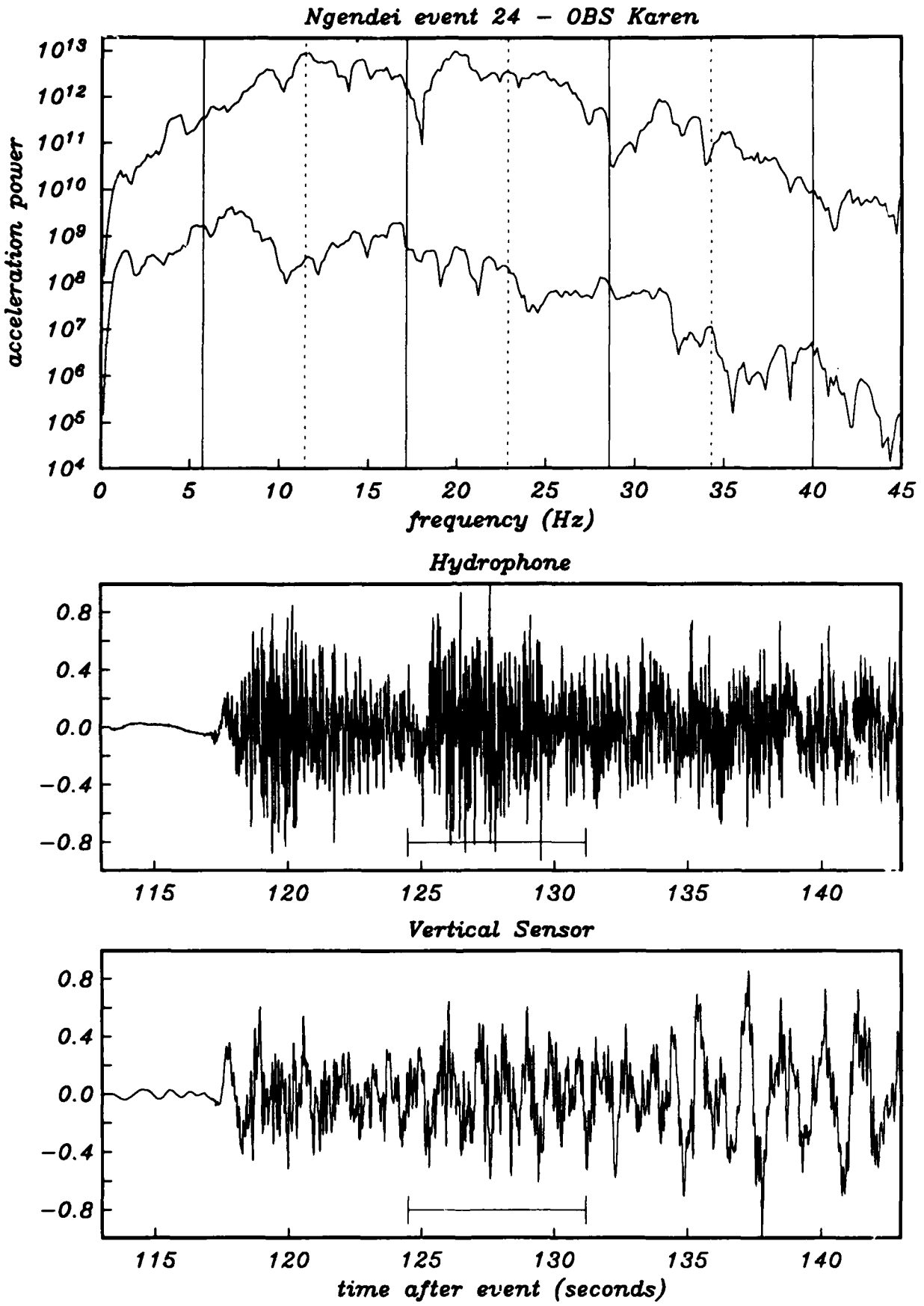
Ngendei event 24 – OBS Karen
acceleration power
frequency (Hz)
Hydrophone
Vertical Sensor
time after event (seconds)

Figure 7

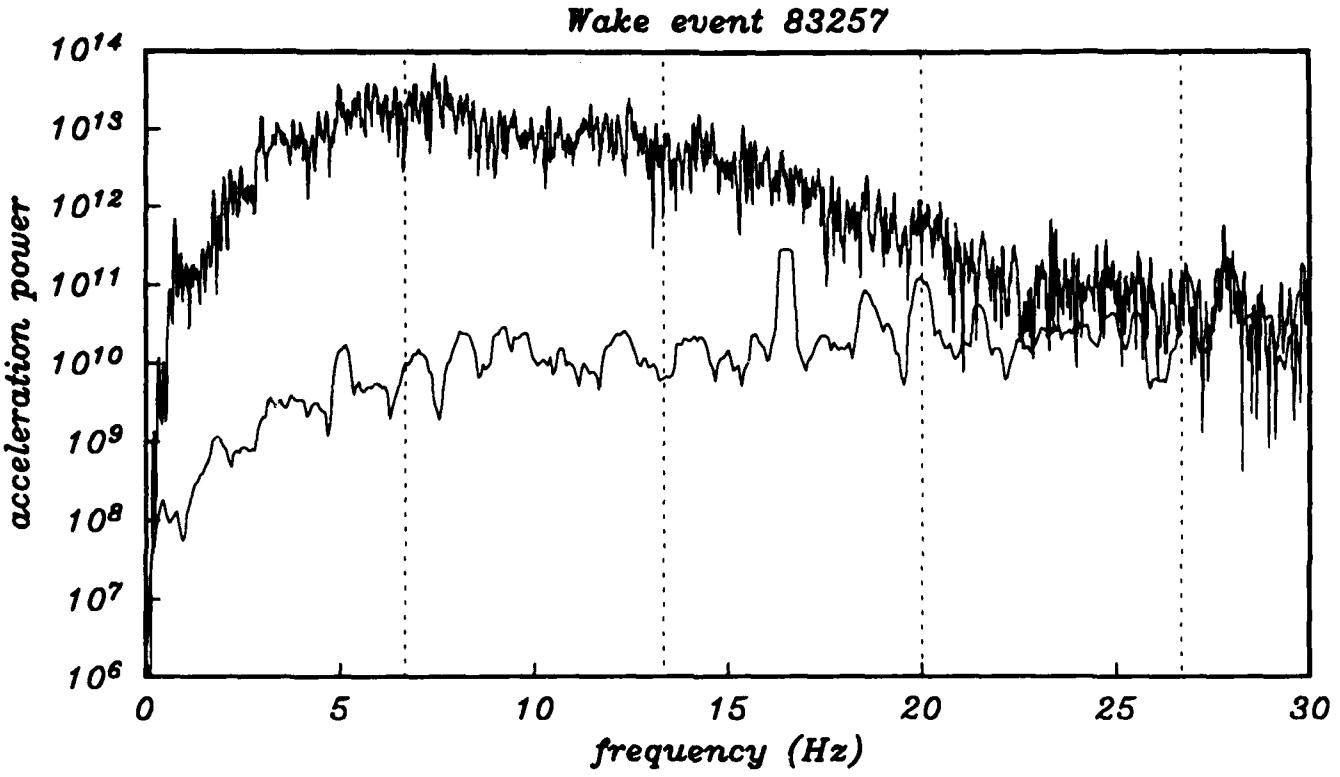
Wake event 83257
acceleration power
10^{14}
10^{13}
10^{12}
10^{11}
10^{10}
10^{9}
10^{8}
10^{7}
10^{6}
0
5
10
15
20
25
30
frequency (Hz)

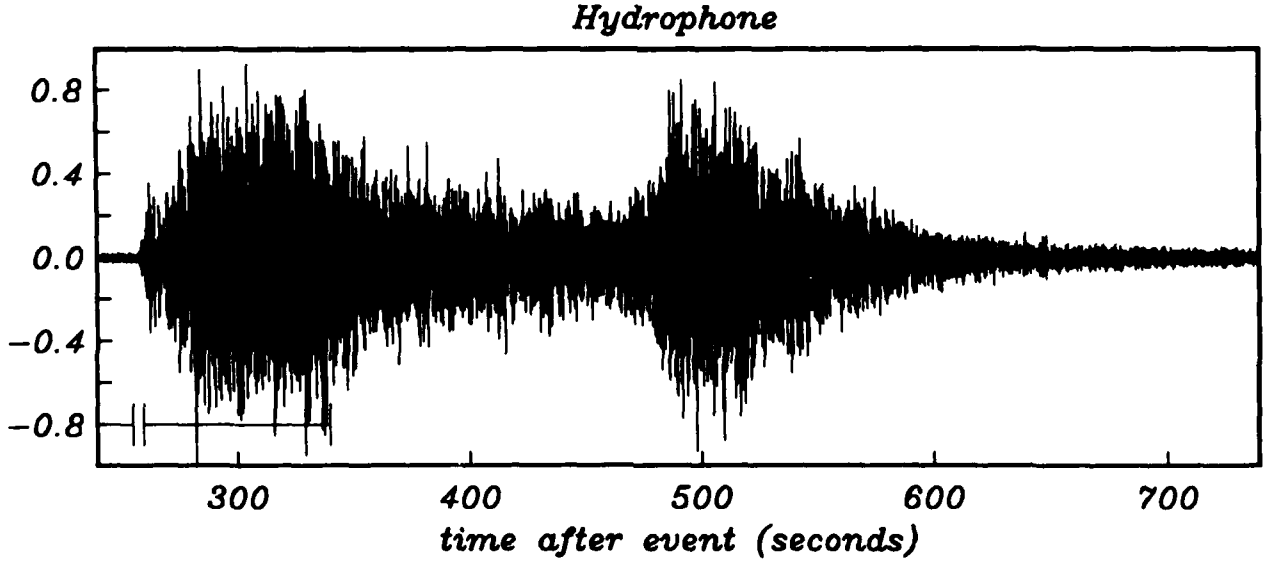
Hydrophone
0.8
0.4
0.0
−0.4
−0.8
300
400
500
600
700
time after event (seconds)

Figure 8

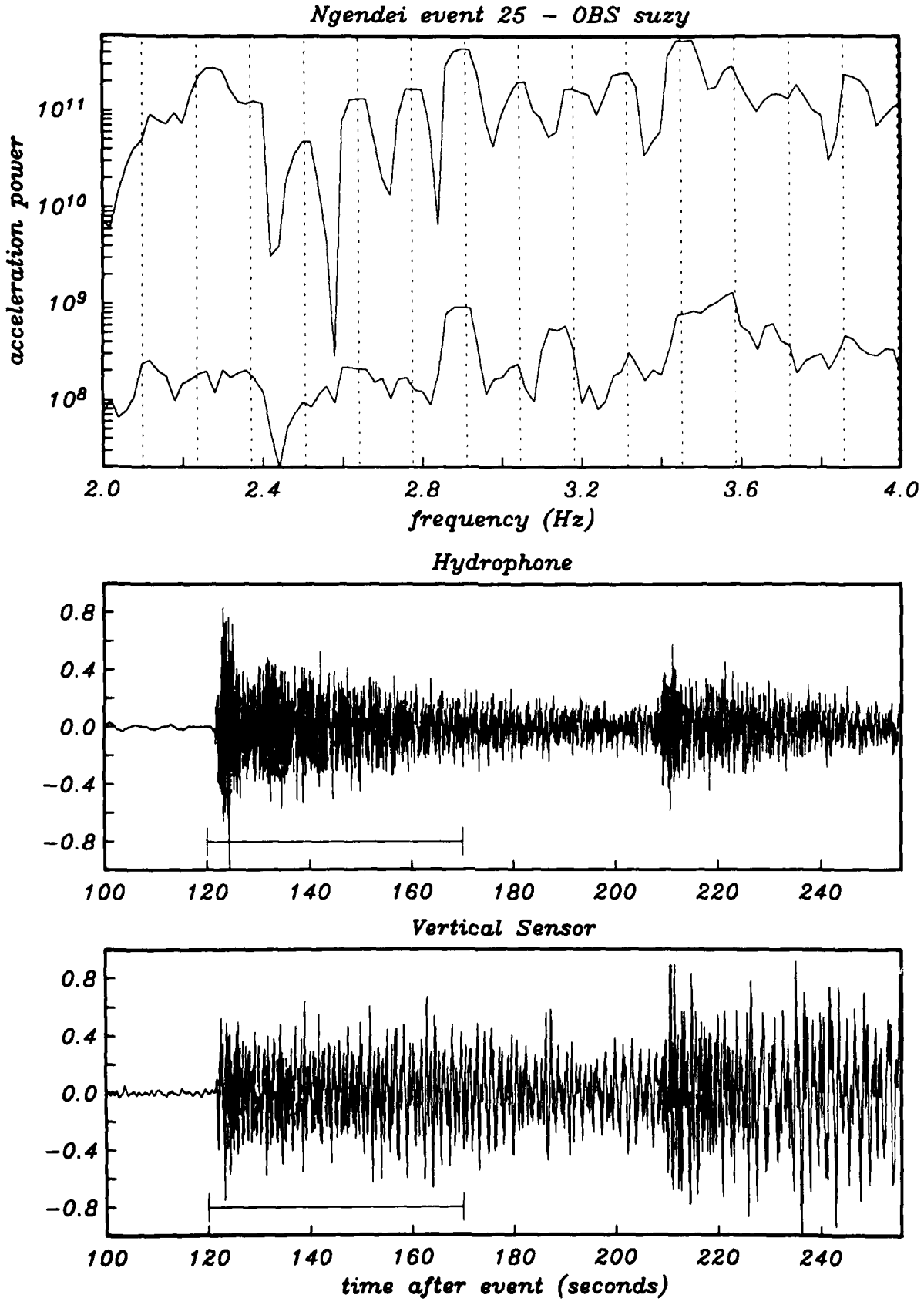
Ngendei event 25 – OBS suzy
acceleration power
10^{11}
10^{10}
10^{9}
10^{8}
2.0
2.4
2.8
3.2
3.6
4.0
frequency (Hz)
Hydrophone
0.8
0.4
0.0
−0.4
−0.8
100
120
140
160
180
200
220
240
Vertical Sensor
0.8
0.4
0.0
−0.4
−0.8
100
120
140
160
180
200
220
240
time after event (seconds)

Figure 9

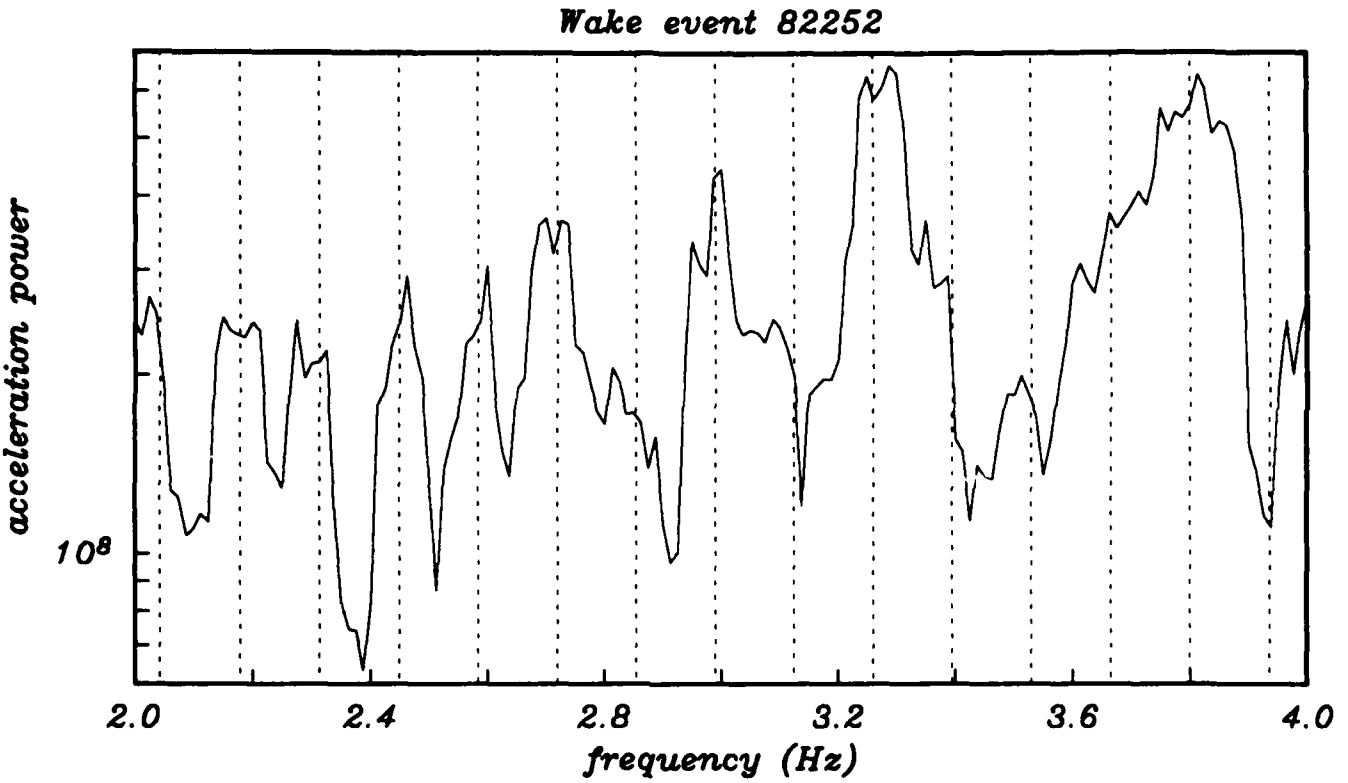
Wake event 82252
acceleration power
10^8
2.0
2.4
2.8
3.2
3.6
4.0
frequency (Hz)

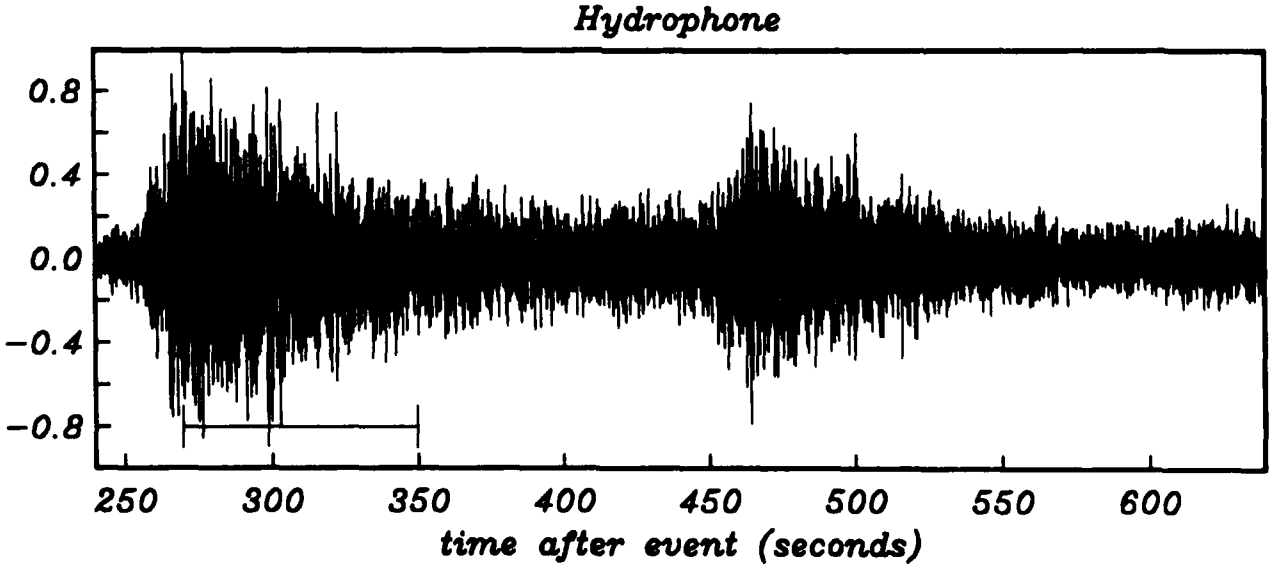
Hydrophone
0.8
0.4
0.0
−0.4
−0.8
250
300
350
400
450
500
550
600
time after event (seconds)

Figure 10

CHAPTER 6

REGIONAL CONTINENTAL PROPAGATION

Michael A.H. Hedlin and John A. Orcutt

SUMMARY

We are currently examining data collected in central Asia and Scandinavia to gain a deeper insight into the nature of the propagation of seismic phases through the continental crust. As has been discussed in the previous chapter, two popular theories exist that attempt to explain the mechanism by which seismic coda is generated in the oceanic crust. These theories involve the scattering of seismic energy by small scale inhomogeneities (Richards and Menke, 1983; Menke and Chen, 1984) and the resonance of energy in low velocity horizons (Sereno and Orcutt, 1985a,b). We attempt to determine the likely dominant coda generation mechanism present in the continental crust by processing the data in two ways. We compute frequency versus time expansions of the energy in synthetic and actual coda in a manner described by Hedlin, Minster and Orcutt (1989). We also compute frequency versus wavenumber spectra from isolated phases in the synthetic and real coda. The synthetic seismograms are computed using Wavenumber Integration (Luco and Apsel, 1983; Apsel and Luco, 1983).

FREQUENCY-TIME ANALYSIS

We have found frequency-time display of seismograms, known as sonograms in acoustics (Markel and Gray, 1976), to be particularly useful for coda analysis because the time dependence information is preserved. We have first applied this processing technique to a synthetic data set created using Wavenumber Integration. This algorithm requires that the Earth be modeled as consisting of a stack of homogeneous layers and includes all seismic phases resulting from the interaction of the propagating wavefield with the interfaces within the model and the free surface. It is thus ideal as a tool to predict the likely features of coda generated in the absence of scattering, simply by the resonance of energy in low velocity horizons. As was demonstrated by Hedlin et al (1988) it is possible to generate significant coda using an Earth model consisting of homogeneous layers and no water column. The model used was representative of the continental crust in the vicinity of the Semipalatinsk nuclear test site in central Asia and was capped by a low velocity horizon representing a near-surface weathered layer or sediment. In figures 1a and 1b are displayed synthetic seismograms, and accompanying sonograms, of the vertical and radial components of motion caused by an explosion buried 30 m at a range of 400 km. Since the Earth model consists of homogeneous layers, the synthetic coda consists solely of reverberations primarily concentrated in the surface layer. Sereno and Orcutt (1985a) showed that coda produced by layer resonance is enriched in power at certain equispaced eigenfrequencies. Peak spacing is inversely proportional to the two-way vertical travel time across the layer, and peak width is controlled by the impedance contrasts between the layer and its neighbors as well as the attenuative properties of the layer itself. As was discussed by Hedlin et al (1988), and is apparent in this figure, when the receiver is a significant distance from the source (so that the incident energy has high phase velocity) the period of the modulation observed on vertical or horizontal component sensors is largely independent of time in the coda. The eigenfrequency spacing in figure 1b is closer than in figure 1a, because at this range the radial component is dominated by shear energy, and the vertical component by faster compressional energy.

We expect that actual coda produced largely by the resonance of energy in low-velocity strata should have frequency-time structure similar to that possessed by these synthetics. We have examined two independent data sets in search of these time independent spectral features. The first data-set consists of high frequency (250 samples/s) recordings of regional mine explosions and single-event calibration explosions made by a triangular array of seismometers deployed in Kazakhstan U.S.S.R. (Eissler et al, 1988; Thurber et al, 1988). The second data-set consists of recordings of regional mine explosions and earthquakes digitized at 40 samples/s by the NORESS array in Norway (Sereno et al, 1987). As has been discussed by Hedlin, Minster and Orcutt (1989) and Hedlin et al (1989) time independent spectral features have been observed in a number of events in central Asia and Scandinavia but these events have all been identified as being mine explosions. The time-independent features are believed to originate at the source from a detonation practice known as ripple firing, in which a number of sub-explosions are closely grouped in space and time. In figure 2 we display the sonogram corresponding to a Blasjo mine explosion recorded at a range of 302 km by the NORESS array. All events believed to be either calibration explosions or earthquakes (and thus likely to have relatively uncolored source spectra) give rise to coda apparently free of time-independent spectral features. In figures 3 and 4 we display the sonograms corresponding to two earthquakes which occurred in Scandinavia and were recorded by the NORESS array. We conclude that the continental crust is not giving rise to significant layer resonance and thus the dominant coda generation mechanism in the vicinity of these two sets of seismometers likely involves some other process. The most likely alternative is the scattering of energy by inhomogeneities. The minor time-independent feature present in the coda of the event displayed in figure 4 exists prior to the onset and is clearly a long lived spectral line in the noise unrelated to the event.

FREQUENCY-WAVENUMBER ANALYSIS

We feel we can gain additional insight regarding the source of seismic coda in the continental crust by isolating various phases within seismic coda and exploiting array data to compute frequency versus wavenumber spectra. It has been demonstrated by many authors (including Mykkeltveit and Bungum,

1984; Dainty, 1985) that wavenumber spectra allow the simultaneous estimation of phase arrival azimuth and velocity. For a preliminary synthetic result we have used seismograms computed using the Earth model discussed in the previous section and linearly stacked it upon itself after time shifting for a phase coming from a back azimuth of 240° with a phase velocity of 8.2 km/s assuming sensor locations in the NORESS array (figure 5). In this example the source was placed 300 km from the array. In figure 6 we display the wavenumber spectrum computed from this synthetic event considering only the energy immediately after the compressional onset in the frequency band from 4.5 to 5.0 Hz. This synthetic event defines the extreme limit in resolution of the NORESS array. Because of the manner in which we constructed the input, all phases arrive with the same phase velocity and from the same azimuth. As a result the true wavenumber spectrum is a delta function at a back azimuth of 240° and a |k| of 0.58 cycles/km. In figure 6 it is clear that the center of the energy distribution is at the correct location; however, the impulse response of the array has smeared the actual wavenumber field out to a "patch" with a half-width of roughly 0.4 cycles/km. In the next section we will discuss the implications of the impulse response somewhat further. We expect that the wavenumber spectrum of a wavefield that has propagated through a medium solely in the plane joining the source and receiver should resemble this event to the extent that the energy should be confined to this plane. Wavenumber spectra computed from the coda of a Norwegian quarry blast (at a range of 302 km, and a back azimuth of 240° from NORESS) is shown in figures 7 to 10. In figure 7 we display the wavenumber spectrum computed from energy in the frequency band from 1.5 to 5.0 Hz arriving in the window from the compressional onset to 6.5 seconds later. At this range we expect this window to include crustal phases as well as the P_n phase. The energy is fairly well constrained to lie on the plane joining the source and the array. In figure 8 we include an additional 13.5 seconds of coda. There is now a fairly considerable amount of apparent "off axis" energy. We have not resolved the ambiguity over whether this indicates out of plane propagation or is due to coherent noise. The average signal levels in this window are somewhat lower than those present in the previous one. In figures 9 and 10 we consider the S_n onset and the following Lg coda. Again there is considerable energy evident due to coherent noise or out of plane propagation. We are currently examining additional events, using a sliding window wavenumber analysis, in

an attempt to establish the origin of the apparent "off-axis" energy. In addition we are producing a full suite of synthetic Green's functions for the NORESS array by considering source to receiver offsets consistent with each individual element in the array.

We can estimate the ability of an array to resolve features in the wavenumber domain by computing the impulse response function, or the response of the array to the simultaneous excitation of every sensor with a delta function. We define the input to the array as:

$$u(x,y) = \frac{1}{N}\sum_{j=1}^{N} \delta(x-x_j)\delta(y-y_j) \tag{1}$$

where N is the number of sensors and (x_j,y_j) are the locations of the sensors. The response in the wavenumber domain is given by

$$U(k_x,k_y) = \frac{1}{N}\sum_{x=x_1}^{x_N}\sum_{y=y_1}^{y_N}\sum_{j=1}^{N} \delta(x-x_j)\delta(y-y_j)e^{-i2\pi(k_x x+k_y y)} \tag{2}$$

where (k_x,k_y) and the x and y wavenumbers in cycles/km. The triple sum simplifies to:

$$U(k_x,k_y) = \frac{1}{N}\sum_{j=1}^{N} e^{-i2\pi(k_x x_j+k_y y_j)} \tag{3}$$

The amplitude of the impulse response equals:

$$|\,U(\mathbf{k})\,| = \frac{1}{N}\sqrt{\sum_{j=1}^{N} e^{-i2\pi(\mathbf{k}\bullet r_j)}\sum_{m=1}^{N} e^{i2\pi(\mathbf{k}\bullet r_m)}} \tag{4}$$

where $\mathbf{k} = (k_x,k_y)$. This can be simplified to:

$$|\,U(\mathbf{k})\,| = \frac{1}{N}\sqrt{\sum_{m=1}^{N}\sum_{j=1}^{N} e^{i2\pi(\mathbf{k}\bullet(r_m-r_j))}} \tag{5}$$

The impulse response of the NORESS array is shown in figure 11. When spatial

periodogram spectral estimates are computed (ie no spatial taper is applied to the recorded wavefield) the true wavenumber spectrum of an event is convolved with this function. As we've discussed earlier, the half-width of the main lobe (roughly the aperture of the array) is approximately 0.4 cycles/km and defines the limit of resolution in the wavenumber domain. No two events separated by less than the resolution can be resolved as being distinct events. Further corruption of the computed wavenumber field occurs because of the sidelobes which, for this array, are small but not infinitesimally so. The true wavenumber spectrum has been blurred to a circular "patch" with a half width of 0.4 cycles/km. The NORESS array is extremely well designed but we feel that some improvement in resolution can be gained by the judicious application of spatial tapers. Currently we are extending the theory of Thompson (1982), who dealt with the computation of optimal tapers for evenly sampled 1-D time series, to the 2-D array data. The primary obstacle to the application of the method is the unevenness of the spatial sampling which complicates the computation of the eigentapers. The theory of Thompson (1982) is readily applicable to the time-frequency transformation required by this method. As is discussed by Hedlin, Minster and Orcutt (1989) it will help us isolate particular phases by allowing shorter time windows.

CONCLUSIONS

Our preliminary analysis of the evolution of frequency spectra as a function of time in seismic coda suggests that layer resonance is not playing a major role in the generation of seismic coda in the continental crust. We are currently employing an analysis of the evolution of the wavenumber spectrum as function of time in an attempt to determine if the likely alternative mechanism, the scattering of energy by small scale inhomogeneities, is responsible.

REFERENCES

Apsel, R.J. and Luco, J.E., 1983, On the Green's Functions for a Layered Half-Space, Part II, Bulletin of the Seismological Society of America, 73, 931-951.

Dainty, A. M., 1985, Coda Observed at NORSAR and NORESS, Unclassified AFGL Final technical report, AFGL-TR-85-0199, ADA166454.

Eissler, H.K., Tarasov, N.T., Zhuravlev, V., Thurber, C.H., Vernon, F.L., Berger, J. & Nersesov, I.L., 1988. High-Frequency Seismic Observations of Chemical Explosions of Known Location and Yield in Eastern Kazakhstan, U.S.S.R.. *Submitted to the J. geophys. Res.*

Hedlin, M. A. H., Orcutt, J. A. & Minster, J. B., 1988. A Comparative Study of High Frequency Signal and Noise in Oceanic and Continental Environments. *Paper presented at the 10th annual AFGL/DARPA seism. Res. Symp.*

Hedlin, M. A. H., Minster, J. B. & Orcutt, J. A., 1989, The Time-Frequency Characteristics of Quarry Blasts and Calibration Explosions Recorded in Kazakhstan U.S.S.R., *Accepted for publication in the Geophysical Journal.*

Hedlin, M. A. H., Orcutt, J. A., Minster, J. B. and Gurrola, H., 1989, The time-Frequency Characteristics of Quarry Blasts, Earthquakes and Calibration Explosions Recorded in Scandinavia and Kazakhstan U.S.S.R., *Paper presented at the 11th annual AFGL/DARPA seism. Res. Symp.*

Luco, J.E. and Apsel, R.J., 1983, On the Green's Functions for a Layered Half-Space, Part I, Bulletin of the Seismological Society of America, 73, 909-929.

Markel, J. D. & Gray, A. H. Jr., 1976. *Linear Prediction of Speech*, Springer-Verlag, Berlin Heidelberg New York.

Menke, W. and Chen, R., 1984, Numerical Studies of the Coda Falloff Rate of Multiply Scattered Waves in a Randomly Layered Media, Bulletin of the Seismological Society of America, 74, 1605-1621.

Mykkeltveit, S. and Bungum, H., 1984, Processing of Regional Seismic Events Using Data From Small-Aperture Arrays, Bulletin of the Seismological Society of America, 74, 2313-2333.

Richards, P. and Menke, W., 1983, The apparent Attenuation of a Scattering Medium, Bulletin of the Seismological Society of America, 73, 1005-1021.

Sereno, T.J. and Orcutt, J.A., 1985a, Synthetic Sesimogram Modelling of the Oceanic Pn Phase, Nature, 316, 246-248.

Sereno, T.J. and Orcutt, J.A., 1985b, Synthesis of Realistic Oceanic Pn Wave Trains, Journal of Geophysical Research, 90, 12755-12776.

Sereno, T.J., Bratt, S.R., Bache, T.C., 1987, Regional Wave Attenuation and Seismic Moment From the Inversion of NORESS Spectra, Unclassified AFGL Semiannual Report No. 2, AFGL-TR-87-0237, ADA187399.

Thompson, D. J., 1982. Spectrum Estimation and Harmonic Analysis. *IEEE Proc.*, **70**, 1055-1096.

Thurber, C. H., Eissler, H., Berger, J., Zhuravlev, V. & Tarasov, N., 1988. Location of Regional Explosions and Earthquakes with the NRDC-Soviet Academy of Sciences Seismic Network in Kazakhstan. *EOS, Trans. of the American geophys.Union*, **69**, 1332.

FIGURE CAPTIONS

Figure 1. Synthetic vertical and radial acceleration sonograms and corresponding time series corresponding to an explosive source buried 30 m at a range of 400 km. The model used in this calculation consisted of a stack of homogeneous layers above a half space. The model is capped by a 100 m thick low velocity horizon representing a weathered or sediment layer.

Figure 2. Seismogram, and binary sonogram, corresponding to a Blasjo mine explosion recorded at a range of 302 km by the NORESS array.

Figure 3. Seismogram, and binary sonogram, corresponding to a presumed earthquake recorded at a range of 343 km by the NORESS array.

Figure 4. Seismogram, and binary sonogram, corresponding to a presumed earthquake recorded at a range of 513 km by the NORESS array.

Figure 5. The NORESS array.

Figure 6. The wavenumber spectrum of a synthetic event at a range of 300 km produced using the model described in the caption for figure 1. The recording by the NORESS array was simulated by placing the displayed time series at the locations of the sensors in the array and offsetting in time for a phase arriving from an azimuth of 240° with an apparent velocity of 8.2 km/s.

Figure 7. The wavenumber spectrum of a Blasjo mine explosion. Only the portion of the Pn coda indicated by the lower figure was considered. The estimate was constructed from sub-estimates spanning the frequency range from 1.5 to 5.0 Hz. The time series has been beamformed for the Pn phase.

Figure 8. The wavenumber spectrum of a Blasjo mine explosion. Only the portion of the Pn coda indicated by the lower figure was considered. The estimate was constructed from sub-estimates spanning the frequency range from 1.5 to 5.0 Hz. The time series has been beamformed for the Pg phase.

Figure 9. The wavenumber spectrum of a Blasjo mine explosion. Only the portion of the Sn coda indicated by the lower figure was considered. The estimate was constructed from sub-estimates spanning the frequency range from 1.5 to 5.0 Hz. The time series has been beamformed for the Sn phase.

Figure 10. The wavenumber spectrum of a Blasjo mine explosion. Only the portion of the Sn coda indicated by the lower figure was considered. The estimated was constructed from sub-estimates spanning the frequency range from 1.5 to 5.0 Hz. The time series has been beamformed for the Lg phase.

Figure 11. The impulse response of the NORESS array.

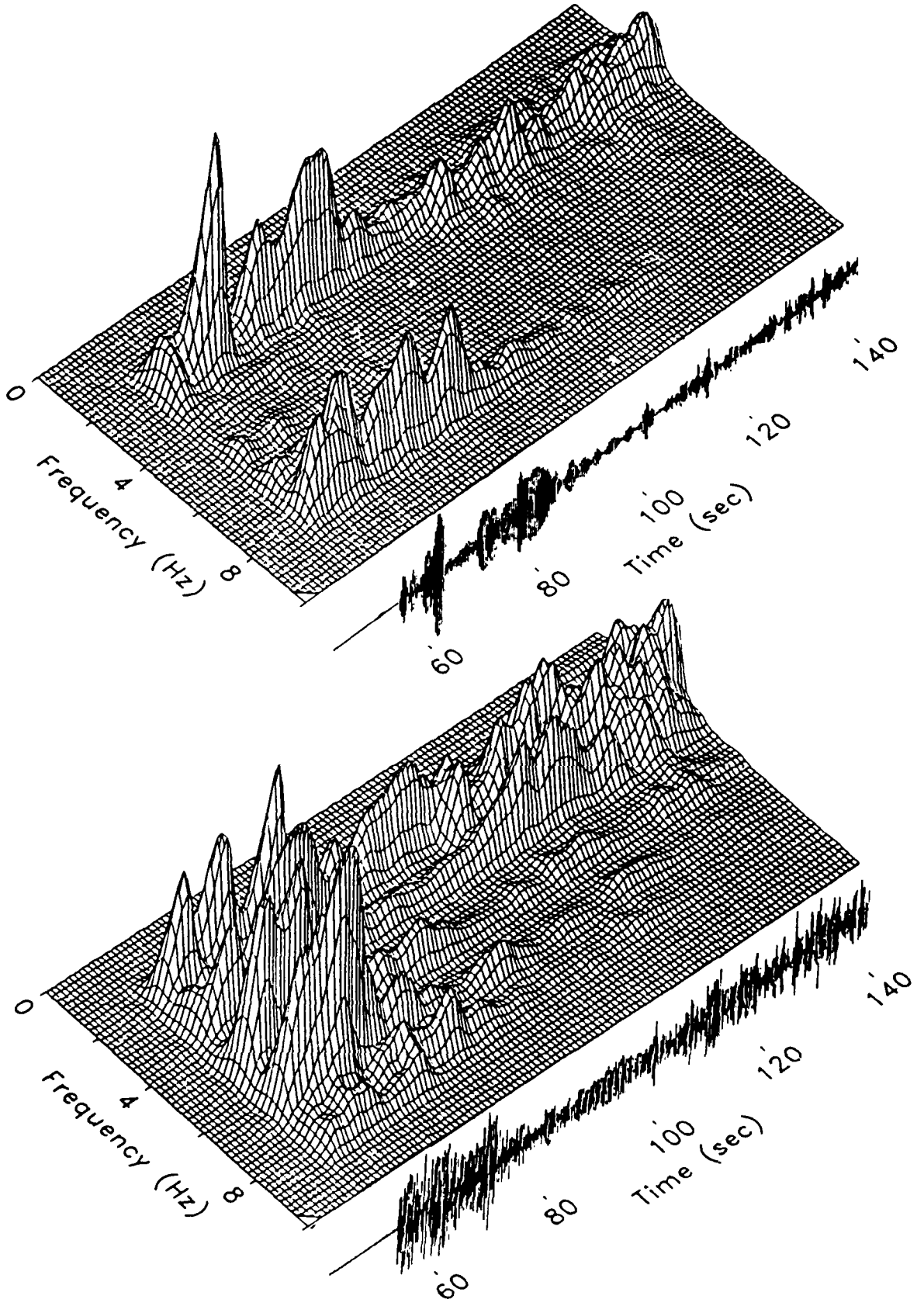

Figures 1a and 1b. Synthetic vertical and radial acceleration sonograms. The source is an explosion buried 30 meters at a range of 400 km.

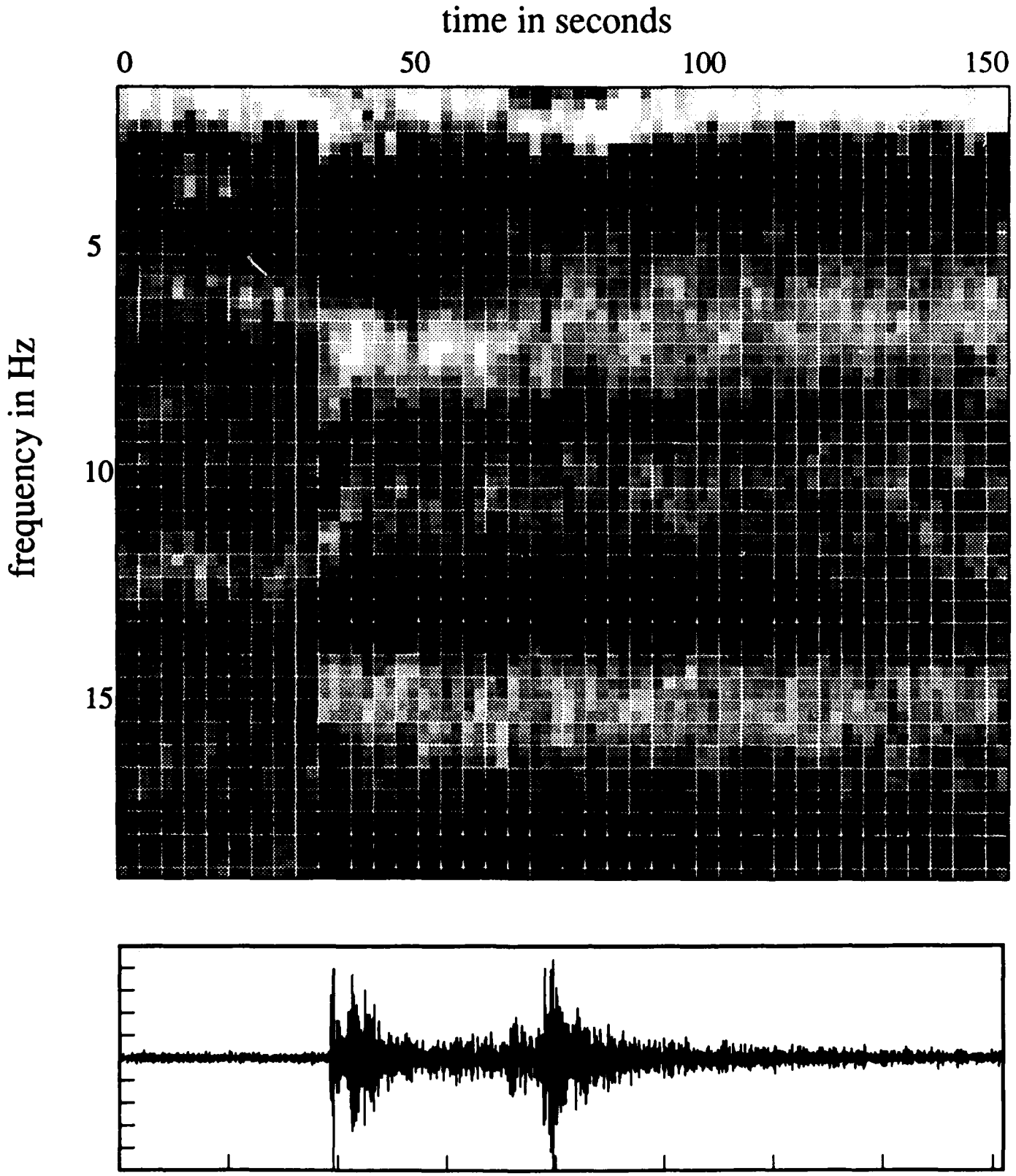

Blasjo explosion 0030 - 302 km from NORESS

Figure 2

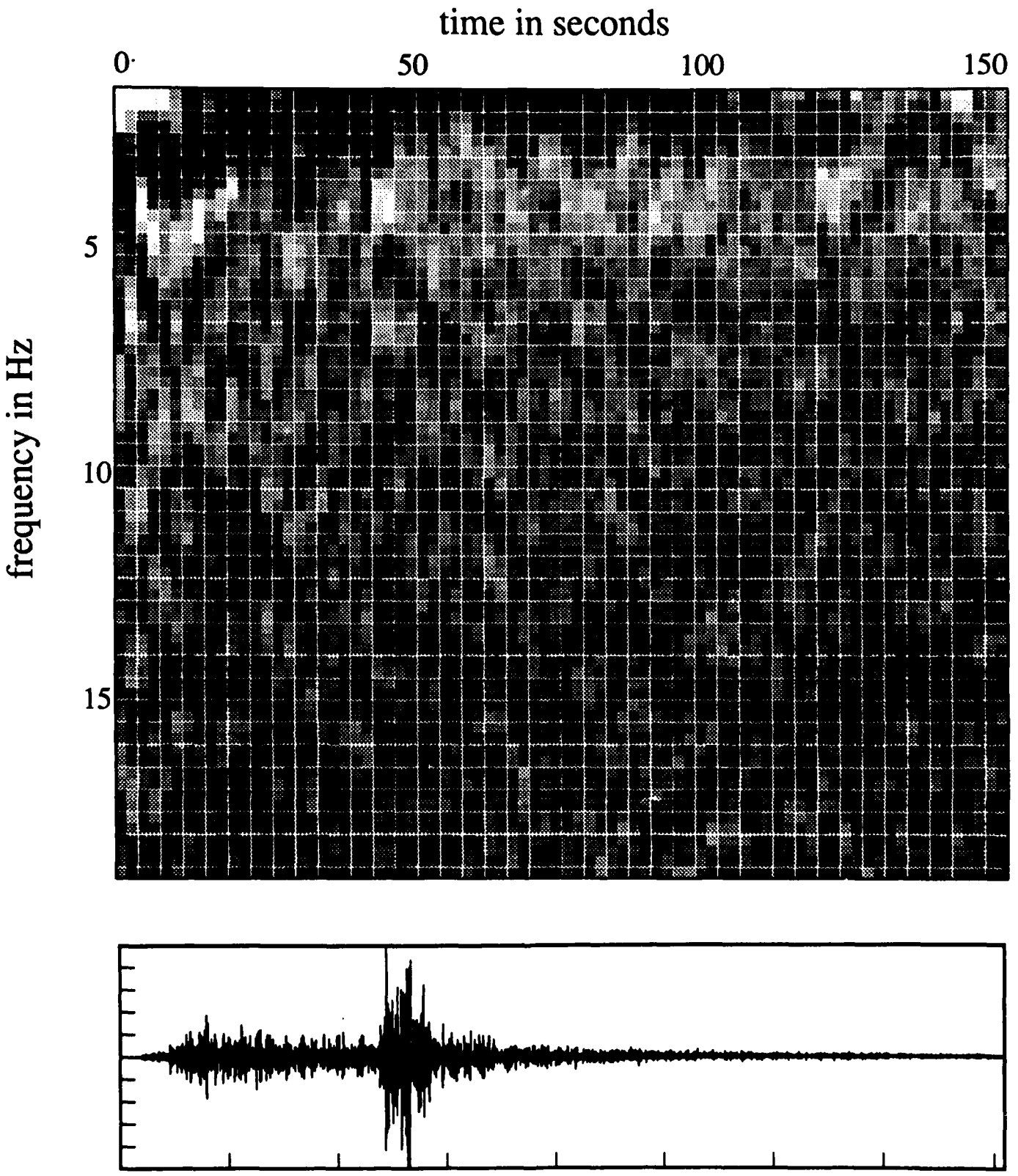

Presumed earthquake 0094 - 343 km from NORESS

Figure 3

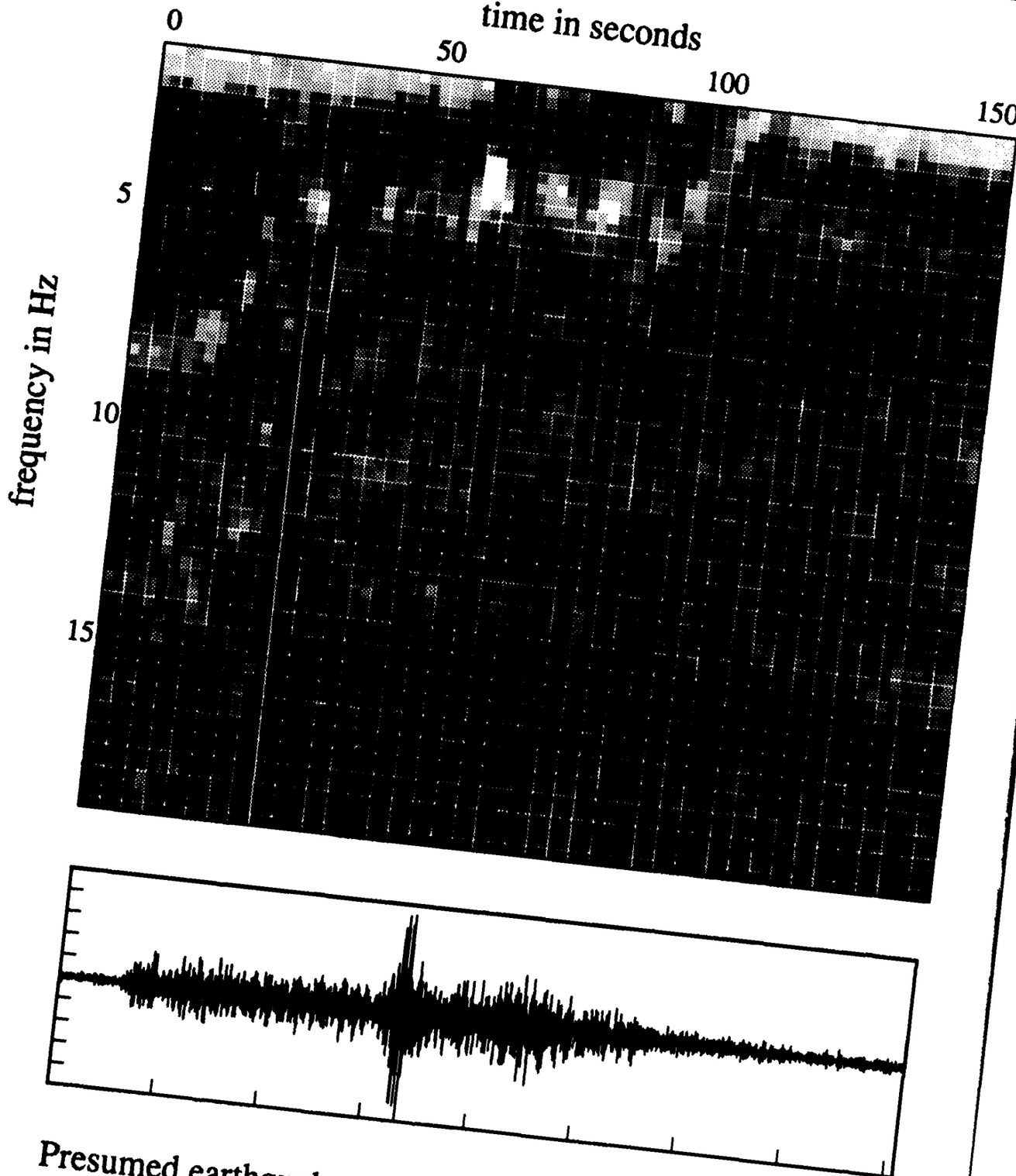

Presumed earthquake 0407 - 513 km from NORESS

Figure 4

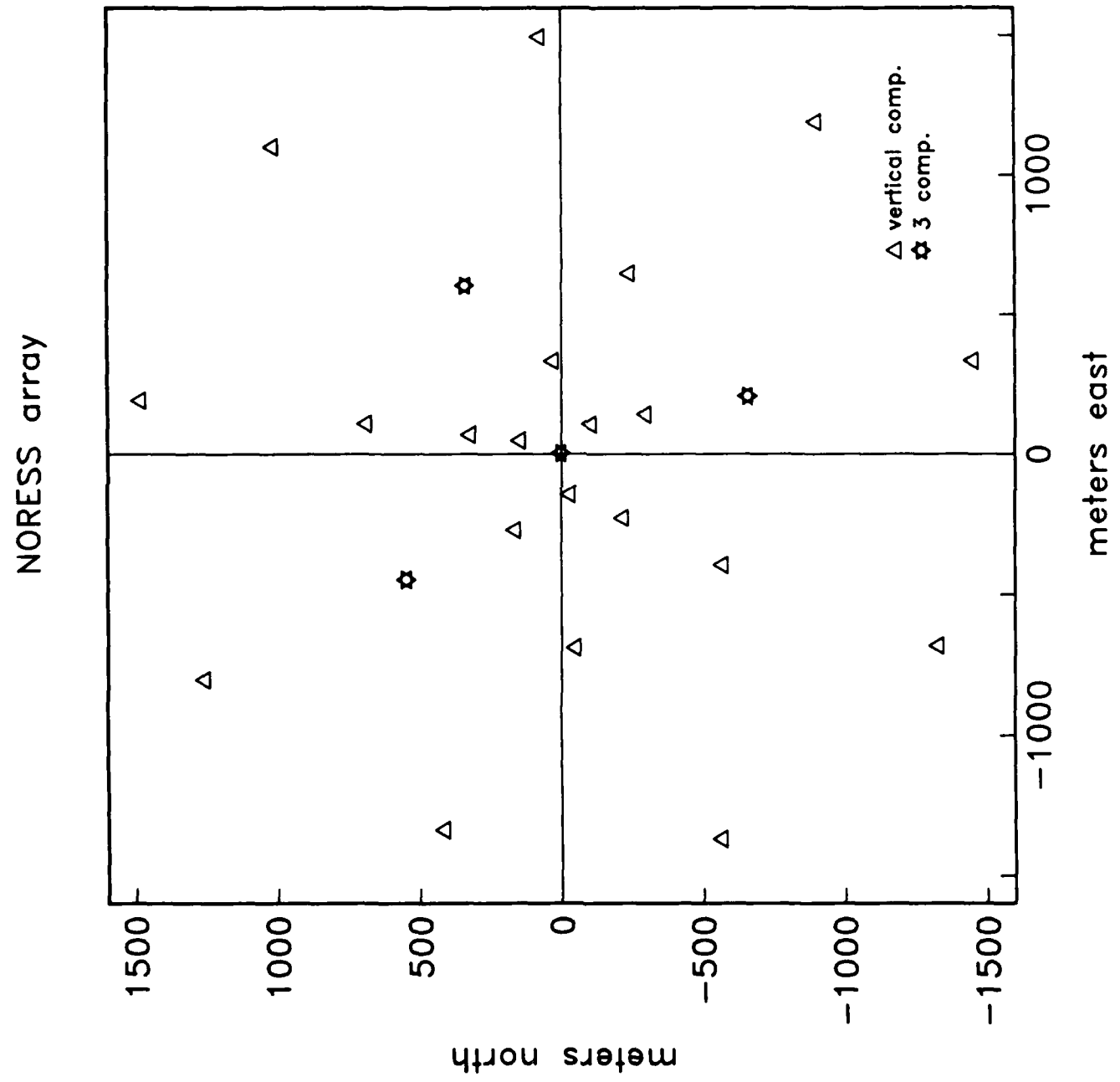
NORESS array
meters north
meters east
1500
1000
500
0
-500
-1000
-1500
1000
0
-1000
△ vertical comp.
✡ 3 comp.

Figure 5

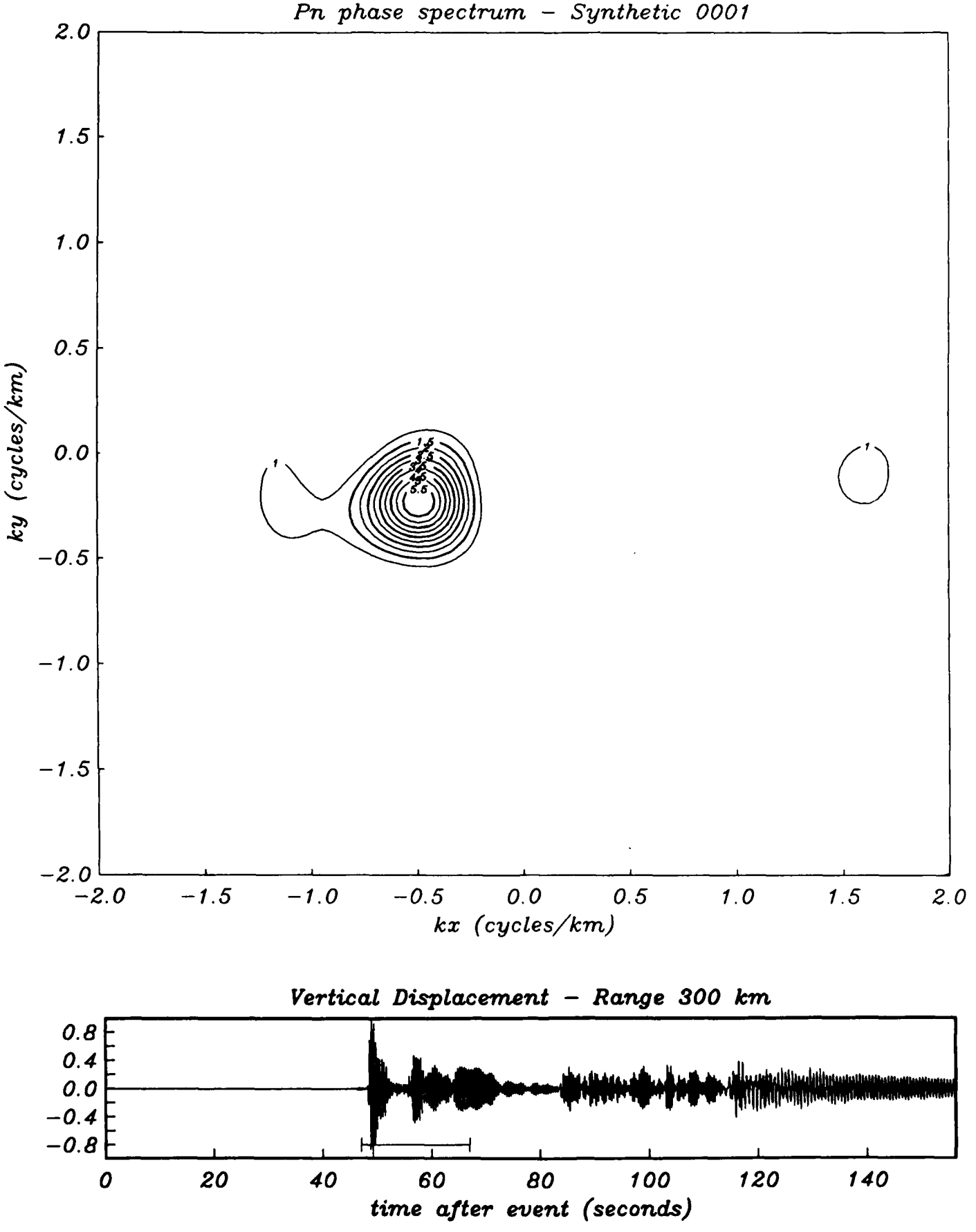
Pn phase spectrum – Synthetic 0001
2.0
1.5
1.0
0.5
0.0
−0.5
−1.0
−1.5
−2.0
ky (cycles/km)
−2.0
−1.5
−1.0
−0.5
0.0
0.5
1.0
1.5
2.0
kx (cycles/km)
1.5
5.5
5.6
Vertical Displacement – Range 300 km
0.8
0.4
0.0
−0.4
−0.8
0
20
40
60
80
100
120
140
time after event (seconds)

Figure 6

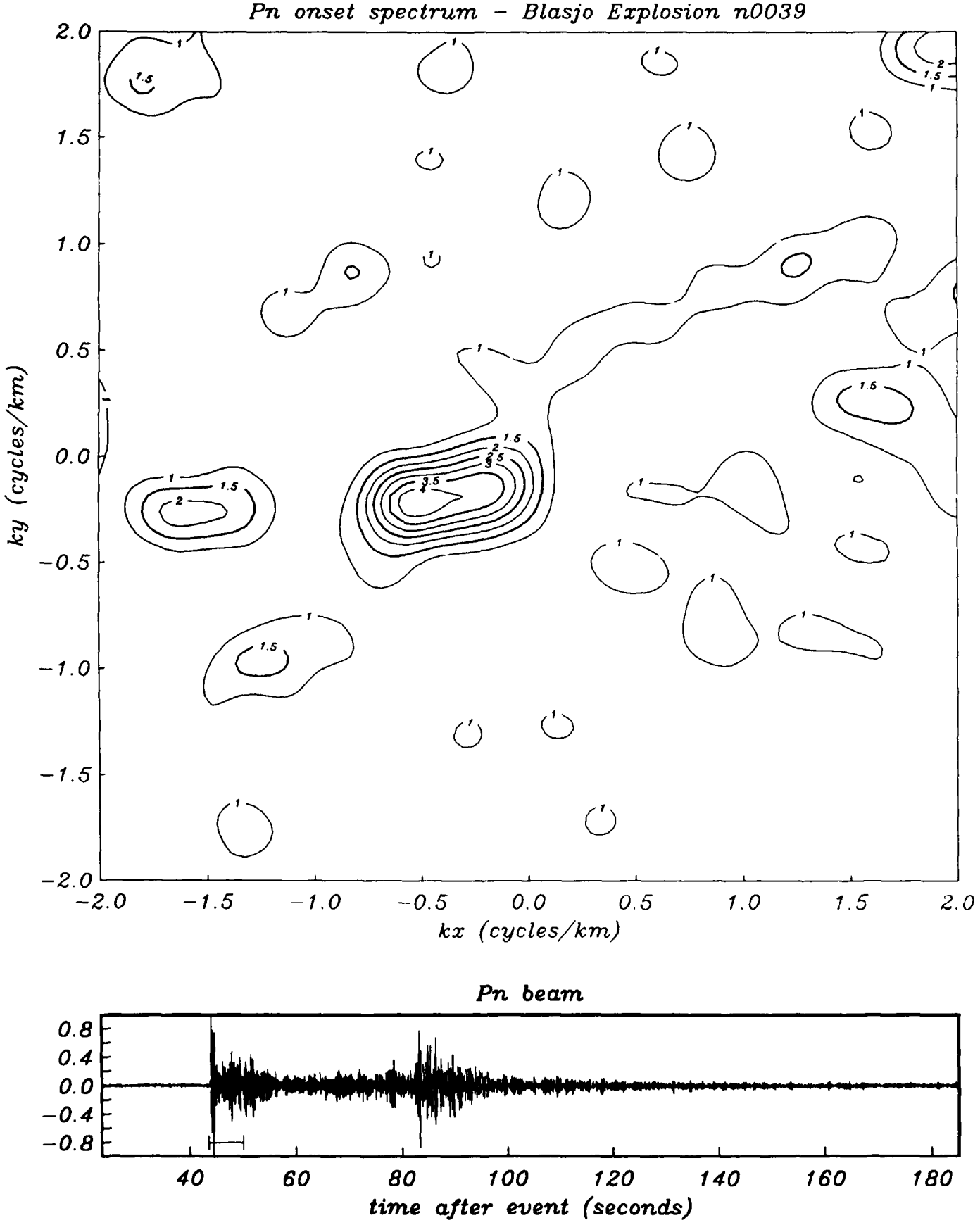
Pn onset spectrum - Blasjo Explosion n0039
ky (cycles/km)
kx (cycles/km)
2.0
1.5
1.0
0.5
0.0
-0.5
-1.0
-1.5
-2.0
Pn beam
0.8
0.4
0.0
-0.4
-0.8
40
60
80
100
120
140
160
180
time after event (seconds)

Figure 7

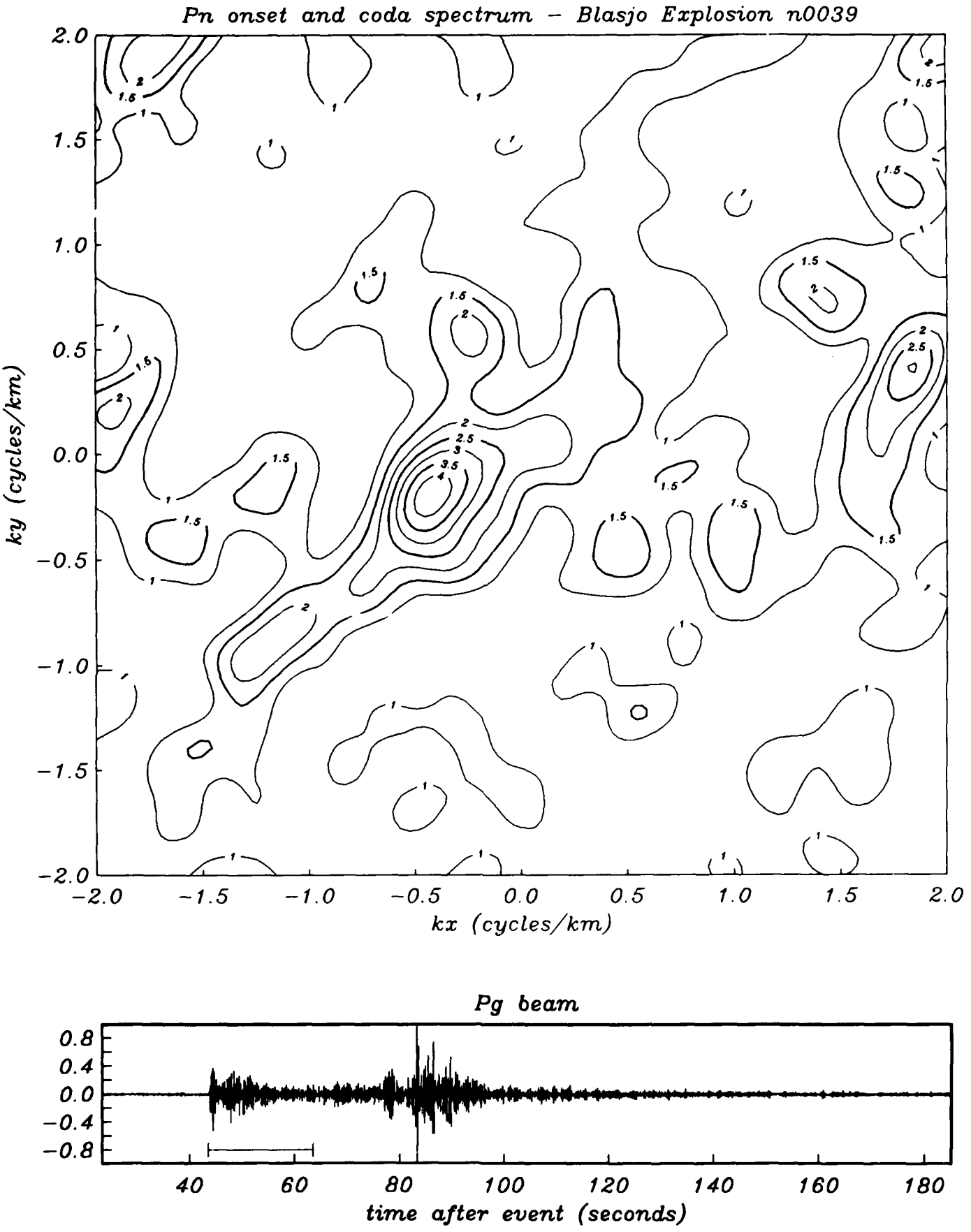
Pn onset and coda spectrum – Blasjo Explosion n0039
ky (cycles/km)
kx (cycles/km)
Pg beam
time after event (seconds)

Figure 8

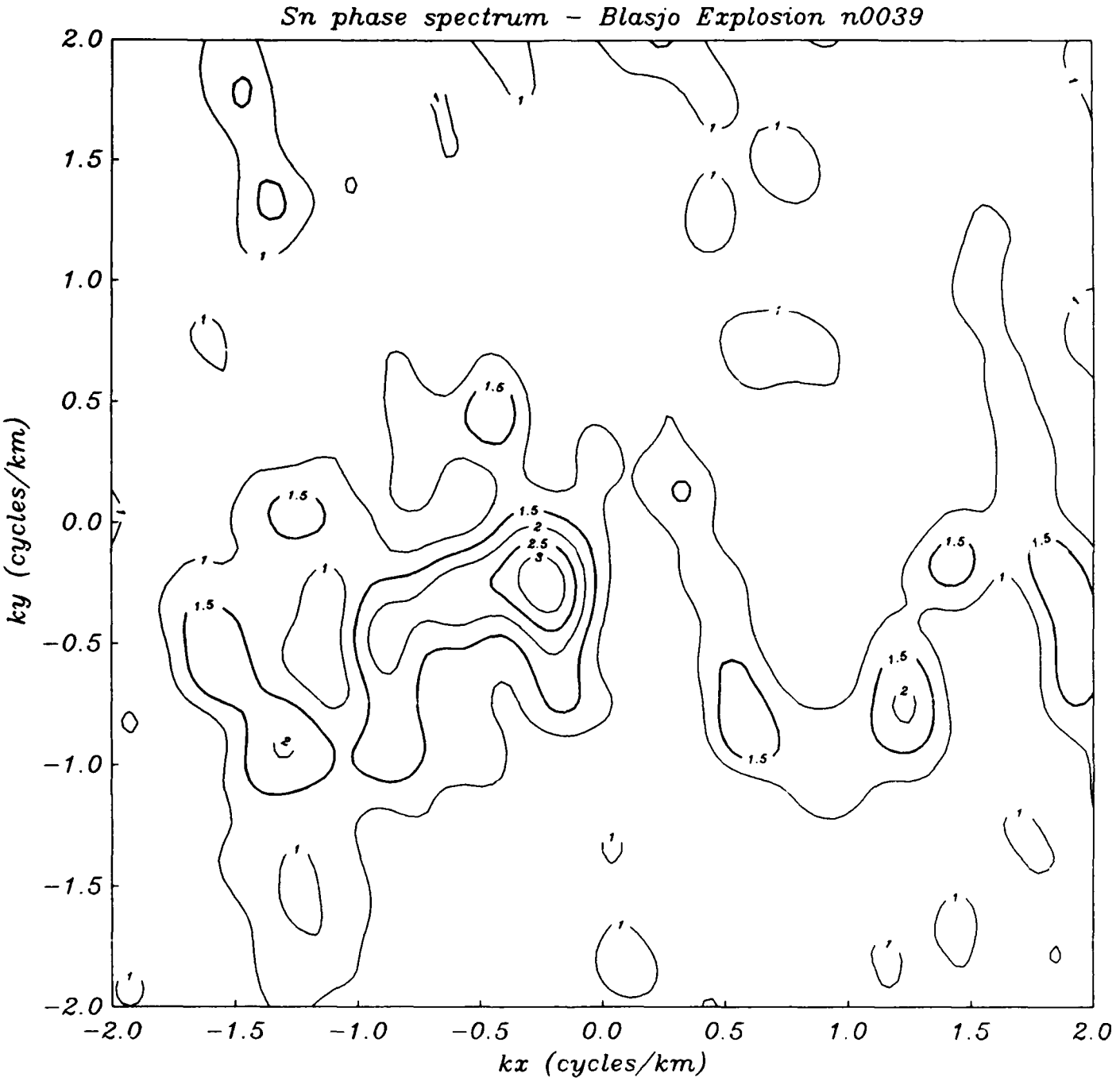
Sn phase spectrum - Blasjo Explosion n0039
ky (cycles/km)
kx (cycles/km)
2.0
1.5
1.0
0.5
0.0
-0.5
-1.0
-1.5
-2.0
-2.0 -1.5 -1.0 -0.5 0.0 0.5 1.0 1.5 2.0

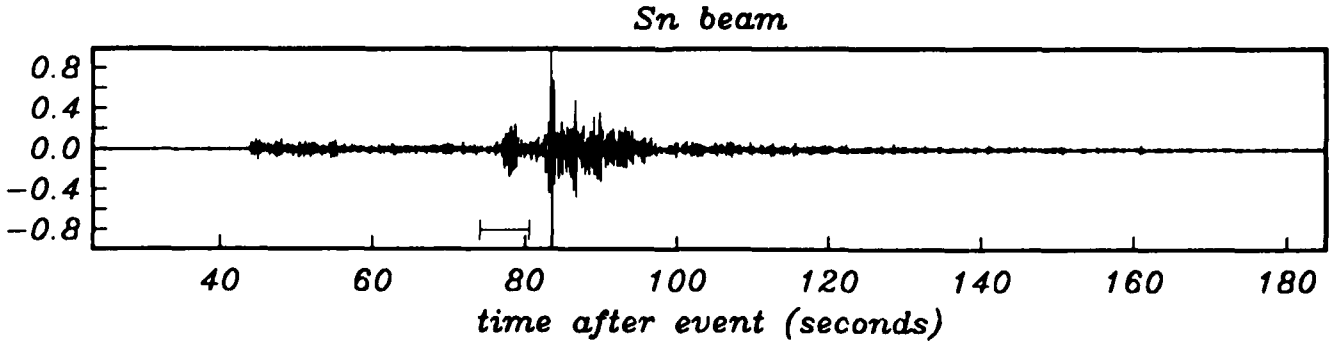
Sn beam
0.8
0.4
0.0
-0.4
-0.8
40 60 80 100 120 140 160 180
time after event (seconds)

Figure 9

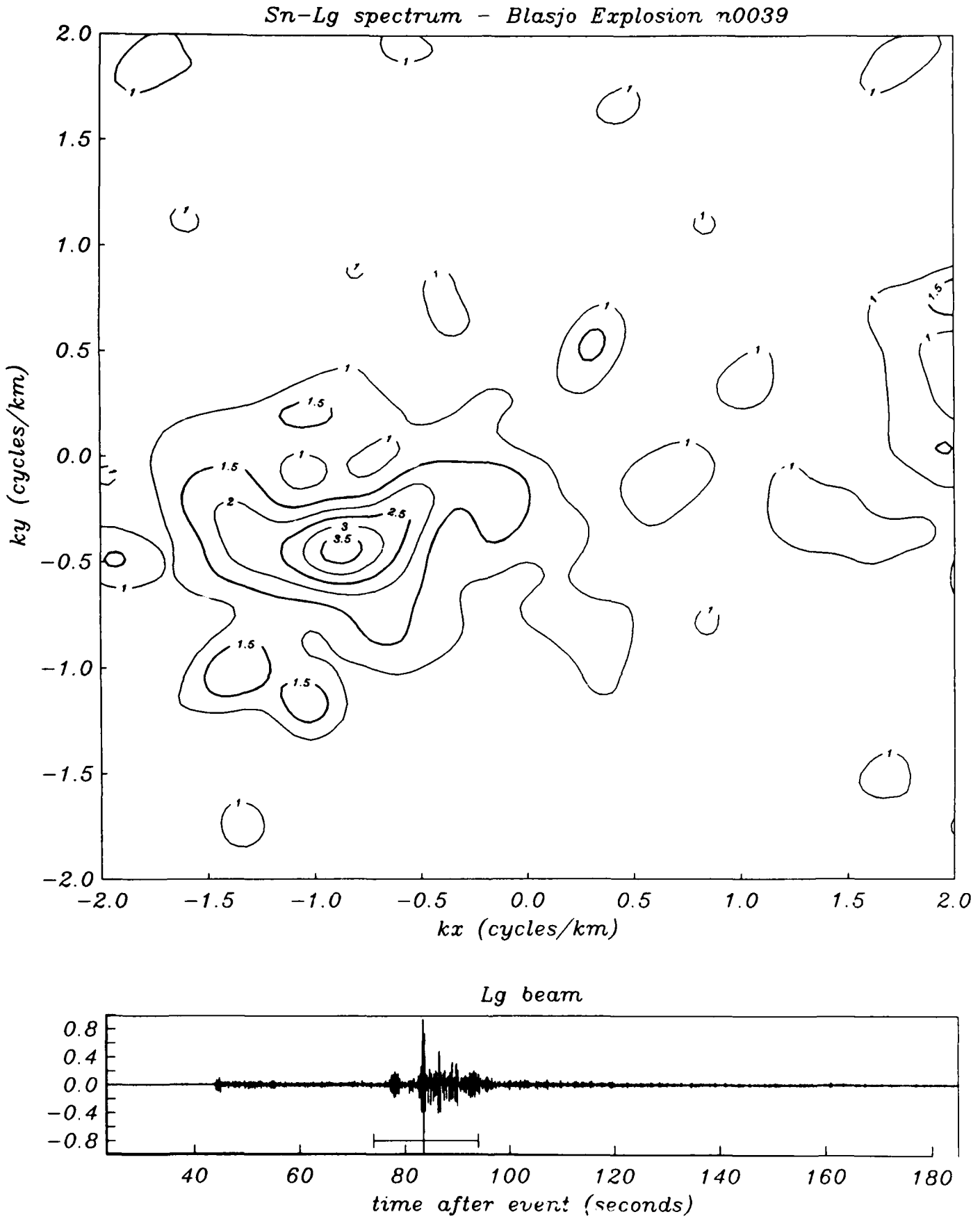
Sn-Lg spectrum - Blasjo Explosion n0039
ky (cycles/km)
kx (cycles/km)
2.0
1.5
1.0
0.5
0.0
-0.5
-1.0
-1.5
-2.0
1
1.5
2
2.5
3
3.5
Lg beam
0.8
0.4
0.0
-0.4
-0.8
40
60
80
100
120
140
160
180
time after event (seconds)

Figure 10

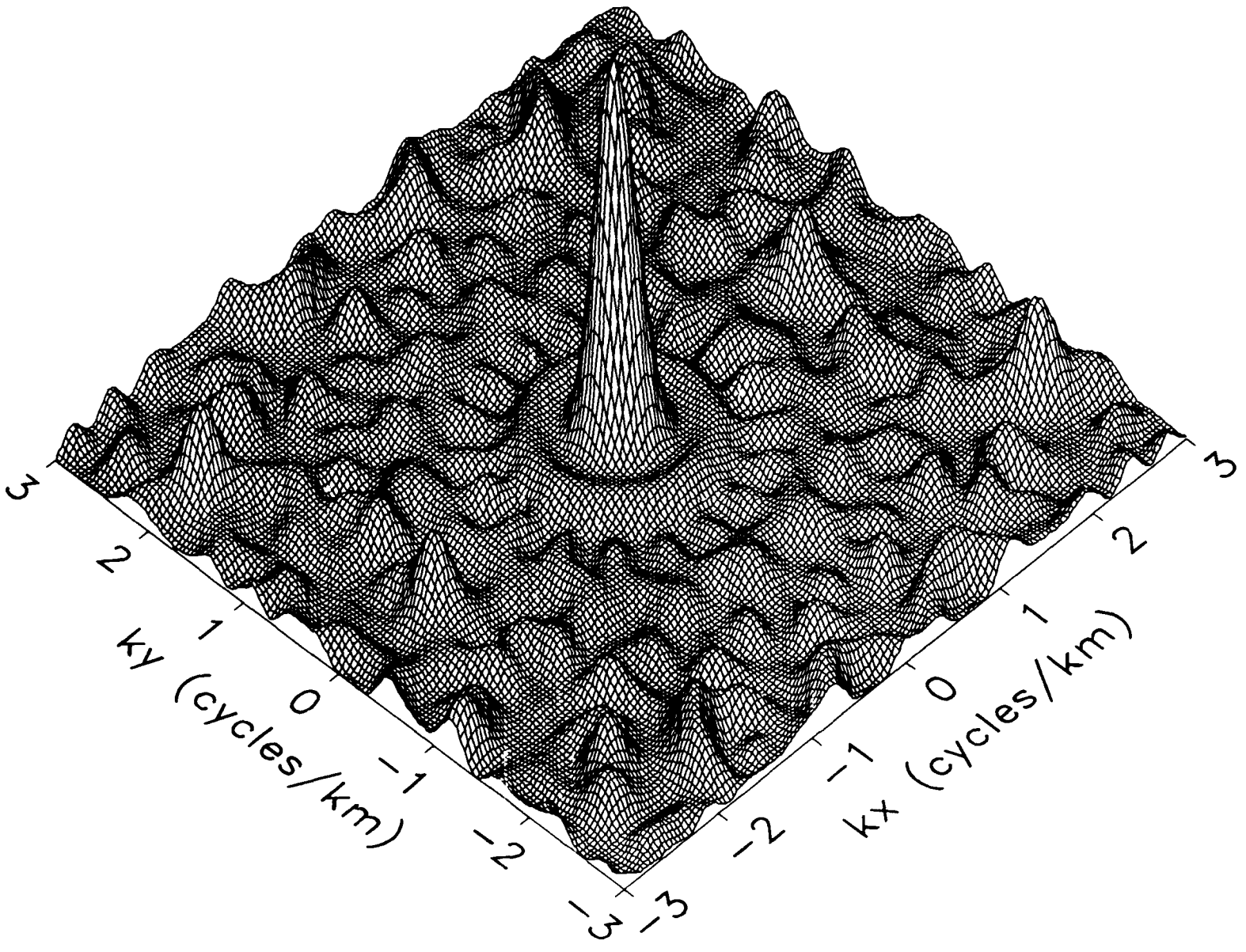

Impulse Response of NORESS array

Figure 11

CONTRACTORS (United States)

Professor Keiiti Aki
Center for Earth Sciences
University of Southern California
University Park
Los Angeles, CA 90089-0741

Professor Thomas Ahrens
Seismological Lab, 252-21
Div. of Geological and Planetary Sciences
California Institute of Technology
Pasadena, CA 91125

Professor Charles B. Archambeau
Cooperative Institute for Resch in Environmental Sciences
University of Colorado
Boulder, CO 80309

Dr. Thomas C. Bache Jr.
Science Applications Int'l Corp.
10210 Campus Point Drive
San Diego, CA 92121 (2 copies)

Dr. Muawia Barazangi
Institute for the Study of of the Continent
Cornell University
Ithaca, NY 14853

Dr. Douglas R. Baumgardt
Signal Analysis & Systems Div.
ENSCO, Inc.
5400 Port Royal Road
Springfield, VA 22151-2388

Dr. Jonathan Berger
Institute of Geophysics and Planetary Physics
Scripps Institution of Oceanography
A-025
University of California, San Diego
La Jolla, CA 92093

Dr. S. Bratt
Science Applications Int'l Corp.
10210 Campus Point Drive
San Diego, CA 92121

Dr. Lawrence J. Burdick
Woodward-Clyde Consultants
P.O. Box 93245
Pasadena, CA 91109-3245 (2 copies)

Professor Robert W. Clayton
Seismological Laboratory/Div. of Geological & Planetary Sciences
California Institute of Technology
Pasadena, CA 91125

Dr Karl Coyner
New England Research, Inc.
76 Olcott Drive
White River Junction, VT 05001

Dr. Vernon F. Cormier
Department of Geology & Geophysics
U-45, Room 207
The University of Conneticut
Storrs, Connecticut 06268

Dr. Steven Day
Dept. of Geological Sciences
San Diego State U.
San Diego, CA 92182

Dr. Zoltan A. Der
ENSCO, Inc.
5400 Port Royal Road
Springfield, VA 22151-2388

Professor John Ferguson
Center for Lithospheric Studies
The University of Texas at Dallas
P.O. Box 830688
Richardson, TX 75083-0688

Professor Stanley Flatte'
Applied Sciences Building
University of California,
Santa Cruz, CA 95064

Dr. Alexander Florence
SRI International
333 Ravenswood Avenue
Menlo Park, CA 94025-3493

Professor Steven Grand
University of Texas at Austin
Dept of Geological Sciences
Austin, TX 78713-7909

Dr. Henry L. Gray
Associate Dean of Dedman College
Department of Statistical Sciences
Southern Methodist University
Dallas, TX 75275

Professor Roy Greenfield
Geosciences Department
403 Deike Building
The Pennsylvania State University
University Park, PA 16802

Professor David G. Harkrider
Seismological Laboratory
Div of Geological & Planetary Sciences
California Institute of Technology
Pasadena, CA 91125

Professor Donald V. Helmberger
Seismological Laboratory
Div of Geological & Planetary Sciences
California Institute of Technology
Pasadena, CA 91125

Professor Eugene Herrin
Institute for the Study of Earth
and Man/Geophysical Laboratory
Southern Methodist University
Dallas, TX 75275

Professor Robert B. Herrmann
Department of Earth & Atmospheric
Sciences
Saint Louis University
Saint Louis, MO 63156

Professor Bryan Isacks
Cornell University
Dept of Geological Sciences
SNEE Hall
Ithaca, NY 14850

Professor Lane R. Johnson
Seismographic Station
University of California
Berkeley, CA 94720

Professor Thomas H. Jordan
Department of Earth, Atmospheric
and Planetary Sciences
Mass Institute of Technology
Cambridge, MA 02139

Dr. Alan Kafka
Department of Geology &
Geophysics
Boston College
Chestnut Hill, MA 02167

Professor Leon Knopoff
University of California
Institute of Geophysics
& Planetary Physics
Los Angeles, CA 90024

Professor Charles A. Langston
Geosciences Department
403 Deike Building
The Pennsylvania State University
University Park, PA 16802

Professor Thorne Lay
Department of Geological Sciences
1006 C.C. Little Building
University of Michigan
Ann Arbor, MI 48109-1063

Dr. Randolph Martin III
New England Research, Inc.
76 Olcott Drive
White River Junction, VT 05001

Dr. Gary McCartor
Mission Research Corp.
735 State Street
P.O. Drawer 719
Santa Barbara, CA 93102 (2 copies)

Professor Thomas V. McEvilly
Seismographic Station
University of California
Berkeley, CA 94720

Dr. Keith L. McLaughlin
S-CUBED,
A Division of Maxwell Laboratory
P.O. Box 1620
La Jolla, CA 92038-1620

Professor William Menke
Lamont-Doherty Geological Observatory
of Columbia University
Palisades, NY 10964

Professor Brian J. Mitchell
Department of Earth & Atmospheric
Sciences
Saint Louis University
Saint Louis, MO 63156

Mr. Jack Murphy
S-CUBED
A Division of Maxwell Laboratory
11800 Sunrise Valley Drive
Suite 1212
Reston, VA 22091 (2 copies)

Professor J. A. Orcutt
IGPP, A-205
Scripps Institute of Oceanography
Univ. of California, San Diego
La Jolla, CA 92093

Professor Keith Priestley
University of Nevada
Mackay School of Mines
Reno, NV 89557

Professor Paul G. Richards
Lamont-Doherty Geological
Observatory of Columbia Univ.
Palisades, NY 10964

Wilmer Rivers
Teledyne Geotech
314 Montgomery Street
Alexandria, VA 22314

Dr. Alan S. Ryall, Jr.
Center of Seismic Studies
1300 North 17th Street
Suite 1450
Arlington, VA 22209-2308 (4 copies)

Professor Charles G. Sammis
Center for Earth Sciences
University of Southern California
University Park
Los Angeles, CA 90089-0741

Professor Christopher H. Scholz
Geological Sciences
Lamont-Doherty Geological Observatory
Palisades, NY 10964

Dr. Jeffrey L. Stevens
S-CUBED,
A Division of Maxwell Laboratory
P.O. Box 1620
La Jolla, CA 92038-1620

Professor Brian Stump
Institute for the Study of Earth & Man
Geophysical Laboratory
Southern Methodist University
Dallas, TX 75275

Professor Ta-liang Teng
Center for Earth Sciences
University of Southern California
University Park
Los Angeles, CA 90089-0741

Dr. Clifford Thurber
State University of New York at
Stony Brooks
Dept of Earth and Space Sciences
Stony Brook, NY 11794-2100

Professor M. Nafi Toksoz
Earth Resources Lab
Dept of Earth, Atmospheric and
Planetary Sciences
Massachusetts Institute of Technology
42 Carleton Street
Cambridge, MA 02142

Professor Terry C. Wallace
Department of Geosciences
Building #77
University of Arizona
Tucson, AZ 85721

Weidlinger Associates
ATTN: Dr. Gregory Wojcik
4410 El Camino Real, Suite 110
Los Altos, CA 94022

Professor Francis T. Wu
Department of Geological Sciences
State University of New York
at Binghamton
Vestal, NY 13901

OTHERS (United States)

Dr. Monem Abdel-Gawad
Rockwell International Science Center
1049 Camino Dos Rios
Thousand Oaks, CA 91360

Professor Shelton S. Alexander
Geosciences Department
403 Deike Building
The Pennsylvania State University
University Park, PA 16802

Dr. Ralph Archuleta
Department of Geological Sciences
Univ. of California at Santa Barbara
Santa Barbara, CA

J. Barker
Department of Geological Sciences
State University of New York at Binghamton
Vestal, NY 13901

Mr. William J. Best
907 Westwood Drive
Vienna, VA 22180

Dr. N. Biswas
Geophysical Institute
University of Alaska
Fairbanks, AK 99701

Dr. G. A. Bollinger
Department of Geological Sciences
Virginia Polytechnical Institute
21044 Derring Hall
Blacksburg, VA 24061

Mr. Roy Burger
1221 Serry Rd.
Schenectady, NY 12309

Dr. Robert Burridge
Schlumberger-Doll Resch Ctr.
Old Quarry Road
Ridgefield, CT 06877

Science Horizons, Inc.
ATTN: Dr. Theodore Cherry
710 Encinitas Blvd., Suite 101
Encinitas, CA 92024 (2 copies)

Professor Jon F. Claerbout
Professor Amos Nur
Dept. of Geophysics
Stanford University
Stanford, CA 94305 (2 copies)

Dr. Anton W. Dainty
Earth Resources Lab
Massachusetts Institute of Technology
42 Carleton Street
Cambridge, MA 02142

Professor Adam Dziewonski
Hoffman Laboratory
Harvard University
20 Oxford St.
Cambridge, MA 02138

Professor John Ebel
Dept of Geology and Geophysics
Boston College
Chestnut Hill, MA 02167

Dr. Donald Forsyth
Dept of Geological Sciences
Brown University
Providence, RI 02912

Dr. Anthony Gangi
Texas A&M University
Department of Geophysics
College Station, TX 77843

Dr. Freeman Gilbert
Institute of Geophysics & Planetary Physics
University of California, San Diego
P.O. Box 109
La Jolla, CA 92037

Mr. Edward Giller
Pacific Seirra Research Corp.
1401 Wilson Boulevard
Arlington, VA 22209

Dr. Jeffrey W. Given
Sierra Geophysics
11255 Kirkland Way
Kirkland, WA 98033

Rong Song Jih
Teledyne Geotech
314 Montgomery Street
Alexandria, Virginia 22314

Professor F.K. Lamb
University of Illinois at
Urbana-Champaign
Department of Physics
1110 West Green Street
Urbana, IL 61801

Dr. Arthur Lerner-Lam
Lamont-Doherty Geological Observatory
of Columbia University
Palisades, NY 10964

Dr. L. Timothy Long
School of Geophysical Sciences
Georgia Institute of Technology
Atlanta, GA 30332

Dr. Peter Malin
University of California at
Santa Barbara
Institute for Central Studies
Santa Barbara, CA 93106

Dr. George R. Mellman
Sierra Geophysics
11255 Kirkland Way
Kirkland, WA 98033

Dr. Bernard Minster
IGPP, A-205
Scripps Institute of Oceanography
Univ. of California, San Diego
La Jolla, CA 92093

Professor John Nabelek
College of Oceanography
Oregon State University
Corvallis, OR 97331

Dr. Geza Nagy
U. California, San Diego
Dept of Ames, M.S. B-010
La Jolla, CA 92093

Dr. Jack Oliver
Department of Geology
Cornell University
Ithaca, NY 14850

Dr. Robert Phinney/Dr. F. A. Dahlen
Dept of Geological
Geological Science University
Princeton University
Princeton, NJ 08540

RADIX System, Inc.
Attn: Dr. Jay Pulli
2 Taft Court, Suite 203
Rockville, Maryland 20850

Dr. Norton Rimer
S-CUBED
A Division of Maxwell Laboratory
P.O. 1620
La Jolla, CA 92038-1620

Professor Larry J. Ruff
Department of Geological Sciences
1006 C.C. Little Building
University of Michigan
Ann Arbor, MI 48109-1063

Dr. Richard Sailor
TASC Inc.
55 Walkers Brook Drive
Reading, MA 01867

Thomas J. Sereno, Jr.
Science Application Int'l Corp.
10210 Campus Point Drive
San Diego, CA 92121

Dr. David G. Simpson
Lamont-Doherty Geological Observ.
of Columbia University
Palisades, NY 10964

Dr. Bob Smith
Department of Geophysics
University of Utah
1400 East 2nd South
Salt Lake City, UT 84112

Dr. S. W. Smith
Geophysics Program
University of Washington
Seattle, WA 98195

Dr. Stewart Smith
IRIS Inc.
1616 N. Fort Myer Drive
Suite 1440
Arlington, VA 22209

Rondout Associates
ATTN: Dr. George Sutton,
Dr. Jerry Carter, Dr. Paul Pomeroy
P.O. Box 224
Stone Ridge, NY 12484 (4 copies)

Dr. L. Sykes
Lamont Doherty Geological Observ.
Columbia University
Palisades, NY 10964

Dr. Pradeep Talwani
Department of Geological Sciences
University of South Carolina
Columbia, SC 29208

Dr. R. B. Tittmann
Rockwell International Science Center
1049 Camino Dos Rios
P.O. Box 1085
Thousand Oaks, CA 91360

Professor John H. Woodhouse
Hoffman Laboratory
Harvard University
20 Oxford St.
Cambridge, MA 02138

Dr. Gregory B. Young
ENSCO, Inc.
5400 Port Royal Road
Springfield, VA 22151-2388

FOREIGN (OTHERS)

Dr. Peter Basham
Earth Physics Branch
Geological Survey of Canada
1 Observatory Crescent
Ottawa, Ontario
CANADA K1A 0Y3

Professor Ari Ben-Menahem
Dept of Applied Mathematics
Weizman Institute of Science
Rehovot
ISRAEL 951729

Dr. Eduard Berg
Institute of Geophysics
University of Hawaii
Honolulu, HI 96822

Dr. Michel Bouchon - Universite
Scientifique et Medicale de Grenob
Lab de Geophysique - Interne et
Tectonophysique - I.R.I.G.M-B.P.
38402 St. Martin D'Heres
Cedex FRANCE

Dr. Hilmar Bungum/NTNF/NORSAR
P.O. Box 51
Norwegian Council of Science,
Industry and Research, NORSAR
N-2007 Kjeller, NORWAY

Dr. Michel Campillo
I.R.I.G.M.-B.P. 68
38402 St. Martin D'Heres
Cedex, FRANCE

Dr. Kin-Yip Chun
Geophysics Division
Physics Department
University of Toronto
Ontario, CANADA M5S 1A7

Dr. Alan Douglas
Ministry of Defense
Blacknest, Brimpton,
Reading RG7-4RS
UNITED KINGDOM

Dr. Manfred Henger
Fed. Inst. For Geosciences & Nat'l Res.
Postfach 510153
D-3000 Hannover 51
FEDERAL REPUBLIC OF GERMANY

Ms. Eva Johannisson
Senior Research Officer
National Defense Research Inst.
P.O. Box 27322
S-102 54 Stockholm
SWEDEN

Tormod Kvaerna
NTNF/NORSAR
P.O. Box 51
N-2007 Kjeller, NORWAY

Mr. Peter Marshall, Procurement
Executive, Ministry of Defense
Blacknest, Brimpton,
Reading FG7-4RS
UNITED KINGDOM (3 copies)

Dr. Robert North
Geophysics Division
Geological Survey of Canada
1 Observatory crescent
Ottawa, Ontario
CANADA, K1A 0Y3

Dr. Frode Ringdal
NTNF/NORSAR
P.O. Box 51
N-2007 Kjeller, NORWAY

Dr. Jorg Schlittenhardt
Federal Inst. for Geosciences & Nat'l Res.
Postfach 510153
D-3000 Hannover 51
FEDERAL REPUBLIC OF GERMANY

University of Hawaii
Institute of Geophysics
ATTN: Dr. Daniel Walker
Honolulu, HI 96822

FOREIGN CONTRACTORS

Dr. Ramon Cabre, S.J.
Observatorio San Calixto
Casilla 5939
La Paz Bolivia

Professor Peter Harjes
Institute for Geophysik
Rhur University/Bochum
P.O. Box 102148, 4630 Bochum 1
FEDERAL REPUBLIC OF GERMANY

Dr. E. Husebye
NTNF/NORSAR
P.O. Box 51
N-2007 Kjeller, NORWAY

Professor Brian L.N. Kennett
Research School of Earth Sciences
Institute of Advanced Studies
G.P.O. Box 4
Canberra 2601
AUSTRALIA

Dr. B. Massinon
Societe Radiomana
27, Rue Claude Bernard
7,005, Paris, FRANCE (2 copies)

Dr. Pierre Mechler
Societe Radiomana
27, Rue Claude Bernard
75005, Paris, FRANCE

Dr. Svein Mykkeltveit
NTNF/NORSAR
P.O. Box 51
N-2007 Kjeller, NORWAY (3 copies)

GOVERNMENT

Dr. Ralph Alewine III
DARPA/NMRO
1400 Wilson Boulevard
Arlington, VA 22209-2308

Dr. Robert Blandford
DARPA/NMRO
1400 Wilson Boulevard
Arlington, VA 22209-2308

Sandia National Laboratory
ATTN: Dr. H. B. Durham
Albuquerque, NM 87185

Dr. Jack Evernden
USGS-Earthquake Studies
345 Middlefield Road
Menlo Park, CA 94025

U.S. Geological Survey
ATTN: Dr. T. Hanks
Nat'l Earthquake Resch Center
345 Middlefield Road
Menlo Park, CA 94025

Dr. James Hannon
Lawrence Livermore Nat'l Lab.
P.O. Box 808
Livermore, CA 94550

Paul Johnson
ESS-4, Mail Stop J979
Los Alamos National Laboratory
Los Alamos, NM 87545

Ms. Ann Kerr
DARPA/NMRO
1400 Wilson Boulevard
Arlington, VA 22209-2308

Dr. Max Koontz
US Dept of Energy/DP 5
Forrestal Building
1000 Independence Ave.
Washington, D.C. 20585

Dr. W. H. K. Lee
USGS
Office of Earthquakes, Volcanoes,
& Engineering
Branch of Seismology
345 Middlefield Rd
Menlo Park, CA 94025

Dr. William Leith
U.S. Geological Survey
Mail Stop 928
Reston, VA 22092

Dr. Richard Lewis
Dir. Earthquake Engineering and
Geophysics
U.S. Army Corps of Engineers
Box 631
Vicksburg, MS 39180

Dr. Robert Masse'
Box 25046, Mail Stop 967
Denver Federal Center
Denver, Colorado 80225

Richard Morrow
ACDA/VI
Room 5741
320 21st Street N.W.
Washington, D.C. 20451

Dr. Keith K. Nakanishi
Lawrence Livermore National Laboratory
P.O. Box 808, L-205
Livermore, CA 94550 (2 copies)

Dr. Carl Newton
Los Alamos National Lab.
P.O. Box 1663
Mail Stop C335, Group ESS-3
Los Alamos, NM 87545

Dr. Kenneth H. Olsen
Los Alamos Scientific Lab.
P.O. Box 1663
Mail Stop C335, Group ESS-3
Los Alamos, NM 87545

Howard J. Patton
Lawrence Livermore National
Laboratory
P.O. Box 808, L-205
Livermore, CA 94550

Mr. Chris Paine
Office of Senator Kennedy
SR 315
United States Senate
Washington, D.C. 20510

AFOSR/NP
ATTN: Colonel Jerry J. Perrizo
Bldg 410
Bolling AFB, Wash D.C. 20332-6448

HQ AFTAC/TT
Attn: Dr. Frank F. Pilotte
Patrick AFB, Florida 32925-6001

Mr. Jack Rachlin
USGS - Geology, Rm 3 C136
Mail Stop 928 National Center
Reston, VA 22092

Robert Reinke
AFWL/NTESG
Kirtland AFB, NM 87117-6008

Dr. Byron Ristvet
HQ DNA, Nevada Operations Office
Attn: NVCG
P.O. Box 98539
Las Vegas, NV 89193

HQ AFTAC/TGR
Attn: Dr. George H. Rothe
Patrick AFB, Florida 32925-6001

Donald L. Springer
Lawrence Livermore National Laboratory
P.O. Box 808, L-205
Livermore, CA 94550

Dr. Lawrence Turnbull
OSWR/NED
Central Intelligence Agency
CIA, Room 5G48
Washington, D.C. 20505

Dr. Thomas Weaver
Los Alamos National Laboratory
P.O. Box 1663
MS C 335
Los Alamos, NM 87545

GL/SULL
Research Library
Hanscom AFB, MA 01731-5000 (2 copies)

Secretary of the Air Force (SAFRD)
Washington, DC 20330
Office of the Secretary Defense
DDR & E
Washington, DC 20330

HQ DNA
ATTN: Technical Library
Washington, DC 20305

DARPA/RMO/RETRIEVAL
1400 Wilson Blvd.
Arlington, VA 22209

DARPA/RMO/Security Office
1400 Wilson Blvd.
Arlington, VA 22209

GL/XO
Hanscom AFB, MA 01731-5000

GL/LW
Hanscom AFB, MA 01731-5000

DARPA/PM
1400 Wilson Boulevard
Arlington, VA 22209

Defense Technical
Information Center
Cameron Station
Alexandria, VA 22314
(5 copies)

Defense Intelligence Agency
Directorate for Scientific &
Technical Intelligence
Washington, D.C. 20301

Defense Nuclear Agency/SPSS
ATTN: Dr. Michael Shore
6801 Telegraph Road
Alexandria, VA 22310

AFTAC/CA (STINFO)
Patrick AFB, FL 32925-6001

Dr. Gregory van der Vink
Congress of the United States
Office of Technology Assessment
Washington, D.C. 20510

Mr. Alfred Lieberman
ACDA/VI-OA'State Department Building
Room 5726
320 - 21St Street, NW
Washington, D.C. 20451

TACTEC
Battelle Memorial Institute
505 King Avenue
Columbus, OH 43201 (Final report only)

*U.S. GOVERNMENT PRINTING OFFICE: 1989-600-000/00023